F 1503/3
FF
8 000000 529237
F 1503/3
T. 42
LSZ
000004 060490

BULETINUL INSTITUTULUI POLITEHNIC DIN IAŞI

Tomul XLII (XLVI)
Fasc. 1-2

Secția III

ELECTROTEHNICĂ
ENERGETICĂ
ELECTRONICĂ

1996

MŰSZAKI INFORMÁCIÓS KÖZPONT ÉS KÖNYVTÁR
ORSZÁGOS
1883

BULETINUL INSTITUTULUI POLITEHNIC DIN IAŞI

Tomul XLII (XLVI)
Fasc. 1–2

Secţia III

ELECTROTEHNICĂ. ENERGETICĂ. ELECTRONICĂ

1996

EDITORIAL STAFF

Prof. Dr. Eng. **MIHAI GAFIŢANU** (President)
Prof. Dr. Eng. **VICTOR BULACOVSCHI** (Vice-President)
Prof. Dr. Eng. **LIVIU GROLL** (Vice-President)
Prof. Dr. Eng. **GHEORGHE ZET** (Secretary)
Prof. Dr. Doc. Eng. **ALFRED BRAIER** (Editor)
Prof. Dr. Eng. **HUGO ROSMAN** (Editor)
Prof. Dr. Eng. **MIHAIL VOICU** (Head of the Exchange Service)
Prof. Dr. Eng. **DIMITRIE ALEXA**
Prof. Dr. Eng. **ION BALASANIAN**
Prof. Dr. **AUREL BEJANCU**
Prof. Dr. Eng. **MIRCEA COZMÎNCĂ**
Prof. Dr. Eng. **SPIRIDON CREŢU**
Prof. Dr. Eng. **ION GIURMA**
Prof. Dr. Eng. **AURELIA GRIGORIU**
Prof. Dr. Eng. **CONSTANTIN PREDA**
Prof. Dr. Eng. **PAULICĂ RĂILEANU**

The Bulletin of the Polytechnic Institute of Jassy is edited by
the Technical University "Gh.Asachi" (the former Polytechnic Institute), Jassy.

TEXredaction:
B. Grigoriu, A. Rotaru
Technical University of Jassy

BULETINUL INSTITUTULUI POLITEHNIC DIN IAŞI
BULLETIN OF THE POLYTECHNIC INSTITUTE OF JASSY
Tomul XLII (XLVI), Fasc. 1–2 1996

Secţia III

ELECTROTEHNICĂ. ENERGETICĂ. ELECTRONICĂ

SUMAR

Pag.

HUGO ROSMAN, LIVIU GORAŞ şi ALFRED BRAIER, Sinteza uniporţilor liniari pasivi excitaţi de semnale modulate în amplitudine, în regimuri de rezonanţă (franc., rez. rom.) 7

DORIN BELAUS, Asupra parametrilor caracteristici ai cuadripolilor generali liniari neautonomi în regim permanent armonic (franc., rez. rom.) 17

IUSTINA ZAHARIA, Reţea neuronală pentru comanda unui braţ robot (franc., rez. rom.) 23

VALERIU MUNTEANU şi DANIELA TĂRNICERIU, Câteva aplicaţii ale entropiei surselor de informaţie cu preferinţe (engl., rez. rom.) 31

N.D. ALEXANDRU, Un nou cod derivat din codul Miller (engl., rez. rom.) 37

PAUL COTAE, Densitatea spectrală de putere a semnalelor digitale cu modulaţie digitală de fază pentru diferite funcţii modulatoare (engl., rez. rom.) 43

DANIELA TĂRNICERIU şi VALERIU MUNTEANU, O metodă de proiectare a filtrelor IIR periodic variante în timp cu aplicaţii în transmultiplexare (I) (engl., rez. rom.) . 53

VIOREL-MIHAIL COSMA, M. LOZOVAN, I. ONCIULESCU şi VIRGIL MOGA, Contribuţii privind analiza oscilatorului de relaxare cu bobină neliniară (engl., rez. rom.) 61

MARIANA BUZDUGA, Asupra condiţiilor de apariţie a oscilaţiilor mecanice într-un sistem electromecanic. III. Extinderea studiului stabilităţii soluţiilor (franc., rez. rom.) 67

ELENA CREŢU, ADRIAN CREŢU şi CARMEN COJOCARU-FILIPIUC, Asupra unei scheme de compensare automată a erorilor transformatoarelor de tensiune (engl., rez. rom.) 77

M. CREŢU şi C. VOINICIUC, Stand de verificare cu PC pentru contoarele electrice (engl., rez. rom.) 83

ADRIAN BARABOI, Asupra funcţionării unui releu de tip ferorezonant (franc., rez. rom.) 89

I. ANDRONE şi ADRIANA PRISĂCARU, Asupra schemelor echivalente ale motorului asincron bifazat nesimetric (engl., rez. rom.) 95

Pag.

ANGEL-RADU-PETRICĂ TODEREAN, IULIAN RĂDUCANU şi LAURENŢIU DIMITRIU, Sistem electronic cu microprocesor pentru controlul injecţiei şi al aprinderii la motoare cu aprindere prin scânteie (engl., rez. rom.) 105

C. POŞA, D. ALEXA şi RADU MUNTEANU, Metodă de autofrânare a unui motor asincron bifazat alimentat de un invertor MID (engl., rez. rom.) 111

KARL SAAL, Determinarea parametrilor interni şi influenţa lor asupra parametrilor de funcţionare impuşi, garantaţi, ai motoarelor asincrone trifazate (germ., rez. rom.).. 119

IULIAN GRAUR, GR. TAŞCĂ, M. ALBU, ADRIAN MAREŞ, V. HORGA şi DORIN LUCACHE, Simularea numerică a regimului de funcţionare stabilizat al unor sisteme de acţionare electrică utilizate în industria metalurgică (engl., rez. rom.) 129

MIRCEA GUŞĂ, MARCEL ISTRATE, N. GAVRILAŞ şi C. ASAFTEI, Detectarea magnetică a scurtcircuitelor pe liniile electrice aeriene de medie tensiune (franc., rez. rom.) 137

JAN IGNAT şi M. PROFIRE, Efectul modificării configuraţiei reţelelor de distribuţie asupra dispozitivelor de localizare a defectului monofazat (engl., rez. rom.) 145

GH. GEORGESCU şi M. GAVRILAŞ, Proiectarea optimală a reţelelor de distribuţie rurală (engl., rez. rom.) 151

RECENZII 157

BULETINUL INSTITUTULUI POLITEHNIC DIN IAŞI
BULLETIN OF THE POLYTECHNIC INSTITUTE OF JASSY
Tome XLII (XLVI), Fasc. 1–2 1996

Section III

ELECTROTECHNICS. ENERGETICS. ELECTRONICS

CONTENTS

Pp.

HUGO ROSMAN, LIVIU GORAŞ et ALFRED BRAIER, Synthèse des uniportes linéaires passifs excités par des signaux modulés en amplitude, en régimes de résonance (French, Romanian summary) 7

DORIN BELAUS, Sur les paramètres caractéristiques des quadripôles généraux linéaires nonautonomes, en régime permanent harmonique (French, Romanian summary) 17

IUSTINA ZAHARIA, Réseau de neurones pour la commande d'un bras robot (French, Romanian summary) 23

VALERIU MUNTEANU and DANIELA TĂRNICERIU, Some Applications of Entropy of Sources with Preferences (English, Romanian summary) 31

N.D. ALEXANDRU, A New Code Based on Delay Modulation (English, Romanian summary) 37

PAUL COTAE, Power Spectral Density of *M*-ary PSK with Various Shaping Functions (English, Romanian summary) 43

DANIELA TĂRNICERIU and VALERIU MUNTEANU, A Design Method for Periodically Time Varying IIR Filters with Application to Transmultiplexing (I) (English, Romanian summary) 53

VIOREL-MIHAIL COSMA, M. LOZOVAN, I. ONCIULESCU and VIRGIL MOGA, Contribution to the Analysis of the Relaxation Oscillator with Non-linear Coil (English, Romanian summary) 61

MARIANA BUZDUGA, Sur les conditions d'apparition des oscillations mécaniques dans un système électromecanique. III. Extension de l'étude de la stabilité des solutions (French, Romanian summary) 67

ELENA CREŢU, ADRIAN CREŢU and CARMEN COJOCARU-FILIPIUC, About a Diagram for the Automatic Error Compensation in Voltage Transformers (English, Romanian summary) 77

M. CREŢU and C. VOINICIUC, Verification Stand-alone Unit with PC for Induction-type Integrating Electricity Meters (English, Romanian summary) 83

ADRIAN BARABOI, Sur le fonctionnement d'un relais type ferrorésonant (French, Romanian summary) 89

I. ANDRONE and ADRIANA PRISĂCARU, On the Equivalent Circuits Diagrams of the Two-phase Unsymmetrical Induction Motors (English, Romanian summary) 95

Pp.

ANGEL-RADU-PETRICĂ TODEREAN, IULIAN RĂDUCANU and LAURENŢIU DIMITRIU, An Electronic Injection and Ignition Microprocessor Control Unit for Spark Ignition Engines (English, Romanian summary) 105

C. POŞA, D. ALEXA and RADU MUNTEANU, The Selfbraking Method of a Two-phase Asynchronous Motor Supplied by a PWM Inverter (English, Romanian summary) .. 111

KARL SAAL, Bestimmung der inneren Parameter und deren Einfluß auf die garantierten Bemessungs-Betriebsparameter von Drehstrom-Asinchronmotoren (German, Romanian summary) 119

IULIAN GRAUR, GR. TAŞCĂ, M. ALBU, ADRIAN MAREŞ, V. HORGA and DORIN LUCACHE, Numerical Simulation of the Stabilized Functioning Regime of Some Electrical Drive Systems Used in Metallurgical Industries (English, Romanian summary) 129

MIRCEA GUŞĂ, MARCEL ISTRATE, N. GAVRILAŞ et C. ASAFTEI, La détection magnétique des court-circuits dans les réseaux aériens de moyenne tension (French, Romanian summary) 137

JAN IGNAT and M. PROFIRE, The Impact of the Layout Modification in the Supply Systems on the One-phase Fault Location Devices (English, Romanian summary) .. 145

GH. GEORGESCU and M. GAVRILAŞ, Optimal Design of the Rural Electric Distribution Networks (English, Romanian summary) 151

BOOK REVIEWS 157

BULETINUL INSTITUTULUI POLITEHNIC DIN IAŞI
Tomul XLII (XLVI), Fasc. 1–2, 1996
Secţia III
ELECTROTEHNICĂ. ENERGETICĂ. ELECTRONICĂ

C.D. 621.3.011; 538.567.4; 538.551.25

SYNTHÈSE DES UNIPORTES LINÉAIRES PASSIFS EXCITÉS PAR DES SIGNAUX MODULÉS EN AMPLITUDE, EN RÉGIMES DE RÉSONANCE

PAR
HUGO ROSMAN, LIVIU GORAŞ et ALFRED BRAIER

Compte tenu des définitions des régimes résonants ou strictement résonants d'un uniporte linéaire passif, en régime permanent, excité par un signal modulé en amplitude, on étudie le problème de la synthèse de tels uniports.

1. Introduction

Dans un travail précédent [1] on a étudié la possibilité d'adapter le concept de résonance à la porte d'accès d'un uniporte linéaire passif (ULP), utilisé d'habitude lorsque l'excitation est périodique, harmonique ou nonharmonique, au cas où l'excitation est un signal modulé en amplitude (MA). À savoir si un ULP est excité par un signal MA dont l'expression est [2]:

$$x(t) = X_m[1 + m\sin(\omega t + \psi)]\sin(\Omega_0 t + \varphi_0), \tag{1}$$

où Ω_0 représente la pulsation de la porteuse, ω – la pulsation du signal modulateur et m – le degré de modulation, on considère que son régime est résonant (RR), si, en régime permanent, le signal réponse a la forme:

$$y(t) = Y_m[1 + m'\sin(\omega t + \psi)]\sin(\Omega_0 t + \varphi_0), \tag{2}$$

avec $m' \neq m$. Si, en outre

$$m' = m \tag{3}$$

on peut dénommer le régime respectif comme strictement résonant (RRS), les relations

$$y(t) = ax(t), \quad Y_m = aX_m, \qquad (a - \text{réel, positif}), \tag{4}$$

en étant satisfaites.

Pour tous les régimes ci-dessus définis on peut écrire les signaux excitation et réponse sous les formes équivalentes:

$$x(t) = \frac{1}{2}mX_m \sin\left(\omega_{-1}t + \phi_0 - \psi + \frac{\pi}{2}\right) + X_m \sin(\Omega_0 t + \phi_0) + \\ + \frac{1}{2}mX_m \sin\left(\omega_1 t + \phi_0 + \psi - \frac{\pi}{2}\right), \tag{5}$$

respectivement

$$y(t) = \frac{1}{2}m'Y_m \sin\left(\omega_{-1}t + \phi_0 - \psi + \frac{\pi}{2}\right) + Y_m \sin(\Omega_0 t + \phi_0) + \\ + \frac{1}{2}m'Y_m \sin\left(\omega_1 t + \phi_0 + \psi - \frac{\pi}{2}\right), \tag{6}$$

où

$$\omega_{-1} = \Omega_0 - \omega, \qquad \omega_1 = \Omega_0 + \omega \tag{7}$$

représentent les pulsations latérales.

Dans un cas plus général si l'excitation MA est de la forme:

$$x(t) = X_m \left[1 + \sum_{k=1}^{\infty} m_k \sin(k\omega t + \psi_k)\right] \sin(\Omega_0 t + \phi_0), \tag{8}$$

c'est-à-dire dans la situation où le signal modulateur est périodique mais nonharmonique, on peut réaliser des RR seulement pour une seule fréquence harmonique, pour certaines fréquences des harmoniques ou bien pour la totalité de celles-ci. Dans ce dernier cas il est nécessaire à réaliser simultanément des résonances (de tensions ou de courants) pour chacune des fréquences Ω_0, $\Omega_0 - k\omega$, $\Omega_0 + k\omega$, $(k = 1, 2, ...)$, le signal réponse ayant la forme:

$$y(t) = Y_m \left[1 + \sum_{k=1}^{\infty} m'_k \sin(k\omega t + \psi_k)\right] \sin(\Omega_0 t + \phi_0), \tag{9}$$

avec $m'_k \neq m_k$. Si $m'_k = m_k$, $(k = 1, 2, ...)$, alors on a affaire avec un RSR.

On peut étudier par une voie analogue le problème similaire où l'ULP est excité par un signal MF ou MP. On peut écrire un tel signal sous la forme [2]:

$$x(t) = X_m \sum_{k=-\infty}^{\infty} \mathrm{Y}_k(\beta) \cos(\Omega_0 + k\omega_0)t, \tag{10}$$

où β représente l'indice de modulation et $Y_k(\beta)$ – les fonctions de Bessel de première espèce, d'ordre k et d'argument β. Si on suppose qu'à la porte de l'ULP on réalise un RR le signal réponse est donné par:

$$y(t) = X_m \sum_{k=-\infty}^{\infty} a_k Y_k(\beta) \cos(\Omega_0 + k\omega_0)t, \tag{11}$$

tandis que dans le cas des RSR:

$$y(t) = Y_m \sum_{k=-\infty}^{\infty} Y_k(\beta) \cos(\Omega_0 + k\omega_0)t. \tag{12}$$

On peut constater aisément que le signal (11) n'est plus MF (ou MP) de sorte qu'un ULP excité par un signal ayant la forme (10) n'admet pas des RR. Au contraire le signal (12) est MF (ou MP) de sorte qu'on peut conclure, quant à la possibilité de réalisation des RR ou RSR à la porte d'un ULP excité par un signal MF (ou MP), qu'on ne peut obtenir, dans ce cas, que des RSR.

Si l'indice de modulation de l'excitation est suffisamment réduit ($\beta < 0,4$) on peut approximer les signaux de la forme (10) avec:

$$x(t) = X_m \cos\omega_0 t - \frac{1}{2}\beta X_m \cos(\omega_0 - \Omega_0)t + \frac{1}{2}\beta X_m \cos(\omega_0 + \Omega_0)t, \tag{13}$$

semblables à ceux ayant la forme (5), donc à des signaux MA.

Le but de cette Note est de réaliser la synthèse des ULP capables à réaliser soit des RR, soit des RSR.

2. Synthèse des uniportes linéaires capables à réaliser des régimes résonants pour des excitations modulées en amplitude

La synthèse proposée a pour but la détermination d'un ULP capable à réaliser au moins trois régimes de résonance (soit des tensions, soit des courants) aux pulsations ω_{-1}, Ω_0, ω_1 de sorte que la composante réactive de l'immitance équivalente de l'ULP ait des zéros ou des pôles pour les trois pulsations ci-dessus [3].

Compte tenu que toute fonction de réactance a les zéros et les pôles situés sur l'axe imaginaire et alternants une première solution est représentée par la synthèse d'une telle fonction ayant la forme:

$$Z_{LC}(s) = \frac{ks(s^2 + \Omega_0^2)}{(s^2 + \omega_{-1}^2)(s^2 + \omega_1^2)}, \tag{14}$$

dont le graphique est représenté dans la Fig.1. Si on utilise la deuxième forme canonique de F o s t e r [3]:

$$Y_{LC}(s) = \frac{(s^2 + \omega_{-1}^2)(s^2 + \omega_1^2)}{ks(s^2 + \Omega_0^2)} = \frac{s}{k} + \frac{k_0}{ks} + \frac{k_1}{s^2 + \Omega_0} \tag{15}$$

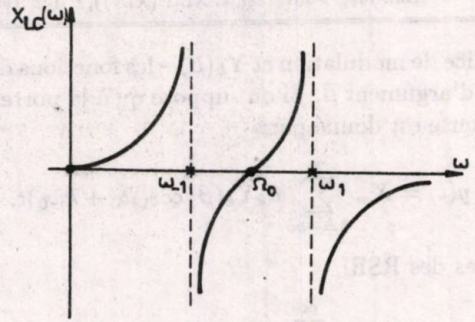

Fig. 1

on obtient

$$k_0 = \frac{\omega_{-1}^2 \omega_1^2}{\Omega_0^2}, \qquad k_1 = \frac{(\omega_{-1}^2 - \Omega_0^2)(\omega_1^2 - \Omega_0^2)}{-\Omega_0^2}, \tag{16}$$

le schéma correspondant en étant représenté dans la Fig.2 *a*.

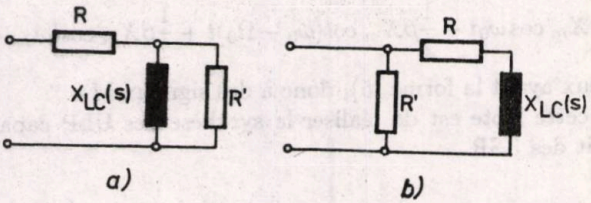

Fig. 2

On peut obtenir une autre solution du même problème en utilisant la première forme canonique de F o s t e r [3], en résultant le schéma représenté dans la Fig.2 *b*, les deux circuits résonants étant accordés aux pulsations ω_{-1}, respectivement ω_1. Pour ces pulsations on réalise des résonances des courants, celle des tensions en l'obtenant à la pulsation Ω_0. Dans la Fig.2 *b* on a utilisé les notations:

$$k_1' = \frac{\Omega_0^2 - \omega_{-1}^2}{\omega_1^2 - \omega_{-1}^2}, \qquad k_2' = \frac{\omega_1^2 - \Omega_0^2}{\omega_1^2 - \omega_{-1}^2}. \tag{17}$$

Plus généralement, on réalise des RR (deux des courants et un des tensions) pour tout ULP ayant le schéma représenté dans la Fig. 3 *a, b*. Si l'excitation est une tension MA ayant la forme (5), c'est-à-dire:

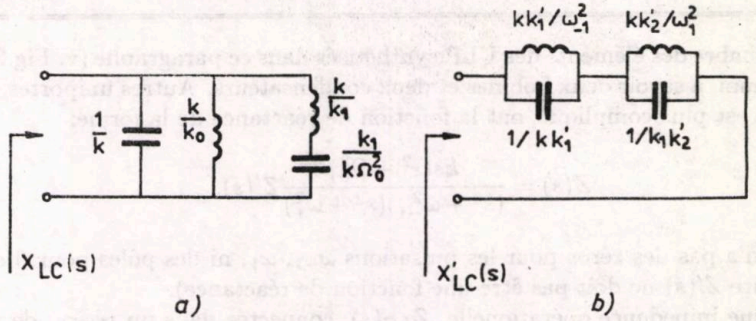

Fig. 3

$$u(t) = \frac{1}{2}mU_m \sin\left(\omega_{-1}t + \phi_0 - \psi + \frac{\pi}{2}\right) + U_m \sin(\Omega_0 t + \phi_0) + \tag{18}$$
$$+ \frac{1}{2}mU_m \sin\left(\omega_1 t + \phi_0 + \psi - \frac{\pi}{2}\right),$$

le courant, en tant que réponse, sera:

$$i(t) = \frac{1}{2} \cdot \frac{mU_m}{R+R'} \sin\left(\omega_{-1}t + \phi_0 - \psi + \frac{\pi}{2}\right) + \frac{U_m}{R} \sin(\Omega_0 t + \phi_0) + \tag{19}$$
$$+ \frac{1}{2} \cdot \frac{mU_m}{R+R'} \sin\left(\omega_1 t + \phi_0 + \psi - \frac{\pi}{2}\right)$$

dans le cas du schéma représenté dans la Fig. 3 *a*, respectivement

$$i(t) = \frac{1}{2} \cdot \frac{mU_m}{R'} \sin\left(\omega_{-1}t + \phi_0 - \psi + \frac{\pi}{2}\right) + \frac{(R+R')U_m}{RR'} \sin(\Omega_0 t + \phi_0) + \tag{20}$$
$$+ \frac{1}{2} \cdot \frac{mU_m}{R'} \sin\left(\omega_1 t + \phi_0 + \psi - \frac{\pi}{2}\right)$$

dans celui du schéma de la Fig. 3 *b*. On peut observer aisément que dans les deux cas considérés ci-dessus le degré de modulation du courant est moindre que celui de la tension, ayant la valeur:

$$m' = \frac{mR}{R+R'} < m. \tag{21}$$

On peut obtenir la solution du problème considéré en effectuant la synthèse de la fonction de réactance:

$$Z_{LC}(s) = \frac{(s^2+\omega_{-1}^2)(s^2+\omega_1^2)}{ks(s^2+\Omega_0^2)}, \tag{22}$$

ayant les zéros et les pôles inversés par rapport au cas précédent. Cette fois on obtient des résonances des tensions pour les pulsations ω_{-1} et ω_1 et des courants pour Ω_0. Dans ce cas quel qu'il soit le schéma adopté, du type représenté dans la Fig. 3, il résulte $m' > m$. Les ULP synthétisés sont, dans ce cas, les duals de ceux représentés dans les Fig. 2 *a, b*.

Le nombre des éléments des ULP synthétisés dans ce paragraphe (v. Fig.2 a, b) est minimum, à savoir deux bobines et deux condensateurs. Autres uniportes, dont le schéma est plus compliqué, ont la fonction de réactance de la forme:

$$Z(s) = \frac{ks(s^2+\Omega_0^2)}{(s^2+\omega_{-1}^2)(s^2+\omega_1^2)} Z'(s), \tag{23}$$

où $Z'(s)$ n'a pas des zéros pour les pulsations ω_{-1}, ω_1, ni des pôles pour 0 et Ω_0 (c'est-à-dire $Z'(s)$ ne doit pas être une fonction de réactance).

Chaque impédance opérationelle, $Z_{LC}(s)$, connectée dans un réseau de résistors mène à une telle condition. Plus encore, chaque réseau dont toutes les impédances operationelles sont soit des résistors, soit de la forme (23) satisfont à ces conditions (pour n'importe quelles valeurs de k_i et $Z_i'(s)$).

On considère, à titre d'exemple, l'ULP représenté dans la Fig. 4, où

$$Z_1(s) = \frac{k_1 s(s^2+\Omega_0^2)}{(s^2+\omega_{-1}^2)(s^2+\omega_1^2)}, \quad Z_2(s) = \frac{k_2 s(s^2+\omega_{-1}^2)(s^2+\omega_1^2)}{s(s^2+\omega_0^2)},$$

$$Z_3(s) = \frac{k_3 s(s^2+\omega_{-1}^2)(s^2+\omega_3^2)}{(s^2+\omega_{-1}^2)(s^2+\omega_1^2)}, \quad \omega_3 > \omega_1, \qquad Z_4(s) = \frac{k_4(s^2+\omega_{-1}^2)(s^2+\omega_1^2)}{s(s^2+\omega_0^2)(s^2+\omega_3^2)}, \quad \omega_3 > \omega_1.$$

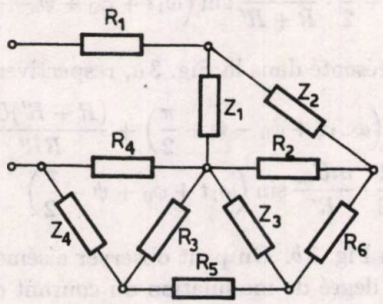

Fig. 4

Le circuit ci-dessus, où coexistent des impédances qui réalisent la résonance des tensions à la pulsation Ω_0 et des résonances des courants aux pulsations ω_{-1}, ω_1, avec des impédances qui, au contraire, réalisent une résonance des courants à la pulsation Ω_0 et des résonances des tensions aux pulsations ω_{-1}, ω_1, est capable à réaliser un RR.

Si on accepte comme impédances des fonctions de circuit plus compliquées, on peut les synthétiser en tant que des ULP capables à réaliser des RR, à condition de préciser la position des autres singularités. Évidemment, le nombre des éléments dont est constitué un tel ULP dépasse celui minimum, de quatre (deux bobines et deux condensateurs).

Dans le cas où on se propose à synthétiser un ULP excité par un signal MA ayant la porteuse supprimée à savoir:

$$x(t) = \frac{1}{2} m X_m \sin\left(\omega_{-1} t + \phi_0 - \psi + \frac{\pi}{2}\right) + \frac{1}{2} m X_m \sin\left(\omega_1 t + \phi_0 + \psi - \frac{\pi}{2}\right), \tag{24}$$

capable à réaliser un RR, il est facile à observer que la fonction de réactance, $Z_{LC}(s)$, doit avoir deux pôles (ou deux zéros) pour les pulsations latérales ω_{-1}, ω_1, la singularité intermédiaire n'ayant aucune signification. Le signal réponse aura la même forme que l'excitation:

$$(25)\quad y(t) = \frac{1}{2}mY_m \sin\left(\omega_{-1}t + \phi_0 - \psi + \frac{\pi}{2}\right) + \frac{1}{2}mY_m \sin\left(\omega_1 t + \phi_0 + \psi - \frac{\pi}{2}\right),$$

avec une même valeur du degré de modulation de sorte que le RR sera, proprement-dit, un RSR. La synthèse de tels ULP sera effectuée dans le § **3**; il est facile a prévoire que ceux-ci auront (dans le cas où tant l'excitation que la réponse ont la porteuse supprimée) au moins quatre éléments réactifs – deux bobines et deux condensateurs.

Pour des ULP ayant des structures plus complexes que celle répresentée dans la Fig. 3 il est possible que, malgré que la fonction de réactance d'un tel ULP ait deux pôles où deux zéros, pour les pulsations latérales ω_{-1}, ω_1, les amplitudes des composantes de la réponse soient différentes:

$$(26)\quad y(t) = \frac{1}{2}mY'_m \sin\left(\omega_{-1}t + \phi_0 - \psi + \frac{\pi}{2}\right) + \frac{1}{2}mY''_m \sin\left(\omega_1 t + \phi_0 + \psi - \frac{\pi}{2}\right),$$

de sorte que pour réaliser le RSR il s'avère nécessaire que la condition supplémentaire

$$(27)\qquad Y'_m = Y''_m$$

soit satisfaite.

Le problème de la synthèse des ULP capables à réaliser le RR, dans le cas où l'excitation est de la forme (8), c'est-à-dire si le signal modulateur est périodique mais nonharmonique ou s'il est MF ou MP, s'avère beaucoup plus difficile a résoudre. Par exemple, la synthèse des ULP capables à réaliser un RR pour un nombre assez grand que possible des harmoniques du signal modulateur peut être effectuée, en principe, dans une manière analogue à celle qui correspond au cas où l'excitation est un signal MA de la forme (5). La différence réside dans le fait que le nombre minimum des éléments réactifs de l'ULP augmente simultanément avec celui des harmoniques du spectre du signal modulateur, en amplifiant le volume des calculs nécesaire à effectuer. Ainsi si n est le nombre des harmoniques et on poursuit à réaliser un RR pour chacune de celles-ci, le nombre minimum des composantes réactives de l'ULP synthétisé est de $4n$.

Il est intéressant à signaler que pour une excitation MF (ou MP) ayant l'indice de modulation suffisamment réduit ($\beta < 0,4$) on peut approximer le signal avec l'expression (13) qui est, d'un point de vue formel, similaire à celle d'un signal MA (v.(5)), de sorte que la synthèse d'un ULP qui réalise un RR se réalise par une même voie et mène à des résultats semblables à ceux représentés dans les Fig. 2*a* et 2*b*.

3. Synthèse des uniportes linéaires passifs capables à réaliser des régimes strictement résonants pour des excitations modulées en amplitude

Si on considère, d'abord, le cas simple d'une excitation MA ayant la forme (5), il est facile à observer qu'on peut réaliser un RSR seulement si les résonances individuelles, qui correspondent aux pulsations ω_{-1}, Ω_0, ω_1, sont d'un même type (des tensions ou des courants).

Une première variante de solutionner le problème ci-dessus est basée sur la synthèse d'une fonction de réactance du type:

$$Z_{LC}(s) = \frac{ks(s^2+\omega'^2)(s^2+\omega''^2)}{(s^2+\omega_{-1}^2)(s^2+\Omega_0^2)(s^2+\omega_1^2)}, \tag{28}$$

ayant le graphique représenté dans la Fig. 5, qui permet à réaliser trois résonances des courants pour les pulsations ω_{-1}, Ω_0, ω_1 et où $\omega' \in [\omega_{-1}, \Omega_0]$ et $\omega'' \in [\Omega_0, \omega_1]$. Si on utilise et dans ce cas la deuxième forme canonique de F o s t e r [3]:

$$Y_{LC}(s) = \frac{(s^2+\omega_{-1}^2)(s^2+\Omega_0^2)(s^2+\omega_1^2)}{ks(s^2+\omega'^2)(s^2+\omega''^2)} = \frac{s}{k} + \frac{k_0}{ks} + \frac{k_1 s}{s^2+\omega'^2} + \frac{k_2 s}{s^2+\omega''^2} \tag{29}$$

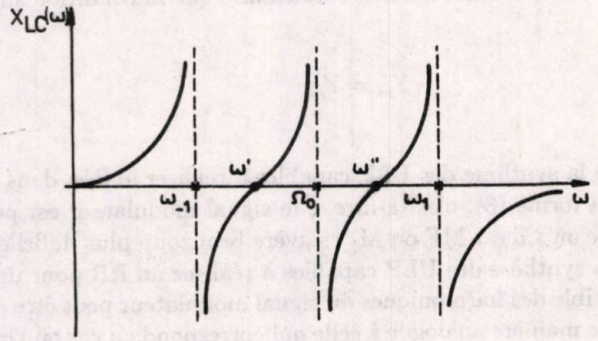

Fig. 5

on obtient

$$k_0 = \frac{\omega_{-1}^2 \Omega_0^2 \omega_1^2}{\omega'^2 \omega''^2}, \quad k_1 = \frac{(\omega_{-1}^2-\omega'^2)(\Omega_0^2-\omega'^2)(\omega_1^2-\omega'^2)}{-\omega'^2(\omega''^2-\omega'^2)},$$
$$k_2 = \frac{(\omega_{-1}^2-\omega''^2)(\Omega_0^2-\omega''^2)(\omega_1^2-\omega''^2)}{-\omega''^2(\omega'^2-\omega''^2)}; \tag{30}$$

le schéma correspondant est représenté dans la Fig. 6 *a*.

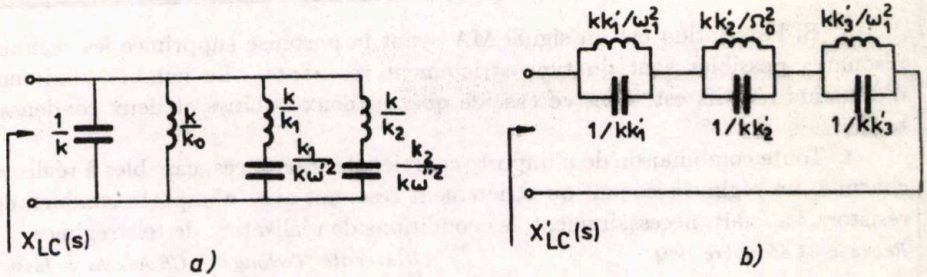

Fig. 6

Si on fait appel à la première forme canonique de F o s t e r [3] alors le schéma qui résulte par synthèse est celle représentée dans la Fig. 6 *b*, où

$$k_1' = \frac{(\omega'^2 - \omega_{-1}^2)(\omega''^2 - \omega_{-1}^2)}{(\Omega_0^2 - \omega_{-1}^2)(\omega_1^2 - \omega_{-1}^2)}, \quad k_2' = \frac{(\omega'^2 - \Omega_0^2)(\omega''^2 - \Omega_0^2)}{(\omega_{-1}^2 - \Omega_0^2)(\omega_1^2 - \Omega_0^2)},$$

(31)

$$k_3' = \frac{(\omega'^2 - \omega_1^2)(\omega''^2 - \omega_1^2)}{(\omega_{-1}^2 - \omega_1^2)(\Omega_0^2 - \omega_1^2)}.$$

Cette fois les trois circuits résonants sont toujours accordés sur les pulsations ω_{-1}, Ω_0, ω_1, mais ils réalisent des résonances des tensions; celles des courants sont obtenus aux pulsations ω', ω''.

Comme dans le cas des RR, on peut obtenir les RSR à l'aide des fonctions de circuit ayant les zéros et les pôles inversés par rapport à ceux de (28) et (29).

Toute combinaison de n'importe combien de telles réactances avec n'importe combien résistors satisfait obligatoirement les conditions nécessaires à réaliser un RSR.

Les ULP synthétisés par le procédé ci-dessus, avec le but de réaliser un RSR, contiennent un nombre minimum d'éléments réactifs – trois bobines et trois condensateurs. Le nombre de ces éléments diminue avec une bobine et un condensateur si l'excitation est un signal MA ayant la porteuse supprimée (v.(24)). En principe la synthèse d'un ULP en telles conditions est réalisée selon le modèle utilisé dans le § **2**, avec la précision que la pulsation Ω_0 peut avoir une valeur quelconque en satisfaisant seulement à la condition $\omega_1 < \Omega_0 < \omega_{-1}$.

4. Conclusions

1. Compte tenu des définitions des régimes résonants et de ceux strictement résonants d'un uniporte linéaire passif, en régime permanent, excité par un signal modulé en amplitude, on réalise la synthèse de tels uniports.

2. Le nombre minimum d'éléments réactifs d'un uniporte linéaire passif, en régime résonant, est de quatre (deux bobines et deux condensateurs) et en régime strictement résonant, de six (trois bobines et trois condensateurs) si l'excitation est un signal MA de la forme (1).

3. Si l'excitation est un signal MA ayant la porteuse supprimée les régimes résonants possibles sont du type strictement résonants. Le nombre minimum d'éléments réactifs est, dans ce cas, de quatre (deux bobines et deux condensateurs).

4. Toute combinaison de n'importe combien de réactances, capables à réaliser, chacune, un régime résonant ou strictement résonant avec n'importe combien de résistors, satisfait, nécessairement, les conditions de réalisation de tels régimes.

Reçue le 28 décembre 1994

Université Technique „Gh. Asachi", Jassy,
Chaire d'Électrotechnique,
Chaire d'Électronique
et
Chaire de Mécanique Théorique

BIBLIOGRAPHIE

1. Rosman H., Braier A., *Sur les régimes de résonance dans les circuits électriques excités par des signaux modulés en amplitude.* Rev. Roum. Sci. Techn., s. Électrot. et Énerg. (sous presse).
2. Mateescu Ad., *Analiza şi sinteza circuitelor electrice.* EDP, Buc., 1975, 73-94.
3. Weinberg L., *Network Analysis and Synthesis.* McGraw Hill, New York, 1962.

SINTEZA UNIPORŢILOR LINIARI PASIVI EXCITAŢI DE SEMNALE MODULATE ÎN AMPLITUDINE, ÎN REGIMURI DE REZONANŢĂ

(Rezumat)

Se realizează sinteza uniporţilor liniari pasivi, în regimuri permanente rezonante sau strict rezonante, atunci când excitaţia este un semnal MA. Dacă purtătoarea excitaţiei este suprimată, atunci singurele regimuri rezonante posibile sunt cele strict rezonante.

Orice combinaţie a unor reactanţe capabile să realizeze, fiecare în parte, un regim rezonant sau strict rezonant, cu oricâte rezistoare, satisface, în mod necesar, condiţiile realizării unor astfel de regimuri.

BULETINUL INSTITUTULUI POLITEHNIC DIN IAŞI
Tomul XLII (XLVI), Fasc. 1–2, 1996
Secţia III
ELECTROTEHNICĂ. ENERGETICĂ. ELECTRONICĂ

C.D. 621.392.5

SUR LES PARAMÈTRES CARACTÉRISTIQUES DES QUADRIPÔLES GÉNÉRAUX LINÉAIRES NONAUTONOMES, EN RÉGIME PERMANENT HARMONIQUE

PAR
DORIN BELAUS

En employant le procédé de représentation d'un quadripôle linéaire général par un quadripôle en sens restreint, dénommé primitif [3], on établit les expressions des impédances caractéristiques à l'alimentation directe et inverse et celles des exposants de transfert sur les impédances caractéristiques, en fonction de $\underline{Z}_3$, pour un quadripôle général linéaire nonautonome nonréciproque et réciproque.

1. Introduction

C'est bien connu le fait (par ex.[1]) que le quadripôle linéaire nonautonome en sens restreint (QLNSR – Fig.1 *a*) peut être considéré comme le cas particulier d'un quadripôle linéaire nonautonome général [2] (QLNG – Fig.1 *b*) si $\underline{Z}_3 \to \infty$.

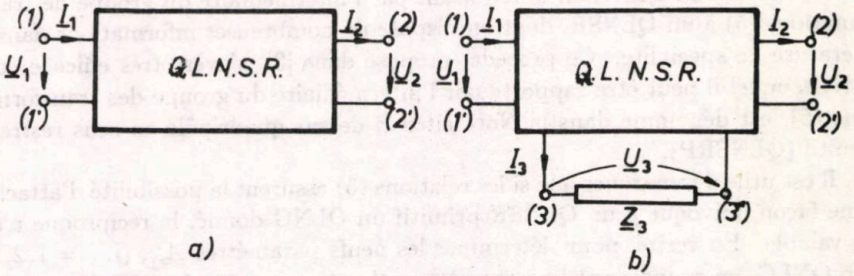

Fig. 1

De même, les équations d'un QLNSR, écrites, par exemple, à l'aide des paramètres fondamentaux:

$$(1) \qquad \begin{bmatrix} \underline{U}_1 \\ \underline{I}_1 \end{bmatrix} = \begin{bmatrix} \underline{A}_{11} & \underline{A}_{12} \\ \underline{A}_{21} & \underline{A}_{22} \end{bmatrix} \begin{bmatrix} \underline{U}_2 \\ \underline{I}_2 \end{bmatrix},$$

dérivent des équations, plus générales, d'un QLNG:

$$\begin{bmatrix} \underline{U}_1 \\ \underline{I}_1 \\ \underline{U}_3 \end{bmatrix} = \begin{bmatrix} \underline{A}_{11} & \underline{A}_{12} & \underline{A}_{13} \\ \underline{A}_{21} & \underline{A}_{22} & \underline{A}_{23} \\ \underline{A}_{31} & \underline{A}_{32} & \underline{A}_{33} \end{bmatrix} \begin{bmatrix} \underline{U}_2 \\ \underline{I}_2 \\ \underline{I}_3 \end{bmatrix}, \tag{2}$$

établies pour la première fois, en régime permanent harmonique, par S i g o r s k y [2].

En effet, si on tient compte que:

$$\underline{U}_3 = \underline{Z}_3 \underline{I}_3 \tag{3}$$

on peut éliminer des équations (2) et (3) les signaux $\underline{U}_3$ et $\underline{I}_3$, les équations (2) devenant:

$$\begin{bmatrix} \underline{U}_1 \\ \\ \underline{I}_1 \end{bmatrix} = \begin{bmatrix} \underline{A}'_{11} & \underline{A}'_{12} \\ \\ \underline{A}'_{21} & \underline{A}'_{22} \end{bmatrix} \begin{bmatrix} \underline{U}_2 \\ \\ \underline{I}_2 \end{bmatrix}, \tag{4}$$

où

$$\begin{cases} \underline{A}'_{11} = \underline{A}_{11} + \frac{\underline{A}_{13}\underline{A}_{31}}{\underline{Z}_3 - \underline{A}_{33}}, \quad \underline{A}'_{12} = \underline{A}_{12} + \frac{\underline{A}_{13}\underline{A}_{32}}{\underline{Z}_3 - \underline{A}_{33}}, \\ \underline{A}'_{21} = \underline{A}_{21} + \frac{\underline{A}_{23}\underline{A}_{31}}{\underline{Z}_3 - \underline{A}_{33}}, \quad \underline{A}'_{22} = \underline{A}_{22} + \frac{\underline{A}_{23}\underline{A}_{32}}{\underline{Z}_3 - \underline{A}_{33}}, \end{cases} \tag{5}$$

avec la restriction $\underline{Z}_3 \neq \underline{A}_{33}$, en géneral satisfaite par tout QLNG. On peut observer que les équations (4) sont de la forme (1), en offrant la possibilité d'étudier les propriétés d'un QLNG en le réduisant par l'intermédiaire du groupe de transformations (5) à un QLNSR, dont on dispose de nombreuses informations dans la littérature de specialité. Ce procédé, proposé dans [3], s'avère très efficace et le QLNG auquel il peut être rapporté par l'intermédiaire du groupe des transformations (5), est dénommé dans la Note citée ci-dessus quadripôle en sens réstreint primitif (QLNSRP).

Il est utile à remarquer que si les relations (5) assûrent la possibilité d'attacher d'une façon univoque à un QLNSR primitif un QLNG donné, la réciproque n'est pas valable. En verité, pour déterminer les neufs paramétres $\underline{A}_{ij}$, $(i,j = 1,2,3)$, d'un QNLG, en connaissant les paramètres $\underline{A}'_{ij}$, $(i,j = 1,2)$, du QNLSR primitif, les quatres relations (5) sont insuffisantes. Si le QLNG est réciproque, les relations qui assûrent le caractère réciproque du quadripôle [3], en nombre de deux:

$$\underline{A}_{11}\underline{A}_{22} - \underline{A}_{12}\underline{A}_{21} = 1, \quad |\underline{A}| = \det \|\underline{A}_{ij}\| = \underline{A}_{33}, \quad (i,j = 1,2,3), \tag{6}$$

ne sont pas suffisantes afin de compléter les relations (5) et de déterminer les paramètres $\underline{A}_{ij}$, $(i,j = 1,2,3)$. Par suite, si à un QLNGR correspond un seul

QNLSR primitif, bien déterminé, inversement, à un tel quadripôle primitif correspond une infinité de QLNGR, soit qu'ils sont réciproques on non.

Dans ce qui suit, en appliquant le procédé ci-dessus, on va étudier les paramètres caractéristiques d'un QLNG.

2. Les impédances caractéristiques

Pour obtenir les expressions des impédances caractéristiques d'un QLNG, on a en vue, d'abord, leurs expressions pour un QLNSR [1], par exemple du celui primitif:

$$(7)\qquad \begin{aligned} \underline{Z}_{c1} &= \frac{\underline{A}'_{11} - \underline{A}'_{22} \pm \sqrt{(\underline{A}'_{11} - \underline{A}'_{22})^2 + 4\underline{A}'_{12}\underline{A}'_{21}}}{2\underline{A}'_{21}}, \\ \underline{Z}_{c2} &= \frac{\underline{A}'_{22} - \underline{A}'_{11} \pm \sqrt{(\underline{A}'_{11} - \underline{A}'_{22})^2 + 4\underline{A}'_{12}\underline{A}'_{21}}}{2\underline{A}'_{21}}. \end{aligned}$$

Evidemment, le signe du radical est choisi de sorte que le quadripôle soit réalisable:

$$(8)\qquad \Re e(\underline{Z}_{c1}) \geq 0, \qquad \Re e(\underline{Z}_{c2}) \geq 0.$$

En substituant dans (6) les paramètres $\underline{A}'_{ij}$, $(i,j = 1,2)$, par les expressions (5) et tous calculs effectués on obtient:

$$(9)\qquad \begin{cases} \underline{Z}_{c1} = \frac{(\underline{A}_{11}-\underline{A}_{22})(\underline{Z}_3-\underline{A}_{33})+\underline{A}_{13}\underline{A}_{31}-\underline{A}_{23}\underline{A}_{32}}{2\underline{A}_{21}(\underline{Z}_3-\underline{A}_{33})+2\underline{A}_{23}\underline{A}_{31}} \pm \\ \pm\sqrt{\left[\frac{(\underline{A}_{11}-\underline{A}_{22})(\underline{Z}_3-\underline{A}_{33})+\underline{A}_{13}\underline{A}_{31}-\underline{A}_{23}\underline{A}_{32}}{2\underline{A}_{21}(\underline{Z}_3-\underline{A}_{33})+2\underline{A}_{23}\underline{A}_{31}}\right]^2 + \frac{\underline{A}_{12}(\underline{Z}_3-\underline{A}_{33})+\underline{A}_{13}\underline{A}_{32}}{\underline{A}_{21}(\underline{Z}_3-\underline{A}_{33})+\underline{A}_{23}\underline{A}_{31}}}, \\ \underline{Z}_{c2} = \frac{(\underline{A}_{22}-\underline{A}_{11})(\underline{Z}_3-\underline{A}_{33})+\underline{A}_{13}\underline{A}_{31}-\underline{A}_{23}\underline{A}_{32}}{2\underline{A}_{21}(\underline{Z}_3-\underline{A}_{33})+2\underline{A}_{23}\underline{A}_{31}} \pm \\ \pm\sqrt{\left[\frac{(\underline{A}_{22}-\underline{A}_{11})(\underline{Z}_3-\underline{A}_{33})+\underline{A}_{13}\underline{A}_{31}-\underline{A}_{23}\underline{A}_{32}}{2\underline{A}_{21}(\underline{Z}_3-\underline{A}_{33})+2\underline{A}_{23}\underline{A}_{31}}\right]^2 + \frac{\underline{A}_{12}(\underline{Z}_3-\underline{A}_{33})+\underline{A}_{13}\underline{A}_{31}}{\underline{A}_{21}(\underline{Z}_3-\underline{A}_{33})+\underline{A}_{23}\underline{A}_{31}}}. \end{cases}$$

Il est utile de faire certaines observations à savoir:

1° Les impédances caractéristiques $\underline{Z}_{c1}$, $\underline{Z}_{c2}$, d'un QLNG sont fonctions de l'impédance $\underline{Z}_3$.

2° Lorsque le quadripôle est réciproque il faut avoir en vue que leurs paramètres fondamentaux, $\underline{A}_{ij}$, $(i,j = 1,2,3)$, satisfont les relations (6) (v.[3]).

Par suite, on peut écrire les relations (9) sous la forme concentrée:

$$(10)\qquad \begin{cases} \underline{Z}_{c1} = \frac{\underline{a}\underline{Z}_3+\underline{b}}{\underline{c}\underline{Z}_3+\underline{d}} \pm \sqrt{\left(\frac{\underline{a}\underline{Z}_3+\underline{b}}{\underline{c}\underline{Z}_3+\underline{d}}\right)^2 + 2\frac{\underline{e}\underline{Z}_3+\underline{f}}{\underline{c}\underline{Z}_3+\underline{d}}}, \\ \underline{Z}_{c2} = -\frac{\underline{a}\underline{Z}_3+\underline{b}}{\underline{c}\underline{Z}_3+\underline{d}} \pm \sqrt{\left(\frac{\underline{a}\underline{Z}_3+\underline{b}}{\underline{c}\underline{Z}_3+\underline{d}}\right)^2 + 2\frac{\underline{e}\underline{Z}_3+\underline{f}}{\underline{c}\underline{Z}_3+\underline{d}}}, \end{cases}$$

où:

$$(11)\qquad \begin{cases} \underline{a} = \underline{A}_{11} - \underline{A}_{22}, \quad \underline{b} = -\underline{A}_{33}(\underline{A}_{11} - \underline{A}_{22}) + \underline{A}_{13}\underline{A}_{31} - \underline{A}_{23}\underline{A}_{32}, \\ \underline{c} = 2\underline{A}_{21}, \quad \underline{d} = -2(\underline{A}_{22}\underline{A}_{33} - \underline{A}_{23}\underline{A}_{31}), \quad \underline{e} = \underline{A}_{12}, \\ \underline{f} = -\underline{A}_{12}\underline{A}_{33} + \underline{A}_{23}\underline{A}_{32}. \end{cases}$$

Compte tenu que $\Re e(\underline{Z}_3) \geq 0$, il résulte que les impédances caractéristiques $\underline{Z}_{c1}$, $\underline{Z}_{c2}$ d'un QLNG, peuvent avoir des valeurs seulement sur la frontière et dans l'intérieur d'un certain domaine. Dans une Note subséquente on s'occupera de la détermination exacte de ce domaine.

Si on note par $\underline{Z}'_{c1}$, $\underline{Z}''_{c1}$ les impédances caractéristiques, pour le cas ou le quadripôle est alimenté en sens direct et par $\underline{Z}'_{c2}$, $\underline{Z}''_{c2}$ – celles correspondant à l'alimentation inverse du quadripôle, on peut écrire les relations:

$$(12)\qquad \underline{Z}'_{c1} + \underline{Z}''_{c1} = 2\frac{\underline{a}Z_3 + \underline{b}}{\underline{c}Z_3 + \underline{d}}, \quad \underline{Z}'_{c1}\underline{Z}''_{c1} = -2\frac{\underline{e}Z_3 + \underline{f}}{\underline{c}Z_3 + \underline{d}},$$

respectivement

$$(13)\qquad \underline{Z}'_{c2} + \underline{Z}''_{c2} = -2\frac{\underline{a}Z_3 + \underline{b}}{\underline{c}Z_3 + \underline{d}}, \quad \underline{Z}'_{c2}\underline{Z}''_{c2} = -2\frac{\underline{e}Z_3 + \underline{f}}{\underline{c}Z_3 + \underline{d}},$$

de tel façon que:

$$(14)\qquad \underline{Z}'_{c1} + \underline{Z}''_{c1} = -(\underline{Z}'_{c2} + \underline{Z}''_{c2}) \quad \text{et} \quad \underline{Z}'_{c1}\underline{Z}''_{c1} = \underline{Z}'_{c2}\underline{Z}''_{c2}.$$

Evidemment, on peut écrire les expressions des impédances caractéristiques d'un QLNG, facilement, en fonction des autres paramétres du quadripôle (les éléments des matrices $[\underline{Y}]$, $[\underline{Z}]$, etc.).

3. Les exposants de transfert sur les impédances caractéristiques

On a en vue qu'on peut déterminer les exposants du QLNSR primitif à l'aide des relations [1]:

$$(15)\qquad \begin{aligned} \underline{g}_{1c} &= \ln \frac{\underline{A}'_{11} + \underline{A}'_{22} \pm \sqrt{(\underline{A}'_{11} - \underline{A}'_{22})^2 + 4\underline{A}'_{12}\underline{A}'_{21}}}{2}, \\ \underline{g}_{2c} &= \ln \frac{\underline{A}'_{11} + \underline{A}'_{22} \pm \sqrt{(\underline{A}'_{11} - \underline{A}'_{22})^2 + 4\underline{A}'_{12}\underline{A}'_{21}}}{2|\underline{A}'|}, \end{aligned}$$

où $|\underline{A}'| = \det \|\underline{A}'_{ij}\|$, $(i, j = 1, 2)$. En tenant compte de (5) il résulte:

$$(16)\qquad \begin{aligned} \underline{g}_{1c} = \ln \Big[\frac{1}{2(\underline{Z}_3 - \underline{A}_{33})} \Big(&(\underline{A}_{11} + \underline{A}_{22})(\underline{Z}_3 - \underline{A}_{33}) + \underline{A}_{13}\underline{A}_{31} + \underline{A}_{23}\underline{A}_{32} \pm \\ &\pm \{[(\underline{A}_{11} - \underline{A}_{22})^2 + 4\underline{A}_{12}\underline{A}_{21}](\underline{Z}_3 - \underline{A}_{33})^2 + \\ &+ 2[(\underline{A}_{11} - \underline{A}_{22})(\underline{A}_{13}\underline{A}_{31} - \underline{A}_{23}\underline{A}_{32}) + \\ &+ 2(\underline{A}_{12}\underline{A}_{23}\underline{A}_{31} + \underline{A}_{13}\underline{A}_{21}\underline{A}_{32})](\underline{Z}_3 - \underline{A}_{33}) + (\underline{A}_{13}\underline{A}_{31} + \underline{A}_{23}\underline{A}_{32})^2\}^{1/2} \Big) \Big], \end{aligned}$$

respectivement:

$$\underline{g}_{2c} = \ln\left[\frac{1}{2[(\underline{A}_{11}\underline{A}_{22} - \underline{A}_{12}\underline{A}_{21})\underline{Z}_3 - |\underline{A}|]}\Big((\underline{A}_{11} + \underline{A}_{22})(\underline{Z}_3 - \underline{A}_{33}) + \right.$$
$$+\underline{A}_{13}\underline{A}_{31} + \underline{A}_{23}\underline{A}_{32} \pm \{[(\underline{A}_{11} - \underline{A}_{22})^2 + 4\underline{A}_{12}\underline{A}_{21}](\underline{Z}_3 - \underline{A}_{33})^2 + \tag{17}$$
$$+2[(\underline{A}_{11} - \underline{A}_{22})(\underline{A}_{13}\underline{A}_{31} - \underline{A}_{23}\underline{A}_{32}) + 2(\underline{A}_{12}\underline{A}_{23}\underline{A}_{31} + \underline{A}_{13}\underline{A}_{21}\underline{A}_{32})]\times$$
$$\left.\times(\underline{Z}_3 - \underline{A}_{33}) + (\underline{A}_{13}\underline{A}_{31} + \underline{A}_{23}\underline{A}_{32})^2\}^{1/2}\Big)\right].$$

En introduisant les notations:

$$\underline{A}_{11} + \underline{A}_{22} = \underline{m}, \quad -\underline{A}_{33}(\underline{A}_{11} + \underline{A}_{22}) + \underline{A}_{23}\underline{A}_{32} + \underline{A}_{13}\underline{A}_{31} = \underline{n},$$
$$(\underline{A}_{11} - \underline{A}_{22})^2 + 4\underline{A}_{12}\underline{A}_{21} = \underline{p}, \tag{18}$$
$$2[(\underline{A}_{11} - \underline{A}_{22})(\underline{A}_{13}\underline{A}_{31} - \underline{A}_{23}\underline{A}_{32}) + 2(\underline{A}_{12}\underline{A}_{23}\underline{A}_{31} + \underline{A}_{13}\underline{A}_{21}\underline{A}_{32})] = \underline{q},$$
$$\underline{A}_{13}\underline{A}_{31} + \underline{A}_{23}\underline{A}_{32} = \underline{r}, \quad \underline{A}_{11}\underline{A}_{22} - \underline{A}_{12}\underline{A}_{21} = |\underline{\tilde{A}}|,$$

on peut écrire les expressions (16) et (17) sous la forme:

(19)

$$\underline{g}_{1c} = \ln\left(\frac{1}{2(\underline{Z}_3 - \underline{A}_{33})}\left\{\underline{m}\underline{Z}_3 + \underline{n} \pm \left[\underline{p}(\underline{Z}_3 - \underline{A}_{33})^2 + 2\underline{q}(\underline{Z}_3 - \underline{A}_{33}) + \underline{r}^2\right]^{1/2}\right\}\right),$$

$$\underline{g}_{2c} = \ln\left(\frac{1}{2|\underline{\tilde{A}}|\underline{Z}_3 - |\underline{A}|}\left\{\underline{m}\underline{Z}_3 + \underline{n} \pm \left[\underline{p}(\underline{Z}_3 - \underline{A}_{33})^2 + 2\underline{q}(\underline{Z}_3 - \underline{A}_{33}) + \underline{r}^2\right]^{1/2}\right\}\right).$$

On constate aisément que les exposants de transfert sur les impédances caractéristiques d'un QLNG sont fonctions de l'impédance $\underline{Z}_3$ et puisque $\Re e(\underline{Z}_3) \geq 0$, ces paramètres de transfert peuvent prendre des valeurs seulement sur la frontière et dans l'intérieur de certains domaines. On se propose à les déterminer dans une Note ultérieure.

De même, on peut observer, que si on note par $\underline{g}'_{1c}$, $\underline{g}''_{1c}$ les deux exposants de transfert sur les impédances caractéristiques, lorsque le quadripôle est alimenté en sens direct et par $\underline{g}'_{2c}$, $\underline{g}''_{2c}$ les exposants de transfert sur les impédances caractéristiques à l'alimentation inverse, résultent les relations:

$$e^{\underline{g}'_{1c}}e^{\underline{g}''_{1c}} = \frac{1}{4}, \quad e^{\underline{g}'_{2c}}e^{\underline{g}''_{2c}} = \frac{1}{4|\underline{\tilde{A}}|^2}. \tag{20}$$

En même temps, si l'on observe que [1]:

$$\frac{1}{2}(e^{\underline{g}_{1c}} + e^{-\underline{g}_{2c}}) = \frac{\underline{A}'_{11} + \underline{A}'_{22}}{2}, \tag{21}$$

conformément aux relations (5) il résulte que dans le cas d'un QLNG:

$$\frac{1}{2}(e^{\underline{g}_{1c}} + e^{-\underline{g}_{2c}}) = \frac{1}{2}\left(\underline{A}_{11} + \underline{A}_{22} + \frac{\underline{A}_{13}\underline{A}_{31} + \underline{A}_{23}\underline{A}_{32}}{\underline{Z}_3 - \underline{A}_{33}}\right). \tag{22}$$

On connaît (par ex. [1]), que l'exposant de transfert peut être défini sur l'impédance caractéristique moyenne:

$$\underline{g}_c = \frac{1}{2}(\underline{g}_{1c} + \underline{g}_{2c}) \tag{23}$$

de tel façon que:

$$\underline{g}_c = \operatorname{arg\,ch} \frac{\underline{A}'_{11} + \underline{A}'_{22}}{2\sqrt{|\underline{A}'|}}, \tag{24}$$

si on se réfère au quadripôle primitif. En passant aux paramètres $\underline{A}_{ij}$, $(i, j = 1, 2, 3)$, du QLNG il résulte l'expression:

$$\underline{g}_c = \operatorname{arg\,ch} \frac{(\underline{A}_{11} + \underline{A}_{22})(\underline{Z}_3 - \underline{A}_{33}) + \underline{A}_{13}\underline{A}_{31} + \underline{A}_{23}\underline{A}_{32}}{(\underline{A}_{11}\underline{A}_{22} - \underline{A}_{12}\underline{A}_{21})\underline{Z}_3 - |\underline{A}|}. \tag{25}$$

Dans le cas où le quadripôle est réciproque, en tenant compte de (6) l'expression (25) devient:

$$\underline{g}_c = \operatorname{arg\,ch}\left(\underline{A}_{11} + \underline{A}_{22} - \frac{\underline{A}_{13}\underline{A}_{31} + \underline{A}_{23}\underline{A}_{32}}{\underline{Z}_3 - \underline{A}_{33}}\right), \tag{26}$$

ce qui est évident, si on a en vue (22).

4. Conclusions

En employant le procedé de [3], d'attacher à un quadripôle linéaire général nonautonome, un quadripôle en sens restreint, dénommé primitif, on établit les expressions des paramètres caractéristiques (impédances caractéristique et exposants de transfert sur les impédances caractéristiques) d'un quadripôle général.

Reçue le 6 novembre 1995

Université Technique „Gh. Asachi", Jassy,
Chaire d'Électrotechnique
Générale et Machines éléctriques

BIBLIOGRAPHIE

1. Şora C., *Cuadripolul electric.* Ed. Tehnică, Bucureşti, 1964.
2. Sigorsky V.P., *Théorie générale des quadripôles* (en russe). Ed. Acad. Sci. Ukraïne, Kiev, 1955.
3. Rosman H., *Sur les conditions de réciprocité et de symétrie d'un quadripôle généralisé nonautonome en régime permanent harmonique.* Bul. Inst. polit., Iaşi, **XL (XLIV)**, *1-4*, s.III, 24-30 (1994).

ASUPRA PARAMETRILOR CARACTERISTICI AI CUADRIPOLILOR GENERALI LINIARI NEAUTONOMI ÎN REGIM PERMANENT ARMONIC

(Rezumat)

Pe baza procedeului de reprezentare al unui cuadripol liniar general printr-un cuadripol în sens restrâns primitiv [3] se stabilesc expresiile impedanţelor caracteristice la alimentarea cuadripolului în sens direct şi invers, precum şi expresiile exponenţilor de transfer pe impedanţele caracteristice, în funcţie de $\underline{Z}_3$, pentru cuadripolul general liniar neautonom, nereciproc şi reciproc.

BULETINUL INSTITUTULUI POLITEHNIC DIN !AŞI
Tomul XLII (XLVI), Fasc. 1–2, 1996
Secţia III
ELECTROTEHNICĂ. ENERGETICĂ. ELECTRONICĂ

C.D. 621-523

RÉSEAU DE NEURONES POUR LA COMMANDE D'UN BRAS ROBOT

PAR
IUSTINA ZAHARIA

On présente une application des réseaux de neurones pour faire exécuter des mouvements à un bras robot. Le réseau utilisé est un réseau moulticouche qui réalise l'association entre chaque couple (x, y) du plan de travail du robot et les angles des divers éléments du bras du robot. Une fois le réseau entraîné, on peut choisir n'importe quel point du plan du robot et le réseau calcule instantanément les angles nécessaires pour faire bouger le bras vers ce point.

1. Introduction

Ayant comme modèle le cerveau humain on a imaginé des réseaux dont les principaux éléments ressemblent aux neurones. La fonction réalisée par un tel réseau dépend des connections réalisées entre ses élements. En général, les éléments composants d'un réseau fonctionnent en parallèle.

Les réseaux de neurones sont entraînées pour réaliser des taches complexes dans divers domaines à savoir: reconnaissance des formes, identification, classification, language, prognose et commande des systèmes. De nos jours les réseaux de neurones sont capables à resoudre les problèmes très difficiles pour les ordinateurs conventionnels ou pour les êtres humains.

Le réseau de neurones, proposé dans ce qui suit, réalise la commande d'un robot en utilisant l'association des modèles. Le réseau doit calculer les valeurs des différents paramètres du bras robot pour le faire exécuter des mouvements.

2. Architecture du réseau

Le réseau utilisé est associatif, moulticouches. La couche d'entrée a R entrées, la couche cachée a S_1 neurones et celle de sortie – S_2 neurones.

Les neurones des divers couches sont connectés de tel façon que chaque neurone soit connecté avec tous ceux de la couche suivante. La fonction des neurones d'entrée et de la couche cachée est logsigmoïde ou tansigmoïde et la fonction des

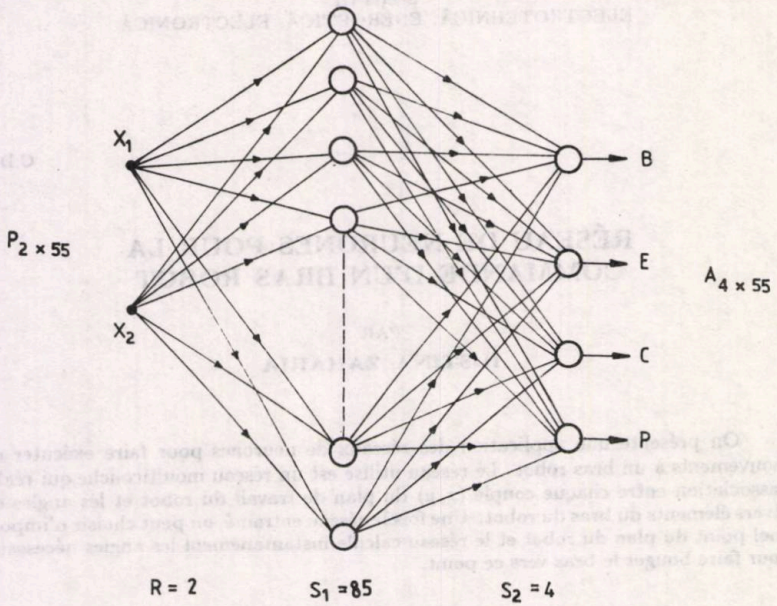

Fig. 1.– L'architecture d'un réseau avec une couche cachée.

neurones de sortie est linéaire.

On applique aux entrées une matrice P ayant les dimensions $R \times Q$ où Q représente le nombre des vecteurs d'entrée $R \times 1$ appliquées en même temps.

Le nombre des neurones de la couche d'entrée correspond aux variables d'entrée choisies – deux variables pour les coordonnées x, y du plan du travail du robot.

Le nombre de neurones de la couche de sortie correspond au variable de sortie choisi pour faire bouger le bras du robot: la base, l'épaule, le coude et le poignet.

3. Base d'apprentissage

Connaissant les longueurs des éléments du bras du robot (Fig. 2):

$$L_1 = 110 \text{ mm}, \quad L_2 = 120 \text{ mm}, \quad L_3 = 155 \text{ mm}, \quad L_4 = 83 \text{ mm},$$

on a calculé premièrement le domaine d'action pour le robot, c'est-à-dire les rayons des cercles maximum et minimum décrites par le bras:

$$R_{\max} = 274 \text{ mm}; \quad R_{\min} = 132 \text{ mm}.$$

En utilisant nombre de procédés fournis par la géometrie classique on a calculé les expressions des angles [4] pour réaliser les mouvements du bras robot:

$$\varphi = \operatorname{arctg} \frac{D}{Z}, \quad \text{où} \quad D = L_1 - L_4,$$

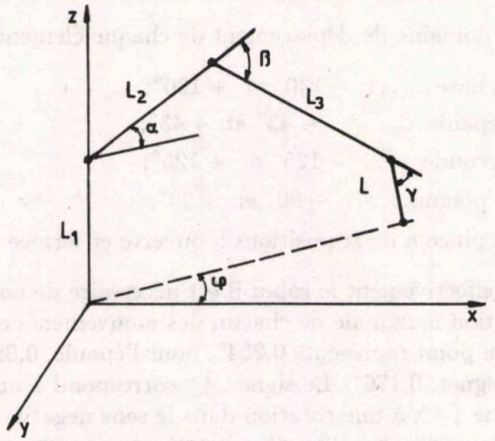

Fig. 2.– Les éléments du bras du robot.

$$\alpha = \arccos \frac{L_3^2 - D^2 - Z^2 - L_2^2}{-2L_2\sqrt{D^2 + Z^2}} - \varphi,$$

$$\beta = \arccos \frac{D^2 + Z^2 - L_3^2 - L_2^2}{-2L_2L_3} - \pi,$$

$$\gamma = \arccos \frac{L_2^2 - D^2Z - Z^2 - L_3^2}{-2L_3\sqrt{D^2 + Z^2}} + \varphi - \frac{\pi}{2}.$$

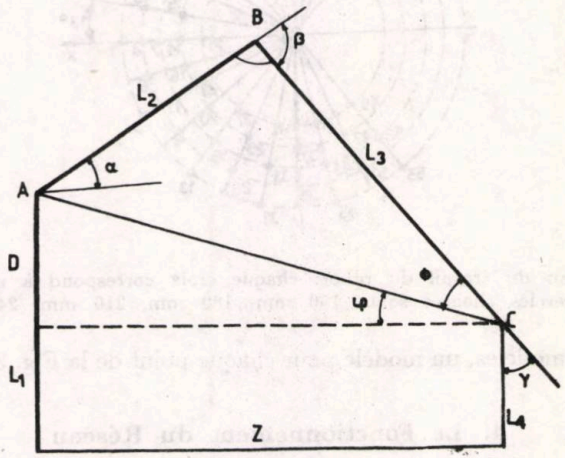

Fig. 3.– La géometrie des éléments du bras du robot.

On a obtenu le domaine de déplacement de chaque élément:

la base..... $-130°$ et $+130°$;
l'épaule..... $-43°$ et $+43°$;
le coude..... $-125°$ et $+125°$;
le poignet..... $-90°$ et $+90°$;
la pince a deux positions : ouverte et fermée.

Pour actionner effectivement le robot il est nécessaire de normaliser les angles en points. La résolution maximale de chacun des mouvements est de 1 024 points. Donc pour la base un point représente 0,254°, pour l'épaule, 0,084°, pour le coude, 0,245° et pour le poignet, 0,176°. Le signe „+" correspond à une rotation dans le sens positif et le signe „−", à une rotation dans le sens negatif.

Pour adapter les valeurs de la base d'apprentissage avec les sorties des neurones on a multiplié tous les valeurs avec 10^{-3}.

Par exemple, si on suppose que le bras du robot doit arriver dans le point de coordonnées $x = 270$ m et $y = 0$ (Fig. 4) alors la base a $\varphi = 0$, l'épaule a $\alpha = 17°$, le coude a $\beta = -11,27°$ et le poignet, $\gamma = 76°$. Le modèle devient, en points:

$$B = +000; \quad E = -203; \quad C = -046; \quad P = -432.$$

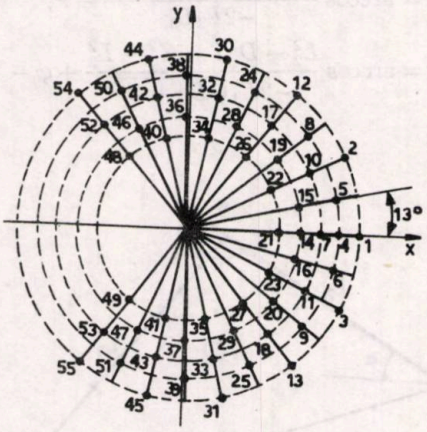

Fig. 4.– Le plan du travail du robot; chaque croix correspond à un couple (x, y); les rayons des cercles choisies sont: 150 mm, 180 mm, 210 mm, 240 mm, 270 mm.

On a utilisé 55 modèles, un modèle pour chaque point de la Fig. 3 (Annexe 1).

4. Le Fonctionnement du Réseau

Un seul neurone réalise deux fonctions (Fig. 5): a) une somme pondérée de tous les entrées; b) une transformation de celle-ci par une fonction dite „de compression".

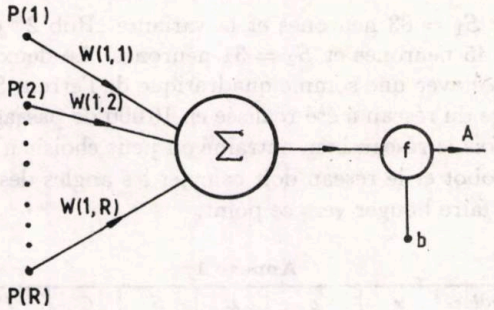

Fig. 5.- La structure d'un neurone.

À cause de leurs interconnections chaque neurone a comme entrée la somme des sorties des neurones de la couche inférieure pondérée par des coefficients denommées *poids synaptiques*, $W(i,j)$, où i représente le numéro du neurone; j – le numéro de l'entrée.

La fonction de compression transforme cette somme en lui donnant une valeur située entre 1 et –1. Cette fonction peut être symmétrique, ce qui correspond à $b = 0$ ou déplacée, ce qui correspond à $b \neq 0$. Donc, le déplacement b est choisi d'habitude $\neq 0$ pour en réaliser un degré de liberté supplémentaire.

La sortie du neurone, calculée à l'aide de la fonction de compression, f, a l'expression:

$$A = f(WP + b),$$

où P est la matrice d'entrée, W – la matrice des poids synaptiques et b – la matrice des déplacements.

On commence par l'apprentissage du réseau en lui présentant des modèles. Un modèle est constitué par un ensemble entrées–sorties désirées. À chaque présentation d'un modèle on calcule, successivement, les sorties des couches du réseau et on compare les sorties du réseau avec celles désirées (la matrice T). Si l'écart dépasse une valeur imposée on modifie les poids synaptiques suivant un algorithme particulier. Cet algorithme a le rôle de minimiser l'erreur définie par la différence entre la sortie calculée et celle désirée. On calcule le gradient de l'erreur dans l'espace des poids synaptiques, on modifie chaque poids d'un quantité proportionnelle à la dérivée partielle correspondante de la fonction erreur, en commençant par la couche de sortie et en finissant par celle d'entrée. La loi d'apprentissage présentée ci-dessus est celle bien connue de retro-propagation.

5. Résultats

À l'aide du logiciel „MATLAB" et de la boîte à outils „Réseaux de neurons" on a imaginé un réseau de neurones moulticouche qui réalise l'association entre chaque couple (x, y) du plan du travail du robot et les angles exprimées en points.

Le réseau de neurones a deux variantes: la variante „Rob 1" qui a une seule

couche cachée avec $S_1 = 83$ neurones et la variante „Rob 2" qui a deux couches cachées avec $S_1 = 45$ neurones et $S_2 = 31$ neurones. Le deux variantes réalisent l'association imposée avec une somme quadratique de l'erreur SSE< 0.1.

L'apprentissage du réseau a été réalisée en 10 000 de passages et il a duré plus d'une heure. Une fois le réseau bien entraîné on peut choisir n'importe quel point (x, y) du plan du robot et le réseau doit calculer les angles des éléments du robot nécessaires pour le faire bouger vers ce point.

Annexe 1

Modèles	x	y	B base	E épaule	C coude	P poignet
1	0,27	0	+,000	−,203	−,046	−,432
2	0,2427	−0,1185	−,102	−,203	−,046	−,432
3	0,2427	+0,1185	+,102	−,203	−,046	−,432
4	0,24	0	+,000	+,053	−,205	−,334
5	0,2338	−0,054	−,051	+,053	−,205	−,334
6	0,2338	+0,054	+,051	+,053	−,205	−,334
7	0,21	0	+,000	+,200	−,296	−,277
8	0,1887	−0,0921	−,102	+,200	−,296	−,277
9	0,1887	+0,0921	+,102	+,200	−,296	−,277
10	0,1865	−0,151	−,153	+,053	−,205	−,334
11	0,1865	+0,151	+,153	+,053	−,205	−,334
12	0,18	0	+,000	+,320	−,370	−,231
13	0,1754	−0,0405	−,051	+,320	−,370	−,231
14	0,1754	+0,0405	+,051	+,320	−,370	−,321
15	0,1662	−0,2128	−,204	−,203	−,046	−,432
16	0,1662	+0,2128	+,204	−,203	−,046	−,432
17	0,15	0	+,000	+,428	−,435	−,192
18	0,1399	−0,1133	−,153	+,320	−,370	−,231
19	0,1399	+0,1133	+,153	+,320	−,370	−,231
20	0,1348	−0,0659	−,102	+,428	−,435	−,192
21	0,1348	+0,0658	+,102	+,428	−,435	−,192
22	0,1293	−0,1655	−,204	+,200	−,296	−,277
23	0,1293	+0,1655	+,204	+,200	−,296	−,277
24	0,1014	−0,2175	−,256	+,053	−,205	−,334
25	0,1014	−0,2175	+,256	+,053	−,205	−,334
26	0,0923	+0,1182	−,204	+,428	−,435	−,192
27	0,0923	+0,1182	+,204	+,428	−,435	−,192
28	0,076	−0,1631	−,256	+,320	−,370	−,231
29	0,076	+0,1631	+,256	+,320	−,370	−,231
30	0,0561	−0,2641	−,307	−,203	−,046	−,432
31	0,0561	+0,2641	+,307	−,203	−,046	−,432
32	0,0437	−0,2054	−,307	+,200	−,296	−,277

Modèles	x	y	B base	E épaule	C coude	P poignet
33	0,0437	+0,2054	+,307	+,200	−,296	−,277
34	0,0312	0,1467	−,307	+,428	−,435	−,192
35	0,0312	+0,1467	+,307	+,428	−,435	−,192
36	−0,0031	−0,18	−,358	+,320	−,370	−,231
37	−0,0031	+0,18	+,358	+,320	−,370	−,231
38	−0,0042	−0,2399	−,358	+,053	−,205	−,334
39	−0,0042	+0,2399	+,358	+,053	−,205	−,334
40	−0,0363	−0,1455	−,409	+,428	−,435	−,192
41	−0,0363	+0,1455	+,409	+,428	−,435	−,192
42	−0,0508	−0,2038	−,409	+,200	−,296	−,277
43	−0,0508	+0,2038	+,409	+,200	−,296	−,277
44	−0,058	−0,2329	−,409	+,053	−,205	−,334
45	−0,058	+0,2329	+,409	+,053	−,205	−,334
46	−0,0817	−0,1604	−,460	+,230	−,370	−,231
47	−0,0817	+0,1604	+,460	+,230	−,370	−,231
48	−0,0964	−0,1149	−,511	+,428	−,435	−,192
49	−0,0964	+0,1149	+,511	+,428	−,435	−,192
50	−0,1089	−0,2139	−,460	+,053	−,205	−,334
51	−0,1089	+0,2139	+,460	−,053	−,205	−,334
52	−0,135	−0,1609	−,511	+,200	−,296	−,277
53	−0,135	+0,1609	+,511	+,200	−,296	−,277
54	−0,1543	−0,1838	−,511	+,053	−,205	−,334
55	−0,1543	+0,1838	+,511	+,053	−,205	−,334

Reçue le 1 mars 1995

Université Technique „Gh. Asachi", Jassy,
Chaire d'Électrotechnique

BIBLIOGRAPHIE

1. Davalo E., Naïm P., *Des réseaux de neurones.* Ed. Eyrolles, Paris, 1990.
2. Bourret T., Reggia R., Samuelides I., *Réseaux neuronaux.* Ed. Teknea, Paris, 1991.
3. Weisbuch G., *Dynamique des systèmes complexes.* Ed. Eyrolles, Paris, 1990.
4. Berrue F., Reveille T., *Commande d'un bras robot.* Rapport no.*1* (1994).
5. Faibish S., Fruchtman G., Dancygier O., *Neural Reflexive Control of a Mobile Robot.* Proc. of the 1992 IEEE Internat. Symp. on Intelligent Control, 1992, 144-146.

REŢEA NEURONALĂ PENTRU COMANDA UNUI BRAŢ ROBOT

(Rezumat)

S-a urmărit realizarea unei reţele neuronale capabile să poată comanda mişcările unui braţ robot. Reţeaua trebuie să calculeze valorile parametrilor (unghiurile) celor patru elemente ale braţului: bază, umăr, cot şi pumn pentru ca aceasta să poată efectua mişcările impuse.

Reţeaua are ca principiu de bază asocierea între perechile de valori (x, y) din planul de lucru al robotului şi unghiurile normalizate exprimate în puncte ale celor patru elemente ce alcătuiesc braţul robotului. Odată reţeaua învăţată şi antrenată prin trecerea succesivă a 55 modele, ea va furniza soluţii corecte pentru orice pereche (x, y) aleasă din planul de lucru.

Reţeaua neuronală realizată are două variante: cu un strat intermediar şi cu două straturi intermediare, având ca regulă de antrenare propagarea inversă.

BULETINUL INSTITUTULUI POLITEHNIC DIN IAŞI
Tomul XLII (XLVI), Fasc. 1–2, 1996
Secţia III
ELECTROTEHNICĂ. ENERGETICĂ. ELECTRONICĂ

D.C. 621.391.51

SOME APPLICATIONS OF ENTROPY OF SOURCES WITH PREFERENCES

BY

VALERIU MUNTEANU and DANIELA TĂRNICERIU

A new characteristic of the information sources with preferences is presented. Based on this characteristic, the absolute maximum entropy is computed. Also, a coding method of sources described only by message utilities for noiseless channel is presented.

1. Introduction

The S h a n n o n's entropy [6] is a measure of both the uncertainty and the information supplied by a probabilistic experiment. Underlining the importance of S h a n n o n's entropy, it is necessary to noticing at the same time that this formula gives only the measure of information as a function of the probabilities with which various events occur. But there are many fields dealing with random events where it is necessary to take into account both these probabilities and some qualitative characteristics of events. A criterion for a qualitative differentiation of the possible events of a given experiment is represented by the relevance, the significance or the utility of the information they carry with respect to a goal, with respect to a qualitative characteristic. The occurrence of an event removes a double uncertainty: a quantitative one, related to the probabilities with which it occurs and a qualitative one, related to a given qualitative characteristic or, generally, to qualitative weights.

We shall suppose that these qualitative weights are nonnegative, finite, real numbers, as the usual weights in physics or as the utilities in decision theory. Also, if one event is more relevant, more significant and more useful (with respect to a given goal or from a given qualitative point of view) than another one, the weight of the first event will be greater than that of the second one.

The entropy, as a measure of uncertainty or of information supplied by a probabilistic experiment depending both on the probabilities of events and of the qualitative weights of the possible event, was denoted as *weighted-entropy* in [3], [4], or *entropy with preferences* in [1], [2].

Let us consider a information source with preferences characterized by the distribution:

$$S: \begin{pmatrix} s_1 & s_2 & \dots & s_N \\ p_1 & p_2 & \dots & p_N \\ u_1 & u_2 & \dots & u_N \end{pmatrix}, \tag{1}$$

with

$$\sum_{i=1}^{N} p_i = 1, \quad 0 < p_i \leq 1, \quad (i = 1, 2, ..., N), \tag{2}$$

$$\sum_{i=1}^{N} u_i = K = \text{const.}, \quad u_i \in \mathbb{R}_+, \quad (i = 1, 2, ..., N), \tag{3}$$

where p_i are the probabilities of the delivered source messages or events s_i and u_i – the qualitative weights of the messages which characterize either their utility, or their importance, or their relevance or significance.

In [1] a relation for the calculus of the entropy of an information source with preferences has been deduced:

$$H(S) = -\sum_{i=1}^{N} p_i \log_2 p_i + \sum_{i=1}^{N} p_i u_i. \tag{4}$$

The maximum value of the above entropy is obtained when [1]:

$$p_i = \frac{2^{u_i}}{\sum_{j=1}^{N} 2^{u_j}}, \quad (i = 1, 2, ..., N). \tag{5}$$

2. Absolute Maximum Entropy Calculus of Sources with Preferences

Since p_i are the probabilities of the delivered messages, the maximum entropy of the source with preferences, denoted by $H_m(S)$, is computed by substituting the probabilities from (5) in (4). Then, it results:

$$H_m(S) = \log_2 \left(\sum_{j=1}^{N} 2^{u_j} \right). \tag{6}$$

Furthermore we want to find the utilities, which the messages s_i have to posses, so that:

$$\left(\sum_{j=1}^{N} 2^{u_j} \right) = \max, \tag{7}$$

under the constraint of (3).

If (7) is satisfied, then the entropy computed by (6) becomes an absolute maximum one and it is denoted by $H_{ma}(S)$.

In order to determine the utilities u_j, for which (7) is satisfied, the Lagrange multipliers method is used. The following function will be constructed:

$$\Phi(u_j) = \sum_{j=1}^{N} 2^{u_j} + \lambda \left(K - \sum_{j=1}^{N} u_j \right), \quad \lambda > 0, \tag{8}$$

where λ is the Lagrange multiplier. The maximum value of $\Phi(u_j)$ is attained simultaneously with the maximum value of (7).

The necessary condition for extreme is:

$$\frac{\partial \Phi(u_j)}{\partial u_j} = 0, \quad (j = 1, 2, ..., N), \tag{9}$$

Substituting (8) in (9) and denoting by u_{jm}, $(j = 1, 2, ..., N)$, the utilities, which agree with (9), it results:

$$u_{jm} = \log_2 \left(\frac{\lambda}{\log_2 e} \right), \quad (j = 1, 2, ..., N). \tag{10}$$

Since:

$$\sum_{j=1}^{N} u_{jm} = K, \tag{11}$$

it results:

$$\lambda = 2^{K/N} \log_2 e. \tag{12}$$

Substituting (12) in (10) the relation:

$$u_{jm} = \frac{\sum_{j=1}^{N} u_j}{N} \tag{13}$$

is obtained. One can easily prove that the so obtained extreme value is a maximum one, because:

$$\frac{\partial^2 \Phi(u_j)}{\partial u_j^2} > 0, \quad \frac{\partial^2 \Phi(u_j)}{\partial u_j \partial u_i} = 0, \quad (i, j = 1, 2, ..., N, \ i \neq j). \tag{14}$$

According to (13), the entropy of the sources with preferences is maximized when all source messages have identical qualitative weights (the same utilities), equal to the arithmetic mean value of the utilities.

Substituting (13) in (6), the absolute maximum entropy of the sources with preferences is obtained:

$$H_{ma}(S) = \log_2 N + \frac{\sum_{j=1}^{N} u_j}{N}. \tag{15}$$

In order to obtain the absolute maximum entropy, $H_{ma}(S)$, the messages have to be delivered with probabilities p_{jm}, which can be determined by substituting (13) in (5) namely:

$$p_{jm} = \frac{1}{N}, \quad (j = 1, 2, ..., N). \tag{16}$$

From (13) and (16) it results that the messages have to be equiprobably delivered in order to ensure the absolute maximum entropy of sources with preferences.

3. Some Applications of Entropy of Sources with Preferences

A first application of entropy of sources with preferences regards the calculus of a binary block code entropy.

Let us consider a binary block code, in which each codeword contains n binary symbols. If k denotes the number of information symbols in each codeword, the number of codewords N is determinated by:

$$N = 2^k. \tag{17}$$

Due to the one-to-one correspondence between the codewords and the information source messages, each codeword will have the same probability and utility as the corresponding message.

Let us suppose also, that in order to correct the errors in each codeword, m parity-check symbols are used.

Considering the utility of each transmitted message and the utility of each transmitted codeword, respectively, equals to the number of parity check symbols, m, it results the following distribution:

$$S : \begin{pmatrix} s_1 & s_2 & \dots & s_N \\ m & m & \dots & m \end{pmatrix}. \tag{18}$$

According to (11), the absolute maximum entropy of this source and implicitly of the code obtained by assigning to each message s_i a codeword c_i of length n, is attained when the messages and respective the codewords are equiprobably delivered. Using (15), the absolute maximum entropy becomes:

$$H_{ma}(S) = \log_2 N + \frac{\sum_{j=1}^{N} m}{N}, \tag{19}$$

or, taking into account (17):

$$H_{ma}(S) = k + m = n. \tag{20}$$

According to (20), the absolute maximum entropy of a binary block error correcting code is equal to the codeword length.

A second application of sources with preferences consists in establishing of the delivering probabilities of unequal protected codewords, so that the average information per codeword be maximum. With this purpose in view let us consider a binary block code of length n, in which the first codeword has m_1 parity check symbols, the second, m_2, and so on, the last codeword having m_N parity check symbols.

Further on we consider the general case, in which many codewords with the same number of parity check symbols could exist. Obviously, since the codeword contains more parity check symbols, more errors could be corrected, so that the above code has an unequal error protection.

We also consider that the parity check symbols in each codeword represents their utilities, because to correct the errors in that codeword, a certain number of parity check symbols is useful.

In order to obtain the maximum average information per codeword, the information source with preferences, characterized by the distribution:

$$S: \begin{pmatrix} s_1 & s_2 & \dots & s_N \\ m_1 & m_2 & \dots & m_N \end{pmatrix}, \tag{21}$$

will provide its messages, respective the corresponding codewords, with the probabilities, which could be computed by (5). For the case we are dealing:

$$p_i = \frac{2^{m_i}}{\sum_{j=1}^{N} 2^{m_j}}, \quad (i = 1, 2, ..., N). \tag{22}$$

The average information per codeword may be computed with help of (6), so that:

$$H_m(S) = \log_2 \left(\sum_{j=1}^{N} 2^{m_j} \right). \tag{23}$$

The average information per symbol in a codeword results:

$$i = \frac{H_m(S)}{n} = \frac{\log_2 \left(\sum_{j=1}^{N} 2^{m_j} \right)}{n}, \tag{24}$$

where N is given by (17).

In the particular case, when all codewords are identically protected:

$$m_1 = m_2 = \cdots = m_N = m, \tag{25}$$

the first application is obtained and $i = 1$ bit/symbol.

The third application consists in an implementation of an encoding method for noiseless channels of the sources with preferences, characterized by the distribution:

$$S: \begin{pmatrix} s_1 & s_2 & \dots & s_N \\ u_1 & u_2 & \dots & u_N \end{pmatrix}, \quad u_i \geq 0, \quad (i = 1, 2, ..., N), \tag{26}$$

so that the average information per codeword be maximum and the average codeword length be minimum.

From (26) one notes that each message utility is known and we want to find the messages delivering probabilities so that the average information per message be maximum. If the source message are delivered with probabilities p_i, (s.(5)), the source entropy becomes maximum, that is the average information per message becomes maximum and it can be calculated by (6).

In order to obtain the codewords of the smallest length, for a noiseless channel, one can use the H u f f m a n encoding procedure, using the above obtained probabilities [5].

4. Conclusions

The main obtained results are the following:

1° Determination of the maximum value of the entropy of a source with preferences, (s.(6)).

2° Determination of the constraints on the utilities and the probabilities (s.(13) and (16)) for obtaining the absolute maximum entropy of a source with preferences (s.(15)).

3° Determination of the maximum absolute entropy of a binary block code with the equal error protected codewords (s.(20)).

4° Determination of the maximum entropy, respective the average information per symbol for a binary block codes, unequal error protected (s.(23), (24)).

5° Derivation of the implementation of an instantaneous code for a noiseless channel when the source messages are characterized only by their utilities or significance. The resulting code ensures a maximum average information per codeword and a minimum average length of codewords.

Received, March 13, 1995

Technical University "Gh.Asachi", Jassy,
Department of Telecommunications

REFERENCES

1. M u n t e a n u V., C o t a e P., *The Entropy with Preference.* AEÜ, **46**, *6*, 429-431 (1992).
2. T u t e j a R.K., *Characterization of Entropy with Preference.* Kybernetyka, **24**, 54-60 (1988).
3. B e l i s M., G u i a ş u S., *A Quantitative Qualitative Measure of Information in Cybernetic Systems.* IEEE Trans. Inform. Theory, **IT-14**, 593-594 (1968).
4. G u i a ş u S., *Weighted Entropy.* Reports on Math. Phys., **2**, 165-179 (1971).
5. H u f f m a n D.A., *A Method for the Construction of Minimum – Redundancy Codes.* In W. J a c k s o n (Ed.), *Communication Theory.* Butterworths Scientific Publications, London, 1953, 102-110.
6. S h a n n o n C.E., *A Mathematical Theory of Communication.* Bull. Syst. Tech. Journal, **27**, 379-423, 623-656 (1948).

CÂTEVA APLICAŢII ALE ENTROPIEI SURSELOR DE INFORMAŢIE CU PREFERINŢE

(Rezumat)

Se prezintă o nouă proprietate a surselor de informaţie cu preferinţe. Pe baza acesteia se calculează entropia maximă absolută. De asemenea, este prezentată o metodă de codare pentru canale neperturbate ale surselor caracterizate numai de utilităţile mesajelor.

BULETINUL INSTITUTULUI POLITEHNIC DIN IAŞI
Tomul XLII (XLVI), Fasc. 1–2, 1996
Secţia III
ELECTROTEHNICĂ. ENERGETICĂ. ELECTRONICĂ

D.C. 621.394.9

A NEW CODE BASED ON DELAY MODULATION

BY

N.D. ALEXANDRU

A new code based on the well-known delay modulation or M i l l e r code is presented. It uses two components, $S1$ and $S2$, transmitted on separate channels. An approximate expression of the power spectral density associated to the proposed code is derived by approximating a recurrence relation between two values of the autocorrelation function which are separated by four bit intervals. The code is interesting for fiber optic digital communications.

1. Introduction

In his paper [1] P r u c n a l proposed a transmission system using two line codes called AMSI (Alternate Mark/Space Inversion), with the property that their modulo-2 sum (EXCLUSIVE OR operation) result in the NRZ-L coded data, which simplifies the implementation of the decoding circuit. The AMSI codes possess very attractive properties such as: zero d.c. content, self-clocking capability, data-rate-transparent decoding and synchronization, as well as baseband bandwidth conservation. The components of AMSI codes are denoted by $S1$ and $S2$.

2. DMT Code

A new code, also with two components, is proposed. It is denoted by DMT (Delay Modulation and T-type flip flop) and is produced by the arrangement shown in Fig. 1.

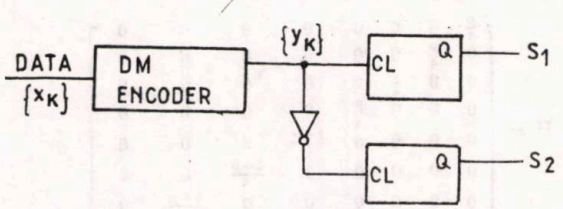

Fig. 1

The associated waveforms are represented in Fig. 2. One can see that the NRZ-L coded data can be obtained by modulo-2 summing of $S1$ and $S2$, followed by a conventional DM decoding. The advantage of this code resides in a spectrum compaction produced by the T-type flip-flop, which divides the frequency by a factor of 2. Its main disadvantage is the non-zero d.c. content.

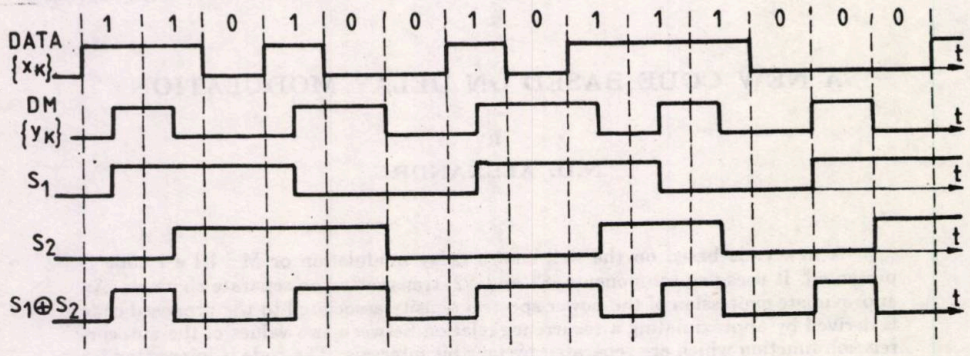

Fig. 2

3. An Approximate Derivation of the P.s.d.

Based on Fig. 1, the transition diagram for the DMT code ($S1$ and $S2$) was extracted and represented in Fig. 3. The matrix P of state transition probabilities is

$$P = \begin{bmatrix} 0 & p & 0 & 0 & 0 & 1-p & 0 & 0 \\ 0 & 0 & p & 0 & 0 & 0 & 1-p & 0 \\ 0 & 0 & 0 & p & 0 & 0 & 0 & 1-p \\ p & 0 & 0 & 0 & 1-p & 0 & 0 & 0 \\ p & 0 & 0 & 0 & 0 & 1-p & 0 & 0 \\ 0 & p & 0 & 0 & 0 & 0 & 1-p & 0 \\ 0 & 0 & p & 0 & 0 & 0 & 0 & 1-p \\ 0 & 0 & 0 & p & 1-p & 0 & 0 & 0 \end{bmatrix}, \tag{1}$$

where p is the probability of a mark in the NRZ-L coded data sequence.

The steady-state probability distribution matrix is

$$\Pi = \begin{bmatrix} \frac{p}{4} & 0 & 0 & 0 & 0 & 0 & 0 & 0 \\ 0 & \frac{p}{4} & 0 & 0 & 0 & 0 & 0 & 0 \\ 0 & 0 & \frac{p}{4} & 0 & 0 & 0 & 0 & 0 \\ 0 & 0 & 0 & \frac{p}{4} & 0 & 0 & 0 & 0 \\ 0 & 0 & 0 & 0 & \frac{1-p}{4} & 0 & 0 & 0 \\ 0 & 0 & 0 & 0 & 0 & \frac{1-p}{4} & 0 & 0 \\ 0 & 0 & 0 & 0 & 0 & 0 & \frac{1-p}{4} & 0 \\ 0 & 0 & 0 & 0 & 0 & 0 & 0 & \frac{1-p}{4} \end{bmatrix} \tag{2}$$

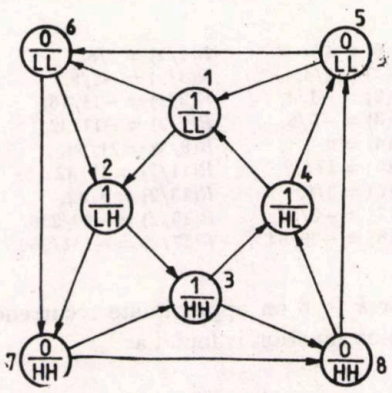

Fig. 3

satisfying relation

$$\Pi P = \Pi. \tag{3}$$

The autocorrelation matrixes Z (full bit interval) and X (half bit interval) are given by

$$Z = \begin{bmatrix} +1 & 0 & -1 & 0 & +1 & +1 & -1 & -1 \\ 0 & +1 & 0 & -1 & 0 & 0 & 0 & 0 \\ -1 & 0 & +1 & 0 & -1 & -1 & +1 & +1 \\ 0 & -1 & 0 & +1 & 0 & 0 & 0 & 0 \\ +1 & 0 & -1 & 0 & +1 & +1 & -1 & -1 \\ +1 & 0 & -1 & 0 & +1 & +1 & -1 & -1 \\ -1 & 0 & +1 & 0 & -1 & -1 & +1 & +1 \\ -1 & 0 & +1 & 0 & -1 & -1 & +1 & +1 \end{bmatrix} \tag{4}$$

and respectively

$$X = \begin{bmatrix} +\frac{1}{2} & +\frac{1}{2} & -\frac{1}{2} & -\frac{1}{2} & +\frac{1}{2} & +\frac{1}{2} & -\frac{1}{2} & -\frac{1}{2} \\ -\frac{1}{2} & -\frac{1}{2} & +\frac{1}{2} & +\frac{1}{2} & -\frac{1}{2} & -\frac{1}{2} & +\frac{1}{2} & +\frac{1}{2} \\ -\frac{1}{2} & -\frac{1}{2} & +\frac{1}{2} & +\frac{1}{2} & -\frac{1}{2} & -\frac{1}{2} & +\frac{1}{2} & +\frac{1}{2} \\ +\frac{1}{2} & +\frac{1}{2} & -\frac{1}{2} & -\frac{1}{2} & +\frac{1}{2} & +\frac{1}{2} & -\frac{1}{2} & -\frac{1}{2} \\ +\frac{1}{2} & +\frac{1}{2} & -\frac{1}{2} & -\frac{1}{2} & +\frac{1}{2} & +\frac{1}{2} & -\frac{1}{2} & -\frac{1}{2} \\ +\frac{1}{2} & +\frac{1}{2} & -\frac{1}{2} & -\frac{1}{2} & +\frac{1}{2} & +\frac{1}{2} & -\frac{1}{2} & -\frac{1}{2} \\ -\frac{1}{2} & -\frac{1}{2} & +\frac{1}{2} & +\frac{1}{2} & -\frac{1}{2} & -\frac{1}{2} & +\frac{1}{2} & +\frac{1}{2} \\ -\frac{1}{2} & -\frac{1}{2} & +\frac{1}{2} & +\frac{1}{2} & -\frac{1}{2} & -\frac{1}{2} & +\frac{1}{2} & +\frac{1}{2} \end{bmatrix}. \tag{5}$$

Using the approach outlined in [2] and [3] we have

$$R(i) = \mathrm{tr}\,[(\Pi P^i)Z], \tag{6}$$

where i is an integer. Also

$$R(i + 1/2) = \mathrm{tr}[(\Pi P^{i-1})X] + \mathrm{tr}[(\Pi P^i)X^T]. \tag{7}$$

For $p = 0.5$ we get

$$\begin{array}{ll} R(0) = 1, & R(1/2) = 5/8, \\ R(1) = 1/4, & R(3/2) = -1/8, \\ R(2) = -1/4, & R(5/2) = -11/16, \\ R(3) = -5/8, & R(7/2) = -11/32, \\ R(4) = 0, & R(9/2) = 21/64, \\ R(5) = 17/32, & R(11/2) = 17/32 \\ R(6) = 3/8, & R(13/2) = 3/32, \\ R(7) = -3/16, & R(15/2) = -99/256, \\ R(8) = -29/64, & R(17/2) = -181/256. \end{array}$$

Denoting $2k = i$, for $k \geq 8$ an approximate recurrence relation among the values of the autocorrelation function is found as

$$R(k+8) = -\frac{17}{32} R(k). \tag{8}$$

Then, using B e n n e t t's formula [4]

(9)

$$W(f) = \left(\frac{m_1}{T}\right)^2 |G(f)|^2 \delta\left(f - \frac{m}{T}\right) + \frac{1}{T}|G(f)|^2 \left\{ R(0) - m_1^2 + 2\sum_{k=1}^{\infty} [R(k) - m_1^2] \cos 2\pi k f T \right\}$$

and after some tedious trigonometric manipulations we can show that

$$\begin{aligned} \sum_{k=0}^{\infty} R(k+1)\cos(k+1)x &= \frac{5}{8}\cos x + \frac{1}{4}\cos 2x - \frac{1}{8}\cos 3x - \frac{1}{2}\cos 4x - \\ &- \frac{11}{16}\cos 5x - \frac{5}{8}\cos 6x - \frac{11}{32}\cos 7x + \sum_{i=8}^{24}\sum_{k=0}^{\infty}\left(-\frac{17}{32}\right)^k R(l)\cos(16k+l)x, \end{aligned} \tag{10}$$

where $x = \pi f T$ and $m_1 = 0$ and finally

$$W(f) = \frac{S(f)}{A^2 T} = \left(\frac{\sin\frac{x}{2}}{\frac{x}{2}}\right)^2 \left[1 + 2\sum_{k=1}^{\infty} R(k)\cos kx\right] \tag{11}$$

or

$$\begin{aligned} W(f) = &\frac{2(1-\cos x)}{x^2}\left(1 + \frac{5}{4}\cos x + \frac{1}{2}\cos 2x - \frac{1}{4}\cos 3x - \right. \\ &\left. - \cos 4x - \frac{11}{8}\cos 5x - \frac{5}{4}\cos 6x - \frac{11}{16}\cos 7x + A\right), \end{aligned}$$

with

$$A = \frac{1}{1313 + 1088\cos 16x}\Big[17\Big(-47\frac{3}{8}\cos x - 22\frac{1}{4}\cos 2x + 11\frac{1}{8}\cos 3x + \\ +65\frac{1}{2}\cos 4x + 56\frac{15}{16}\cos 5x + 55\frac{1}{8}\cos 6x + 32\frac{27}{32}\cos 7x\Big) + \\ +32\Big(21\cos 9x + 34\cos 10x + 34\cos 11x + 48\cos 12x + 6\cos 13x - \\ -12\cos 14x - \frac{99}{4}\cos 15x - 29\cos 16x - 22\frac{5}{8}\cos 17x - 10\frac{1}{4}\cos 18x + \\ +5\frac{1}{8}\cos 19x + 17\frac{1}{2}\cos 20x + 22\frac{15}{16}\cos 21x + 21\frac{1}{8}\cos 22x + \\ +11\frac{27}{32}\cos 23x\Big)\Big]. \tag{12}$$

The approximative p.s.d. of the DMT code is represented in Fig. 4.

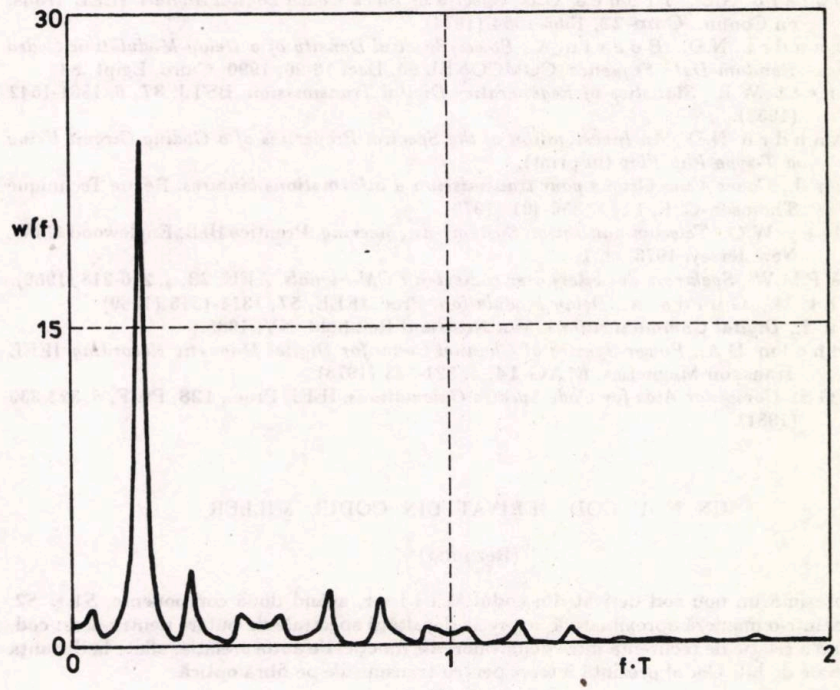

Fig. 4

4. Conclusions

1° A new code derived from M i l l e r code (delay modulation) using two components transmitted on different channels is proposed.

2° Its p.s.d. bears some similarity with the M i l l e r code, but it is more compact.

3° Its decoding implies an exclusive-or operation performed on its two components $S1$ and $S2$, followed by a conventional DM decoding.

Received, April 30, 1992

Technical University "Gh.Asachi", Jassy, Department of Telecommunications

REFERENCES

1. P r u c n a l P.R., P e r r i e r, *A Rate-Transparent Self-Clocking Line Code.* Proc. IEEE, **75**, *8*, 1123-1125 (1987).
2. C a r i o l a r o G.L., T r o n c a G.P., *Spectra of Block Coded Digital Signals.* IEEE Trans. on Comm., **Com-22**, 1555-1564 (1974).
3. A l e x a n d r u N.D., B o a r i u A., *Power Spectral Density of a Delay-Modulation Coded Random Data Sequence.* COMCONEL 90, Dec. 16-20, 1990, Cairo, Egipt, 83.
4. B e n n e t t W.R., *Statistics of Regenerative Digital Transmission.* BSTJ, **37**, *6*, 1501-1542 (1958).
5. A l e x a n d r u N.D., *An Investigation of the Spectral Properties of a Coding Circuit Using a T-type Flip Flop* (in print).
6. V a l i n J., *Codes d'impulsions pour transmission d'informations binaires.* Revue Technique Thomson-CSF, **11**, *2*, 356-401 (1979).
7. L i n d s e y W.C., *Telecommunication Systems Engineering.* Prentice Hall, Englewood Cliffs, New Jersey, 1973, ch.**1**.
8. N a v é P.M.W., *Spektrum des biternärer codierten PCM-Signals.* AEÜ, **23**, *4*, 216-218 (1969).
9. H e c h t M., G u i d a A., *Delay Modulation.* Proc. IEEE, **57**, 1314-1316 (1969).
10. K o r n I., *Digital Communications.* Van Nostrand Reinhold, NY, 1985.
11. L i n d h o l m D.A., *Power Spectra of Channel Codes for Digital Magnetic Recording.* IEEE Trans. on Magnetics, **MAG-14**, *5*, 321-323 (1978).
12. P o o G.S., *Computer Aids for Code Spectra Calculations.* IEEE Proc., **128**, Pt. F, *5*, 323-330 (1981).

UN NOU COD DERIVAT DIN CODUL MILLER

(Rezumat)

Se prezintă un nou cod derivat din codul M i l l e r, având două componente, $S1$ şi $S2$. Se deduce, într-o manieră aproximativă, expresia densităţii spectrale de putere pentru acest cod, aproximând o relaţie de recurenţă între două valori ale funcţiei de autocorelaţie, aflate la distanţa de 4 intervale de bit. Codul prezintă interes pentru transmisiile pe fibră optică.

BULETINUL INSTITUTULUI POLITEHNIC DIN IAŞI
Tomul XLII (XLVI), Fasc. 1–2, 1996
Secţia III
ELECTROTEHNICĂ. ENERGETICĂ. ELECTRONICĂ

D.C. 538.567.4

POWER SPECTRAL DENSITY OF *M*-ARY PSK WITH VARIOUS SHAPING FUNCTIONS

BY
PAUL COTAE

Analytic expressions for the power spectral density of digital phase modulations signals for various shapes of the base-band modulating signal are derived. The proposed method is more general than those known from the literature and allows the derivation of DSP for correlated modulating signals (partial response signals).

1. Introduction

The phase of PSK modulated signal is proportional to the base-band waveform sequence:

$$\Phi(t) = K_p d(t, a_i) = K_p \sum_i a_i h(t - iT), \tag{1}$$

where K_p is a constant and a_i are real numbers, so that (1) may be expressed as:

$$y(t) = A\cos\left[2\pi f_p t + K_p \sum_i a_i h(t - iT) + \Phi_0\right]. \tag{2}$$

At every sampling times $t_k = KT + T/2$, (1) becomes:

$$\Phi(t_k) = K_p a_k, \tag{3}$$

because for all the base-band impulse responses, $h(T/2) = 1$, [1].

In order to obtain the complex envelope, (2) and (3) are used and observing that:

$$x(t) = A\exp\left\{\mathrm{j}\left[K_p \sum_i a_i h(t - iT)\right]\right\}$$

it results:

$$x(t) = a\sum_i d(t - iT, a_i) = A\exp\left\{\mathrm{j}\left[K_p \sum_i a_i h(t - iT)\right]\right\}. \tag{4}$$

Although $h(t)$ is defined only over the range $0 \leq t \leq T$, the complex envelope expression is defined over $KT \leq t < (K+1)T$. After few mathematical manipulation of (4) a similar expression of the modulated QASK signal may be obtained. Indeed, considering:

$$a_i = \frac{\exp\left[\mathrm{j}Kah(t-kT)\right]}{h(t-kT)}$$

relation (4) becomes:

$$x(t) = A\sum_i a_i h(t-iT). \tag{5}$$

The initial phase, Φ_0, from (2) is a random variable too, which is supposed to have a uniform distribution over the range $[0,\pi]$. It is known that in the case of coherent receivers, the local signal have to be generated of the same frequency and phase as the received modulated signal.

In order to simplify the complexity of the receiver equipment, an alternative of PSK modulation, named DPSK (Differential PSK), is used.

In this case the phase of the modulated signal still doesn't vary in absolute values proportional to information symbols a_i as in PSK modulation, but in succesive differences of the phase, determined by the symbols a_i, as in following relation:

$$a'_i = a'_{i-1} + a_i. \tag{6}$$

The form of the DPSK modulated signal is:

$$y(t) = A\cos\left[2\pi f_p t + K_p \sum_i a'_i h(t-iT)\right] \tag{7}$$

so that at two successive sampling times, the phase difference is:

$$\Phi\left(KT+\frac{T}{2}\right) - \Phi\left(KT-\frac{T}{2}\right) = K_p\sum_k a'_k h\left(\frac{t}{2}\right) - K_p\sum_k a'_{k-1}\left(\frac{T}{2}\right) = a + kK_p$$

and according to (7) the complex envelope of the DPSK modulated signal is:

$$x(t) = A\sum_i a'_i h(t-iT). \tag{8}$$

2. Power Spectral Density Calculus for *M*-ary PSK

Three distinct cases are treated:

1° *Full response signals* (K=1). The impulse response of the shaping filter is defined in the time domain over the same range $[0,T]$ as the waveform sequence $d(t,a_i)$ at its output.

The typical case of PSK modulated signal is that for which the shaping filter function remains the same for any input waveform sequence.

2° *Partial response signals* (K=2). In this case the data modulation rate, $R = 1/T$, remains unchanged, that is the symbols are defined over the range $[0, T]$ too and the impulse response of the shaping filter is defined over the range $[0, 2T]$.

3° *General case* ($K > 2$). In this case the modulation rate remains the same and the impulse response is defined over the range $[0, KT]$.

For PSK modulation, the base-band waveform sequence is:

$$d(t, \alpha_i) = \exp[\mathrm{j}K_p h(t, \alpha_i)]\, u_T(t), \tag{9}$$

and for PSD calculus terms as

$$X_{d,i}(f) = \overline{D(f, \alpha_i) D^*(f, \alpha_0)}. \tag{10}$$

are useful. In principle, the Fourier Transforms of sequences $d(t, \alpha_i)$ and $d(t, \alpha_0)$ could be calculated and then their average value have to be computed, according (10).

An efficient procedure is to calculate first the average of $d(t, \alpha_i)$, denoted by $m_d(t)$, according to:

$$m_d(t) = \overline{D(t, \alpha_i)} \tag{11}$$

and then $M_d(f) = F[m_d(t)]$ will be computed.

2.1. Total Response Signals

The sequence α_i consists of a single symbol a_i, which are uncorrelated. According to (11):

$$X_{d,1}(f) = |M_d(f)|^2 \tag{12}$$

and based on the autocorrelation function, $X_{d,0}(f)$, it follows:

$$R_{d,0}(t, t') = \overline{d(t, a_i) d^*(t, a_0)} = \overline{\exp\{\mathrm{j}K_p[h(t, a_i) - h(t', a_0)]\}}. \tag{13}$$

For M-ary modulation the symbols average is:

$$m_d(t) = \frac{\sum_{i=1}^{M} \exp[\mathrm{j}(2i - M - 1)K_p h(t)]}{M} = \frac{\sin M K_p h(t)}{M \sin K_p h(t)}. \tag{14}$$

Analogously, using the above relation, (13) becomes:

$$R_{d,0}(t, t') = \frac{\sin M K_p [h(t) - h(t')]}{M \sin K_p [h(t) - h(t')]}. \tag{15}$$

Since $R_{d,0}(t,t')$ above obtained is real, it can be computed as:

$$X_{d,0}(f) = 2\int_0^T \left(\int_0^{T-z} R_{d,0}(x, x+z)\,\mathrm{d}z \right) \cos 2\pi f z\,\mathrm{d}z, \tag{16}$$

which allows the PSD calculus for M-ary PSK according to:

$$X(f) = 2\frac{A^2}{T}\int_0^T \left(\int_0^{T-z} R_{d,0}(x, x+z)\,\mathrm{d}z \right) \cos 2\pi f z\,\mathrm{d}z - |M_d(f)|^2 + \\ + \left(\frac{A}{T}\right)|M_d(f)|^2 \sum_k \delta\left(f - \frac{k}{T}\right). \tag{17}$$

The particular cases are obtained by specifying the impulse response of the shaping filter for chosen M.

a) *PSD of M-ary PSK for h(t)=1NRZ*

We choose $K_p = \pi/M$ and according to (14):

$$m_d(t) = \frac{\sin\left(\pi \frac{M}{\pi}\pi\right)}{M \sin\frac{\pi}{M}}$$

and obviously $M_d(f) = 0$. From (15) $R_{d,0}(t,t') = 1$, so that (16) becomes:

$$X_{d,0}(f) = 2\int_0^T (T-z)\cos 2\pi f z\,\mathrm{d}z = T^2 \sin c^2 fT;$$

thus finally (17) becomes:

$$X(f) = A^2 T \sin c^2 fT. \tag{18}$$

One can observe that PSD have not discrete part and it doesn't depend on M.

b) *PSD of M-ary PSK for h(t)=1HR, 1RC, 1TR*

For $M = 2$, 2PSK is obtained, that is binary PSK, named BPSK. With (14) it results:

$$m_d^{(2)}(t) = \cos\frac{\pi}{2}h(t) = \begin{cases} \cos\left(\frac{\pi}{2}\sin\frac{\pi t}{T}\right), & 0 \le t \le T, \text{ BPSK 1HS;} \\ \cos\frac{\pi}{4}\left(1 - \cos\frac{2\pi t}{T}\right), & 0 \le t \le T, \text{ BPSK 1RC;} \\ \cos\frac{\pi t}{T}, & 0 \le t \le T, \text{ BPSK 1TR.} \end{cases} \tag{19}$$

For $M = 4$, 4PSK or PSK with 4 levels, named QPSK, are obtained. QPSK modulation for $h(t)$=1NRZ is the same to OQASK, for which the symbols a_i are

symmetrically arranged on a circle or on a quadrate. Thus, according to (14) the average becomes:

$$m_d^{(4)}(d) = \cos\frac{\pi}{4}h(t)\cos\frac{\pi}{2}h(t) = \cos\frac{\pi}{4}h(t)m_d^{(2)}(t). \tag{20}$$

Analogously, for $M = 8$ one obtains:

$$m_d^{(8)}(d) = \cos\frac{\pi}{8}h(t)\cos\frac{\pi}{4}h(t)\cos\frac{\pi}{2}h(t) = \cos\frac{\pi}{8}h(t)m_d^{(4)}(t). \tag{21}$$

This time the Fourier Transform of $m_d^2(t), m_d^4(t)$ and $m_d^8(t)$ are nonnegative and the calculus procedure from a) cannot be applied.

The obtained relations for M-ary PSK are very important, because they allows to conclude about the PSD of the shaping filter characteristics directly in the time domain.

2.2. Partial Response Signals (K=2)

Although the impulse response of the shaping function is defined over the range $[0, 2\pi]$, a single equivalent impulse response over a single elementary interval is computed. It depends on the last $K = 2$ symbols sanded by the source. So:

$$\begin{aligned} d(t,\alpha_i) &= d(t,a_i,a_{i-1}) = d_0(t,a_i)d_1(t,a_{i-1}), \\ m_d(t,\alpha_i) &= \overline{d_0(t,a_i)d_1(t,a_{i-1})}. \end{aligned} \tag{22}$$

Also:

$$\begin{aligned} h(t,a_i) &= h_0(t,a_i)u_T(t) + h_1(t-T,a_i)u_T(t-T), \\ h_k(t,a_i) &= h(t+KT,a_i)u_T(t), \end{aligned} \tag{23}$$

according to (1), which is true for PSK modulation. Although in (23) the impulse response is defined in the range $[0, 2T]$, in (22) one can observe that the signal $d(t,\alpha_i)$ is defined over $[0, T]$. With this notes (3) becomes:

$$m_{d,k}(t) = \overline{d_k(t,a_0)} \tag{24}$$

and thus:

$$R_{d,i}(t,t') = \overline{d(t,\alpha_i)d^*(t',\alpha_0)} = \overline{d_0(t,a_0)d^*(t,a_1)d_0^*(t,a_0)d_1^*(t,a_{-1})}. \tag{25}$$

In order to simplify the above computation, the product of two terms from (25) is denoted by:

$$p_{k,n}(t,t') \triangleq \overline{d_k(t,a_i)d_n^*(t,a_i)}. \tag{26}$$

Based on the autocorrelation function, for $K = 2$ and for $i \geq 2$, $X_{d,0}(f)$, $X_{d,1}(f)$ and $X_{d,i}(f)$ have to be computed. Due to the symbols stationarity, the pair (a_i, a_{i-1}) may be replaced with (a_1, a_0).

For $i = 0$, the symbols are independent and according to (25), it results:

$$R_{d,1}(t,t') = \overline{d_0(t,a_1)d_1(t,a_0)d_0^*(t,a_0)d_1^*(t',a_{-1})} = p_{0,0}(t,t')p_{1,1}(t,t'). \tag{27}$$

For $i = 1$, (25) becomes:

$$\begin{aligned} R_{d,1}(t,t') &= \overline{d_0(t,a_1)d_1(t,a_0)d_0^*(t',a_0)d_1^*(t,a_{-1})} = \\ &= d_0(t,a_1)p_{1,0}(t,t')d_1^*(t',a_0) = m_{d,0}(t)p_{1,0}(t,t')m_{d,1}^*(t'). \end{aligned} \tag{28}$$

For $i \geq 2$, (25) becomes:

$$R_{d,i}(t,t') = m_d(t)m_d^*(t') = m_{d,0}(t)m_{d,0}(t')m_{d,1}^*(t)m_{d,1}^*(t'). \tag{29}$$

Analogously:

$$M_{d,k}(t) = \overline{d_k(t,a_0)} = \frac{\sin MK_p h_k(t)}{M \sin K_p h_k(t)}. \tag{30}$$

a) *PSD of M-ary PSK and Duobinary h(t)*

Relation (30) becomes:

$$m_{d,k}(t) = \frac{1}{M \sin \frac{\pi}{2M}}. \tag{31}$$

According to (5) and (7), (31) becomes:

$$p_{k,n}(t,t') = 1 = p_{k,n}(t',t), \tag{32}$$

and consequently:

$$R_{d,0}(t,t') = 1 = R_{d,0}(t',t). \tag{33}$$

Thus:

$$X_{d,0}(f) = 2\int_0^T \left(\int_0^{T-z} R_{d,0}(x, x-z)\,dx \right) \cos 2\pi f z\,dz = T^2 \sin c^2 fT. \tag{34}$$

For $X_{d,1}(f)$ computation (33) is used:

$$R_{d,1}(t,t') = \frac{1}{M \sin \frac{\pi}{2M}}$$

obtaining:

$$X_{d,1}(f) = \frac{T^2 \sin c^2 fT}{\left(M \sin \frac{\pi}{2M}\right)^2}. \tag{35}$$

Analogously:

$$X_{d,i}(f) = X_{d,2}(f) = \frac{T^2 \sin c^2 fT}{\left(M \sin \frac{\pi}{2M}\right)^4}. \tag{36}$$

For $K = 2$ it results:

$$X(f) = TA^2(\sin cfT)^2 \left[1 + \frac{2\cos 2\pi fT}{\left(M \sin \frac{\pi}{2M}\right)^2} - \frac{1 + \cos 2\pi fT}{\left(M \sin \frac{\pi}{2M}\right)^4} + \right. \tag{37}$$
$$\left. + \frac{1}{T\left(M \sin \frac{\pi}{2M}\right)^4} \sum_k \delta\left(f - \frac{k}{T}\right)\right].$$

$M = 2$ represents the BPSK case, with duobinary $h(t)$.

Particularizing (37) for $M = 2$, PSD of Duobinary PSK is obtained:

$$X(f) = \frac{T}{4} A^2 \sin c^2 fT \left[3 + 2\cos 2\pi fT + \frac{1}{T} \sum_k \delta\left(f - \frac{k}{T}\right)\right]. \tag{38}$$

Analogously, the forms for PSD of QPSK with $h(t)$=2RC, 2TR and 2HS are obtained by imposing $M = 4$.

2.3. General Case ($K > 2$)

The impulse response of the shaping filter is defined over the range $[0, KT]$ and its response depends on the last K information symbols.

As in case $K = 2$, the response for each information symbols is deduced.

The filter response for a single symbol is:

$$h(t, a_i) = \sum_{k=0}^{K-1} h_k(t - kT, a_i) u_T(t - kT). \tag{39}$$

The sequence $\alpha_i = (a_i, a_{i-1}, ..., a_{i-k})$ results:

$$h(t, \alpha_i) = \sum_{k=0}^{K-1} h_k(t, a_{i-k}) u_T(t). \tag{40}$$

In order to compute the autocorrelation function $R_{d,0}(t,t')$ according to (30), based on (39) and (40), the difference $h(t,\alpha_i)-h(t',\alpha_0)$ has to be evaluated. Thus:

$$h(t,\alpha_i)-h(t',\alpha_0)=\left\{\sum_{k=0}^{K-1}h_k(t,a_{i-k})+\right.$$
$$\left.+\sum_{k=i}^{K-1}[h_k\ (t,a_{i-k})-h_{k-i}(t,a_{i-k})]-\sum_{k=0}^{K-1}h(t,a_{i-k})\right\}u_T(t). \tag{41}$$

Due to the fact that the sequence from the shaping filter input is defined as (4), it was truncated in K bits groups.

For $i \geq K$ the terms $h(t,\alpha_i)$ and $h(t',\alpha_0)$ are independent, if the information symbols are independent too.

Based on (41), (1) becomes:

$$d(t,\alpha_i)=e^{jK_p h(t,\alpha_i)}=\prod_{k=0}^{K-1}d_k(t,a_{i-k}). \tag{42}$$

Two cases are considered: a) $i \leq K$, for which the symbols are correlated; b) $i > K$, for which the symbols are uncorrelated.

According to (5) the autocorrelation function is:

$$R_{d,i}(t,t')=d(t,\alpha_i)d^*(t',\alpha_0)=\prod_{k=0}^{i-1}m_{d,k}(t)\prod_{k=i}^{K-1}p_{k,k-1}(t,t')\prod_{k=i}^{K-1}m^*_{d,k}(t'). \tag{43}$$

The necessary terms $X_{d,i}(f)$ are obtained considering the Fourier Transform of (43).

If $i \geq K$, then:

$$R_{d,i}(t,t')=\prod_{k=0}^{i-1}m_{d,k}(t)m^*_{d,k}(t')=m_d(t)m^*_d(t'), \tag{44}$$

where:

$$m_d(t)=d(t,\alpha_0)=\sum_{k=0}^{K-1}m_{d,k}(t). \tag{45}$$

For an effective computation, $K_p=\pi/KM$ is chosen and the component parts of PSD for a given case are computed.

In literature, the computer simulation for partial response signals are used. but the method is not exact and spectral efficient calculus needs an analytical formula.

3. Conclusions

Using the proposed procedure, the statistical mean of data sequence is first computed and then its Fourier Transform. The treatment of PSK modulation is unitary, which allows the PSD deducing for partial response signals.

Received, May 16, 1994

Technical University "Gh.Asachi", Jassy,
Department of Telecommunications

REFERENCES

1. C o t a e P., *Contributions to the Improving of the Modulation Techniques for High Speed Data Transmission* (in Romanian). Ph. D. Thesis, Technical University Bucureşti, 1992.
2. C o t a e P., *Digital Communication.* Part **I**, *Digital Modulation* (in Romanian). Technical University „Gh.Asachi", Jassy, 1992.
3. C o t a e P., *A General Method for Computation Power Spectral Density of Phase Shift Keying M-ary Modulated Signals.* Bul. Inst. polit., Iaşi (in print).

DENSITATEA SPECTRALĂ DE PUTERE A SEMNALELOR DIGITALE CU MODULAŢIE DIGITALĂ DE FAZĂ PENTRU DIFERITE FUNCŢII MODULATOARE

(Rezumat)

Se deduc expresiile analitice pentru densitatea spectrală de putere (DSP) în cazul semnalelor digitale cu modulaţie digitală de fază, pentru diferite forme ale semnalului modulator din banda de bază (BB). Metoda propusă este mai generală decât cea cunoscută în literatura de specialitate şi permite deducerea DSP şi în cazul semnalelor modulatoare corelate (semnale cu răspuns parţial).

BULETINUL INSTITUTULUI POLITEHNIC DIN IAŞI
Tomul XLII (XLVI), Fasc. 1–2, 1996
Secţia III
ELECTROTEHNICĂ. ENERGETICĂ. ELECTRONICĂ

D.C. 621.318.7

A DESIGN METHOD FOR PERIODICALLY TIME VARYING IIR FILTERS WITH APPLICATION TO TRANSMULTIPLEXING (I)

BY

DANIELA TĂRNICERIU and VALERIU MUNTEANU

Based on the decomposition of a periodically time varying (PTV) IIR filter into a linear time invariant IIR section and a periodically varying FIR one, a design method of the global PTV IIR filter is proposed. So, rotating simultaneously the poles and zeros of a high performances prototype filter, a repeating pole structure is obtained.

1. Introduction

Periodically time varying (PTV) filters are those whose coefficients vary periodically with time. PTV FIR (Finite Impulse Response) filters suffer from the same limitation as time invariant FIR filters, i.e. the filter order is too large to create a sharp cutoff characteristic. This is the reason why the IIR (Infinite Impulse Response) PTV filter study is an actual problem. The above filters have been studied for a number of specific problems and their design was made based on the frozen time approximation [8]. Because the PTV filters present a frequency characteristic at every time moment, these may be design using a method specific to the time invariant filters. For the PTV filters one can define the generalized transfer function (GTF), $H(z,n)$, which represents the filter transfer function at moment n.

The GTF may be represented in a three dimensional, system, $Oxyz$, where the axis Ox, Oy and Oz correspond, respectively, to normalized frequency f, time moment n and magnitude $|H(z,n)|$. This method presents some disadvantages. After reviewing PTV system notation and representation based on the idea that a PTV IIR filter may be implemented as a time invariant IIR system cascaded with an PTV FIR filter [1], in what follows design technique with well defined error and stability characteristics is presented.

2. PTV IIR Filters Analysis

The input–output relationship of a time varying system is given by:

$$y[n] = \sum_{k=-\infty}^{\infty} h[n,k]\, x[k], \tag{1}$$

where $x[k]$ is the input sequence, $y[k]$ – the output sequence and $h[n,k]$ – the response of the system at time n to an impulse at time k, called G r e e n's function. Two others forms of the G r e e n's function are:

$$r[m,k] = h[m+k,k], \tag{2}$$

$$p[n,m] = h[n,n-m]. \tag{3}$$

The corresponding input–output relationships are:

$$y[n] = \sum_{k=-\infty}^{\infty} r[n-k,k]\, x[k], \tag{4}$$

$$y[n] = \sum_{k=-\infty}^{\infty} p[n,n-k]\, x[k]. \tag{5}$$

The difference equation form of a time varying filter is:

$$y[n] = \sum_{j=0}^{M-1} a_j[n]\, x[n-j] + \sum_{l=1}^{N} b_l[n]\, y[n-l]. \tag{6}$$

For a PTV filter with periodicity P the G r e e n's functions are characterized by:

$$h[n,k] = h[n+P,k+P], \quad \forall n,k; \tag{7}$$

$$r[m,k] = r[m,k+P], \quad \forall m,k; \tag{8}$$

$$p[n,m] = p[n+P,m], \quad \forall n,m, \tag{9}$$

with difference equation coefficients:

$$a_j[n] = a_j[n+P], \tag{10}$$

$$b_l[n] = b_l[n+P]. \tag{11}$$

Since $r[m,k]$ is periodic w.r.t. k it can be expanded in Fourier series:

$$r[m,k] = \sum_{l=0}^{P-1} q_l[m] e^{-j\frac{2\pi}{P}lk}, \tag{12}$$

where:

$$q_l[m] = \frac{1}{P} \sum_{k=0}^{P-1} r[m,k] e^{j\frac{2\pi}{P}lk} \tag{13}$$

are the Fourier coefficients, with the Fourier transform:

$$Q_l(\omega_y) = \sum_{i=-\infty}^{\infty} q_l[i] e^{-j\omega_y i}. \tag{14}$$

This yields an input–output relationship called a *bifrequency map* [1], as in Fig.1:

$$Y(\omega_y) = \sum_{l=0}^{P-1} Q_l(\omega_y) X(\omega_x), \tag{15}$$

where:

$$\omega_x = \omega_y - \frac{2\pi l}{P}. \tag{16}$$

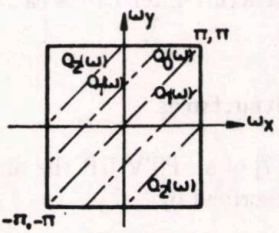

Fig. 1.– The bifrequency map.

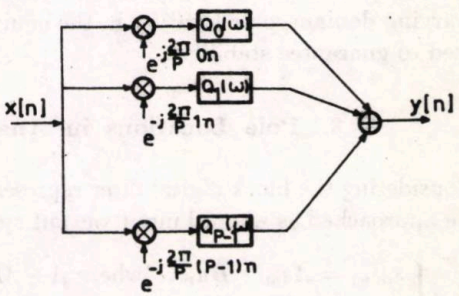

Fig. 2.– Q-form modulator filter structure.

Relation (15) describes a parallel bank of time invariant filters with modulated inputs, as in Fig.2.

Taking into account relations (4) and (5), other two analysis structures of PTV filters can be achieved:

$$\begin{aligned} y[n] = &\sum_{k=-\infty}^{\infty} r[n-kP, kP]\, x[kP] + \sum_{k=-\infty}^{\infty} r[n-kP-1, kP+1]\, x[kP+1] + \\ &+ \cdots + \sum_{k=-\infty}^{\infty} r[n-kP-P+1, kP+P-1]\, x[kP+P-1]. \end{aligned} \tag{17}$$

Every sum can represent the input–output relationship of a linear time invariant (LTI) filter, whose input is attacked with samples of $x[n]$ taken from P in P. Thus, relation (17) may be implemented with P filters $R_i(z)$ with coefficients $r[n,i]$, $(i = 0, ..., P-1)$, preceded by a commutator switch, as in Fig.3. Similarly, relation

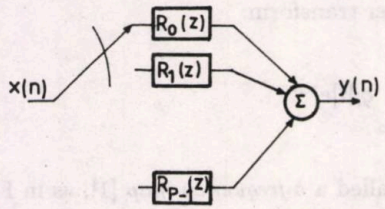

Fig. 3.– Commutator switch followed by filter bank structure.

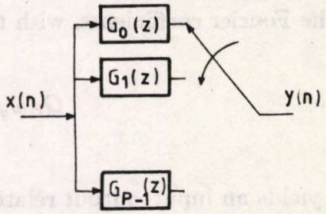

Fig. 4.– Filter bank followed by commutator switch.

(5) may be decomposed in P filters $G_i(z)$, with $i = 0, ..., P-1$, corresponding to $p[i,n]$ coefficients, followed by a commutator switch, as in Fig.4.

In the Q-form system, the modulators give rise to PTV behaviour, while in Figs.3 and 4, the commutators give rise to PTV behaviour. A PTV IIR filter may be implemented in one way as above, using LTI filters, each of order N, but this results in many multiplication. The stability of an PTV IIR filter is guaranteed if each LTI filter in the structure is stable. While poles and zeros do not exist in the time varying domain, pole location in the equivalent structure filter banks can be analyzed to guarantee stability.

3. Pole Locations in Analysis Structures

Considering the block digital filter representation [7] of an PTV IIR the filter may be approached as a multi input–output system, described by:

$$(18)\qquad \begin{cases} s_{m+1} = As_m + Bu_m, & \text{where } A \in M_{N\times N}(R),\ B \in M_{N\times P}(R), \\ v_m = Cs_m + Du_m, & \text{where } C \in M_{P\times N}(R),\ D \in M_{P\times P}(R). \end{cases}$$

$u_m = [x[mP], x[mP+1], ..., x[mP+P-1]]^t$ is the blocked input sequence created from filter input x and $v_m = [y[mP], y[mP+1], ..., y[mP+P-1]]^t$ is the blocked output sequence from which filter output y is obtained. The system can be diagonalized [6] namely:

$$(19)\ T\overline{s}_m = s_m; \qquad (20)\ \overline{s}_{m+1} = T^{-1}AT\overline{s}_m + T^{-1}Bu_m,\ v_m = CT\overline{s}_m + Du_m.$$

Introducing the notations:

$$(21)\qquad \Lambda = T^{-1}AT,\ \overline{B} = T^{-1}B,\ \overline{C} = CT,$$

it results:

$$(22)\qquad \overline{s}_{m+1} = \Lambda\overline{s}_m + \overline{B}u_m,\ v_m = \overline{C}\overline{s}_m + Du_m,$$

where:

$$(23)\qquad \Lambda = \text{diag}\,[\lambda_0, \lambda_1, ..., \lambda_{N-1}],$$

with: λ_i – the eigenvalue of matrix A. The recursive solution of these equations are:

$$v_0 = Du_0, \quad v_m = \sum_k \overline{C}\Lambda^{m-k} B u_{k-1} + Du_m. \tag{24}$$

In order to obtain the impulse response of the system, i.e. G r e e n's functions, the following condition are imposed:

$$u_m = 0, \quad \forall m \neq 0 \quad \text{and} \quad u_0 \in \{E_0, E_1, ..., E_{P-1}\}, \tag{25}$$

where:

$$\begin{cases} E_0 = [1\ 0\ ...\ 0]^t, \\ E_1 = [0\ 1\ 0\ ...\ 0]^t, \\ ..... \\ E_{P-1} = [0\ 0\ ...\ 0\ 1]^t. \end{cases} \tag{26}$$

If the input is E_i, it results:

$$v_0 = DE_i, \quad v_m = \overline{C}\,\Lambda^{m-1}\,\overline{B}E_i, \quad m > 0. \tag{27}$$

The kth element of the output vector can be written as:

$$v_{km} = \sum_{l=0}^{N-1} c_{kl} b_{li} \lambda_l^{m-1}, \quad m > 0, \quad v_{k0} = d_{ki}. \tag{28}$$

The z-transform of the kth output is:

$$V_k^i(z) = \sum_{m=0}^{\infty} v_{km}^i z^{-m} = \sum_{m=1}^{\infty} \sum_{l=0}^{N-1} c_{kl} b_{li} \lambda_l^{m-1} z^{-m} + d_{ki} z^{-0} = \tag{29}$$

$$= \sum_{l=0}^{N-1} c_{kl} b_{li} \frac{z^{-1}}{1 - \lambda_l z^{-1}} + d_{ki}.$$

One notes that each input of the block version is attached by an interpolated signal. In order to go the data rate of the scalar system, the above transfer function is interpolated by P:

$$V_k^i(z) = \sum_{l=0}^{N-1} c_{kl} b_{li} \frac{z^{-P}}{1 - \lambda_l z^{-P}} + d_{ki}, \quad \text{with} \quad k = 0, ..., P-1. \tag{30}$$

The scalar output y is obtained by aligning and adding in time the interpolated output functions:

$$Y^i(z) = \sum_{k=0}^{P-1} V_k^i(z) z^{-k} = \sum_{k=0}^{P-1} \left(\sum_{l-0}^{N-1} c_{kl} b_{li} \frac{z^{-P} z^{-k}}{1 - \lambda_l z^{-P}} + d_{ki} z^{-k} \right), \tag{31}$$

which represent the impulse responses of the system to an impulse at time i:

$$Y^i(z) = \sum_{k=0}^{P-1} \sum_{l=0}^{N-1} \frac{d_{ki} z^P + c_{kl} b_{li} - d_{ki} \lambda_l}{z^P - \lambda_l} z^{-k}. \tag{32}$$

Relation (32) may by written as:

$$Y^i(z) = \frac{N(z)}{D(z^P)}, \quad \text{where} \quad D(z^P) = \prod_{l=0}^{N-1} (z^P - l_1). \tag{33}$$

From (33) it results the following properties of PTV IIR filters.

In block structure the filters have the same repeated pole denominator and, consequently, the same repeated structure. These can be chosen to ensure stability of the overall structure. Since each filter has the same denominator with periodicity P, $D(z^P)$ can be pulled out of time varying part of the system. So any direct form of a PTV IIR filter is equivalent to a PTV FIR cascaded with a LTI filter of the form $1/D(z^P)$.

In the next step, the zeros of each filter of PTV filter in Q-form will be chosen. Thus, for each P filters, the denominator are:

$$N_i^*(z) = \prod_k (z - z_k) N_i(z), \tag{37}$$

where $\prod_k (z - z_k)$ represents the zeros needed to cancel the unwanted poles of the P groups of poles and $N_i(z)$ represents zeros necessary to form the frequency characteristic. For the first filter with index 0 the first group of poles will be cancel with zeros from the term $\prod_k (z - z_k)$ from (37). Because the number of poles and zeros of a transfer function of an IIR filter are the same, it results that terms $N_i(z)$ have the same degree, for any $i = 0, ..., P-1$. The number of zeros of $N_i(z)$ will be equal to the number of poles of prototype filter. There are two ways to locate these zeros. One consists in considering the relation:

$$N_0(z) = N_1(z) = \cdots = N_{P-1}(z), \tag{38}$$

which means that the zeros will have fixed position on unit circle between the groups of poles, otherwise the frequency response of the filter that corresponds to the pole group, will be altered. Thus, K zeros will be placed (K is the prototype filter order) in P domains.

If $K < P$, there are domains between pole groups without zeros. This is a very unfavourable case. When $K > P$ there are domains between pole groups with different number of zeros and their placement couldn't be made judiciously for each domain.

A second solution consists in considering the terms $N_i(z)$ defined for each domain namely: a) the condition that the zeros be located in the same place as a pole group haven't to be still fulfill, which increase the domain of zeros location; b) the frequency response of the LTI filters in Q-form could approach the ideal one, by judicious placement of zeros.

4. Design Method

A method to design the prototype filter with high performances as in Fig.5 (with zeros in desired positions) is proposed. The basic idea of the method is to turn round the zeros simultaneously with poles. This idea is encouraged by the fact that elliptic filters have no zeros in the range $[-\pi/2P, \pi/2P]$, (for the prototype filter).

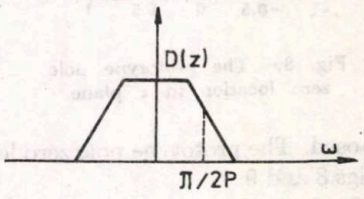

Fig. 5.– The prototype characteristic.

Due to this reason at a simultaneous turning of poles and zeros with the same angle, there is no danger to overlap the zeros over poles, as in Figs.6 and 7. This last solution gives substantial improvements on the global filter performances. The LTI IIR filter coefficients are easily obtained, using the prototype filter:

$$D_1(z^P) = \prod_{i=0}^{P-1} D(zW^iW^{1/2}), \tag{39}$$

where $D(z)$ is the denominator of the prototype filter.

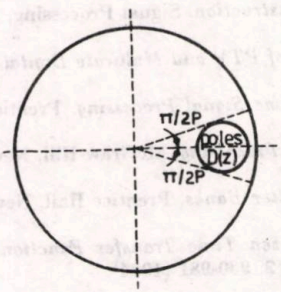

Fig. 6.– Pole location of the prototype filter.

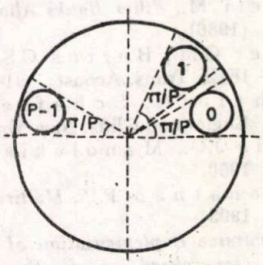

Fig. 7.– Repeated pole structure.

In order to calculate the PTV FIR coefficients, the denominator coefficients, $N_i^*(z)$, will be computed and relation (36) will be applied.

Based on the decomposition of an PTV IIR filter in two sections, a PTV FIR one and a LTI IIR filter, a repeated pole structure obtained by turning round simultaneously the poles and zeros of a prototype filter, with high performances is

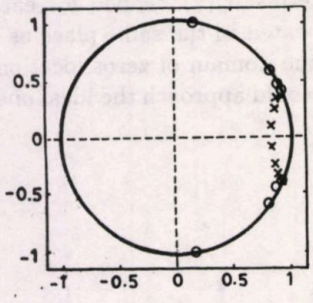

Fig. 8.– The prototype pole zero location in z plane.

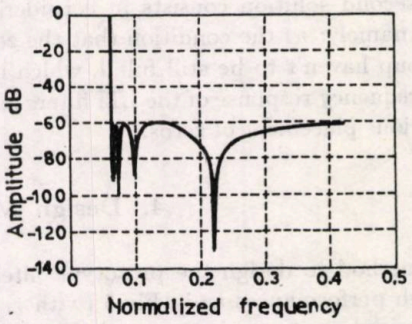

Fig. 9.– The prototype transfer function.

proposed. The prototype pole zero location and its transfer function are presented in Figs.8 and 9.

In the basic method, the order of PTV FIR filters were $(n-1)P+n$, where $(n-1)P$ represents the number of zeros necessary to cancel the unwanted poles and n – the number of filter zeros. The proposed method requires order n and the filter may be implemented in one of direct or transposed form I or II.

Received, July 5, 1995

Technical University "Gh.Asachi", Jassy,
Department of Telecommunications

REFERENCES

1. Prater J.S., Loeffler C.M., *Analysis and Design of PTV IIR Filters, with Applications to Transmultiplexing.* IEEE Trans. Signal Processing, 2715-2725 (1992).
2. Ferrara E.R., *Frequency Domain Implementations of PTV Filters.* IEEE Trans. Acoust., 883-892 (1985).
3. Vetterli M., *Filter Banks Allowing Perfect Reconstruction.* Signal Processing, 219-244 (1986).
4. Loeffler C.M., Burrus C.S., *Optional Design of PTV and Multirate Digital Filters.* IEEE Trans. Acoust., 991-997 (1984).
5. Oppeheim A., Schaffer R., *Discrete Time Signal Processing.* Prentice Hall, Englewood Cliffs, New York, 1989.
6. Proakis J.G., Manolakis A., *Digital Signal Processing.* McGraw-Hill, New York, 1990.
7. Vaidyanathan P.P., *Multirate Systems and Filter Banks.* Prentice Hall, New York, 1993.
8. * * * *Recursive Implementation of LTV Filters – Frozen Time Transfer Function versus Generalized Transfer Function.* Proc. IEEE, **72**, 980-981 (1984).

O METODĂ DE PROIECTARE A FILTRELOR IIR PERIODIC VARIANTE ÎN TIMP CU APLICAŢII ÎN TRANSMULTIPLEXARE (I)

(Rezumat)

Plecând de la descompunerea unui filtru IIR periodic variant în timp (PTV) în două secţiuni, una IIR liniar invariantă în timp şi alta FIR periodic variantă în timp, se propune o metodă de proiectare a filtrului global IIR PTV, obţinând o structură de poli repetitivi prin rotirea simultană a polilor şi zerourilor unui filtru prototip de performanţe ridicate.

BULETINUL INSTITUTULUI POLITEHNIC DIN IAŞI
Tomul XLII (XLVI), Fasc. 1–2, 1996
Secţia III
ELECTROTEHNICĂ. ENERGETICĂ. ELECTRONICĂ

D.C. 621.319.55

CONTRIBUTION TO THE ANALYSIS OF THE RELAXATION OSCILLATOR WITH NON-LINEAR COIL

BY
VIOREL-MIHAIL COSMA, M. LOZOVAN,
I. ONCIULESCU and VIRGIL MOGA

This work aims to establish the period of the relaxation oscillations occurring in the electric circuits that include a non-linear resistor with dynatron characteristics and a loss-free non-linear coil. With the view to simplify the analysis, the characteristics of the two elements are considered as piecewise linearized.

1. Introduction

Let's consider the electric circuit presented in Fig.1, where L is a loss-free non-linear coil, whose piecewise linearized characteristics:

$$\Psi = L(i)i, \quad \Psi = \begin{cases} L_1 i, & \text{for } i \in (0, I_k), \\ L_1 I_k + L_2(i - I_k), & \text{for } i > I_k, \end{cases} \tag{1}$$

are presented in Fig.2, L_1 and L_2 representing the inductances corresponding to the two segments of the characteristics $\Psi(i)$ $(L_2 < L_1)$.

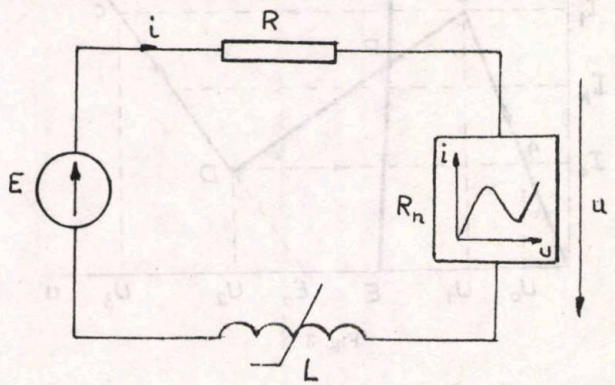

Fig. 1

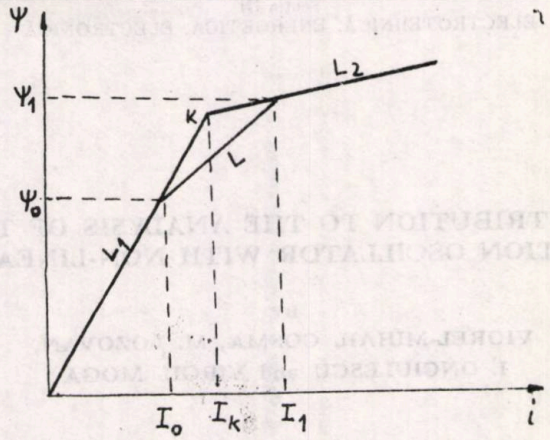

Fig. 2

The non-linear resistor R_n (Fig.1) has its dynatron characteristics $i(u)$ approximated by three line segments (Fig.3). It is preferably to express the positive resistances segments R_1, R_2 of the characteristics under the form:

$$(2) \qquad u = \begin{cases} R_1 i, & \text{for } i \in (0, I_1), \\ U_2 + R_2 i, & \text{for } i > I_0, \text{ with } U_2 = E_0 + R_2 I_0, \end{cases}$$

where the value E_0 is graphically established (Fig.3).

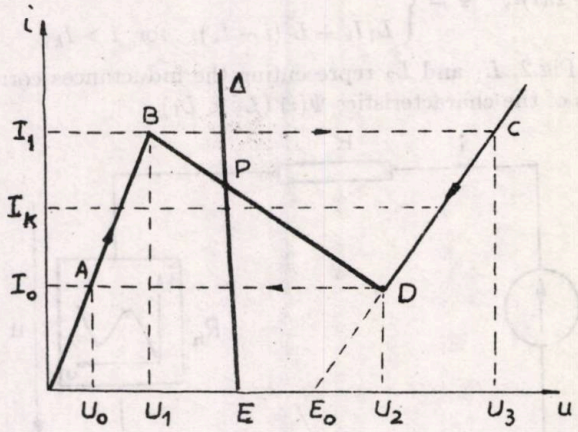

Fig. 3

If the self-excitation conditions are satisfied in the given circuit, by the intersection of the load line $\Delta(E - Ri)$ with the static characteristics of the non-linear

resistor in the region of negative resistance (point P, Fig.3), the unstable operating point will travel along the relaxation cycle $ABCD$ in the plane of the $i(u)$ characteristics (Fig.3). The form of the generated oscillations depends on the inductance value in the circuit and on the maximum excursion of the voltage and current during the operation.

This self-excitation process is described by the differential equation:

$$\frac{d\Psi}{dt} + Ri + u = E, \tag{3}$$

obtained by applying the generalized Ohm's law to the electric circuit presented in Fig.1.

2. Considerations on the Relaxation Oscillation Period

Since the commutation times corresponding to the jumps of the operation point from B to C, and from D to A respectively, are very short, the relaxation oscillations period practically corresponds to the slow evolution of the operation point on the rising portion of the non-linear resistor characteristics, with the resistances R_1 and R_2.

Let's note by t_1 and t_2 the two times corresponding to the evolutions on the AB and CD portions respectively. These times are calculated from the relation (4) where the expressions (1),...,(3) are taken into account, also correlating the current excursion corresponding to the non-linear resistor and coil characteristics (Figs.2 and 3):

$$dt = \frac{L(i)\,di}{E - Ri - u(i)}. \tag{4}$$

The case is considered where the maximum current excursion, $\Delta I_{max} = I_1 - I_0$, occurs near the angular point K of the non-linear coil characteristics (Fig.2).

From relation (4) the expressions of the two times result:

$$\begin{aligned} t_1 &= L_1 \int_{I_0}^{I_k} \frac{di}{E-(R+R_1)i} + L_2 \int_{I_k}^{I_1} \frac{di}{E-(R+R_1)i} = \\ &= \frac{L_1}{R+R_1} \ln \frac{E-(R+R_1)I_0}{E-(R+R_1)I_k} + \frac{L_2}{R+R_1} \ln \frac{E-(R+R_1)I_k}{E-(R+R_1)I_1}, \end{aligned} \tag{5}$$

$$\begin{aligned} t_2 &= L_2 \int_{I_1}^{I_k} \frac{di}{E-E_0-(R-R)i} + L_1 \int_{I_k}^{I_0} \frac{di}{E-E_0-(R+R_2)i} = \\ &= \frac{L_2}{R+R_2} \ln \frac{E_0+(R+R_2)I_1-E}{E_0+(R+R_2)I_k-E} + \frac{L_1}{R+R_2} \ln \frac{E_0+(R+R_2)I_k-E}{E_0+(R+R_2)I_0-E}. \end{aligned} \tag{6}$$

The notations:

$$\beta_1 = \frac{(R+R_1)(I_1-I_0)}{E-(R+R_1)I_0}, \quad \beta_1 \in (0,1), \tag{7}$$

$$\beta_2 = \frac{(R+R_2)(I_1-I_0)}{E_0+(R+R_2)I_0-E}, \quad \beta_2 > 0, \tag{8}$$

will be utilized.

The time constants of the electric circuit during the slow evolution of the operation point have the expressions:

$$\tau_{11} = \frac{L_1}{R+R_1}, \qquad \tau_{12} = \frac{L_2}{R+R_1} \tag{9}$$

and

$$\tau_{21} = \frac{L_1}{R+R_2}, \qquad \tau_{22} = \frac{L_2}{R+R_2}, \tag{10}$$

respectively.

The parameter:

$$\alpha = \frac{I_k - I_0}{I_1 - I_0} \tag{11}$$

is introduced.

For a certain characteristics $i(u)$, by shifting the maximum current excursion, $\Delta I_{\max}$, around the angular point (by means of a current generator) ($I_k \in (I_0, I_1)$) it follows:

$$\alpha \in (0,1). \tag{12}$$

By replacing the notations (7),...,(11) in the expressions (5) and (6) of the times t_1 and t_2 respectively, the expression of the relaxation oscillations period will result:

$$T \simeq t_1 + t_2 = (\tau_{11}-\tau_{12}) \ln \frac{1}{1-\alpha\beta_1} + \tau_{12} \ln \frac{1}{1-\beta_1} + \tag{13}$$
$$+ (\tau_{21}-\tau_{22}) \ln(1+\alpha\beta_2) + \tau_{22} \ln(1+\beta_2) = T(\alpha).$$

The shape of the $T(\alpha)$ characteristics is represented in Figs.4 and 5 by the curves *1*, depending on the coordinates of the $ABCD$ relaxation cycle.

Let

$$L = \frac{\Psi_1 - \Psi_0}{I_1 - I_0} \tag{14}$$

be the incremental inductance corresponding to the maximum current excursion ΔI_{max} (Fig.2). This inductance can be expressed in terms of the parameter α:

$$L = L_2 + \alpha(L_1 - L_2), \quad L \in (L_2, L_1). \tag{15}$$

Taking into account the relations (15), (9), (10) the expression of the relaxation oscillation period corresponding to this inductance may be written:

$$T = [\tau_{12} + \alpha(\tau_{11} - \tau_{12})] \ln \frac{1}{1 - \beta_1} + [\tau_{22} + \alpha(\tau_{21} - \tau_{22})] \ln(1 + \beta_2). \tag{16}$$

The $T(\alpha)$ dependence is given by the curves *2* in Figs.4 and 5.

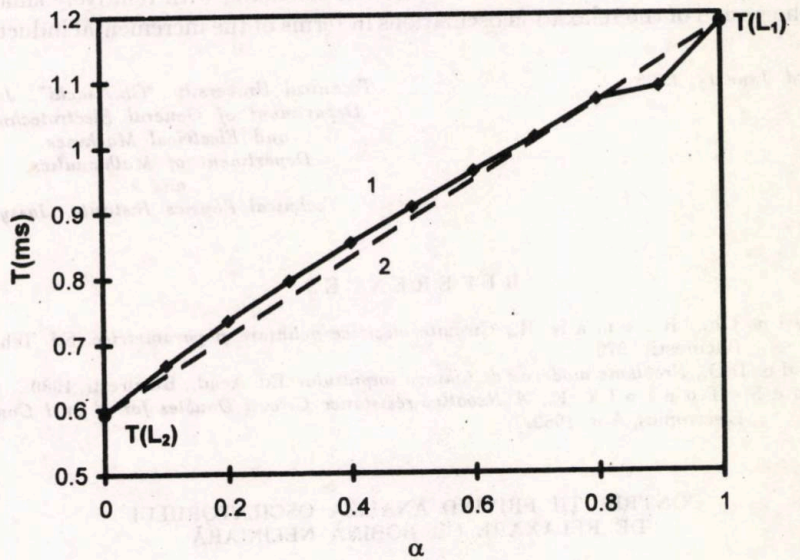

Fig. 4

The values of the period T correspond to the electric circuit that has a nonlinear resistor with controlable characteristics $i(u)$ and the following parameters:

1. I_1=39 mA, I_0=21 mA, E_0=7.5 V, R_1=160 Ω and R_2=200 Ω;
2. I_1=28 mA, I_0=21 mA, E_0=6.4 V, R_1=160 Ω and R_2=200 Ω.

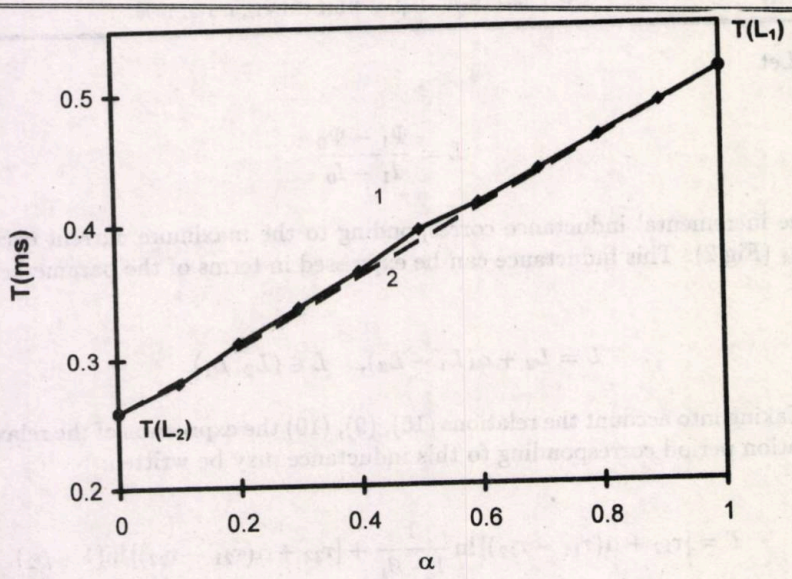

Fig. 5

By reducing the current excursion one can calculate, with relatively small errors, the period of the relaxation oscillations in terms of the incremental inductance (16).

Received, June 14, 1995

Technical University "Gh.Asachi", Jassy,
Department of General Electrotechnics and Electrical Machines
Department of Mathematics,
and
Technical Physics Institute, Jassy

REFERENCES

1. S a v i n Gh., R o s m a n H., *Circuite electrice neliniare şi parametrice.* Ed. Tehnică, Bucureşti, 1973.
2. S a n d u D.D., *Probleme moderne de tehnica impulsului.* Ed. Acad., Bucureşti, 1980.
3. B r o c h - T o n i o l a F., *A Negative-resistance Circuit Doubles for V or I Control.* Electronics, Apr. 1969.

CONTRIBUŢII PRIVIND ANALIZA OSCILATORULUI DE RELAXARE CU BOBINĂ NELINIARĂ

(Rezumat)

Se urmăreşte determinarea perioadei oscilaţiilor de relaxare ce apar în circuitele electrice ce conţin un rezistor neliniar cu caracteristică $i(u)$ de tip dynatron şi o bobină neliniară fără pierderi. În scopul simplificării analizei se consideră caracteristicile celor două elemente de circuit liniarizate pe porţiuni.

BULETINUL INSTITUTULUI POLITEHNIC DIN IAŞI
Tomul XLII (XLVI), Fasc. 1-2, 1996
Secţia III
ELECTROTEHNICĂ. ENERGETICĂ. ELECTRONICĂ

C.D. 621.3.018.6

SUR LES CONDITIONS D'APPARITION DES OSCILLATIONS MÉCANIQUES DANS UN SYSTÈME ÉLECTROMECANIQUE

III. EXTENSION DE L'ÉTUDE DE LA STABILITÉ DES SOLUTIONS

PAR
MARIANA BUZDUGA

On détermine l'influence exercée par les paramètres de construction de l'instrument magnétoélectrique d'un circuit qui contient aussi une diode tunel, sur les conditions d'apparition des oscillations mécaniques du système mobile.

L'analyse est effectuée dans le cas où le point de fonctionnement du circuit se trouve n'importe où sur l'arc à pente négative de la caractéristique de la diode et pour un tel domaine de variation de la résistance du circuit qui assure la monotonie de la fonction $d\alpha'(u'')/dt$.

1. Introduction

Les oscillations mécaniques qui apparaissent dans un système électromécanique hybride, formé par un circuit électrique qui contient une diode tunel et un instrument magnétoélectrique, ont été étudiées en [1] et [2] dans le cas particulier quand le point de fonctionnement du système se trouve au centre de la zone descendante de la caractéristique de la diode tunel.

Dans ce qui suit on élargit l'analyse pour le cas, plus général, d'un point de fonctionnement situé n'importe où sur l'arc à pente négative de la caractéristique.

2. Equations de fonctionnement du système

Par rapport au cas analysé dans les Notes antérieures [1] et [2], l'origine du système de coordonnées est déplacée de O' en $O''(U_1', -I_1')$, avec $U_1' < U_V'$, conformément à la Fig.1, qui devient le point de régime permanent du circuit.

Dans ce qui suit, les variables considérées face à la nouvelle origine seront notées par $(\,'')$.

On peut écrire les relations évidentes:

$$(1) \qquad i' = i'' - I_1', \qquad u' = u'' + U_1', \qquad \alpha' = \alpha_1' + \alpha'',$$

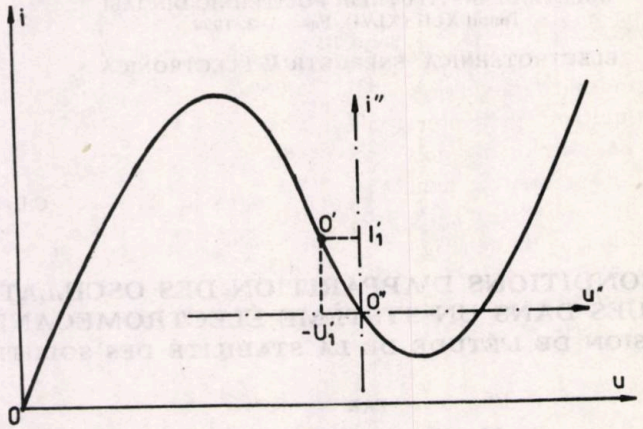

Fig. 1

tandis que l'équation qui approxime la caractéristique de la diode devient:

$$i'' - I_1' = -a_1(u'' + U_1') + a_3(u'' + U_1')^3, \tag{2}$$

d'où résulte que, pour le régime permanent:

$$-I_1' = -a_1 U_1' + a_3 U_1'^3. \tag{3}$$

Les équations de fonctionnement du système hibride de la Fig.2 devienent:

$$\begin{cases} R'i'' + u'' + N\Phi_0 \frac{d\alpha''}{dt} = 0, \\ J\frac{d^2\alpha''}{dt^2} + B\frac{d\alpha''}{dt} + C\alpha'' = N\Phi_0 i''. \end{cases} \tag{4}$$

En remplaçant (3) en (4) on a:

Fig. 2

$$\frac{d\alpha''}{dt} = Pu''^3 + Nu''^2 + Mu'', \tag{5}$$

avec:

$$P = -\frac{a_3 R'}{N\Phi_0}; \quad M = -\frac{1}{N\Phi_0}(1 - R'a_1 + 3a_3 R' U_1'^2); \quad N = -\frac{3a_3 R' U_1'}{N\Phi_0}. \tag{6}$$

De l'analyse du comportement de la fonction (5) et de sa dérivée on a établi qu'elle présente un domaine de stricte monotonie pour $R' \in (0, 1/a_1)$ où elle est décroissante (Fig.3 *a*) et elle prend la forme de la Fig.3 *b* pour $R' > 1/a_1$.

Pour l'intervalle $R' \in (0, 1/[a_1(1 - \frac{1}{4}(U_1'/U_V')^2])$ la fonction (5) a un seul zéro, en O''; pour $R' = 1/[a_1(1 - \frac{1}{4}(U_1'/U_V')^2]$ elle devient tangente à l'axe $O''u''$ et pour des valeurs plus grandes de R' elle présente trois zéros.

Pour l'analyse qui suit c'est intéressant de savoir le position des extrêmums de la fonction (5), par rapport au point de fonctionnement O'' du système. Les calculs montrent qu'ils sont situés dans le domaine $u'' \leq 0$ pour $R' \in (1/[a_1(1 - -\frac{1}{4}(U_1'/U_V')^2)], 1/[a_1(1-(U_1'/U_V')^2)])$, pour $R' = 1/[a_1(1-(U_1'/U_V')^2)]$ l'un d'entre eux se situant juste dans l'origine (Fig.3 *c*) et pour des valeurs plus grandes de R' un des extrêmums est situé dans le domaine $u'' > 0$. Il s'ensuit, évidemment, que la pente de la fonction (5) dans le point de fonctionnement du système est négative tant que $R' < 1/(a_1[1 - (U_1'/U_V')^2])$.

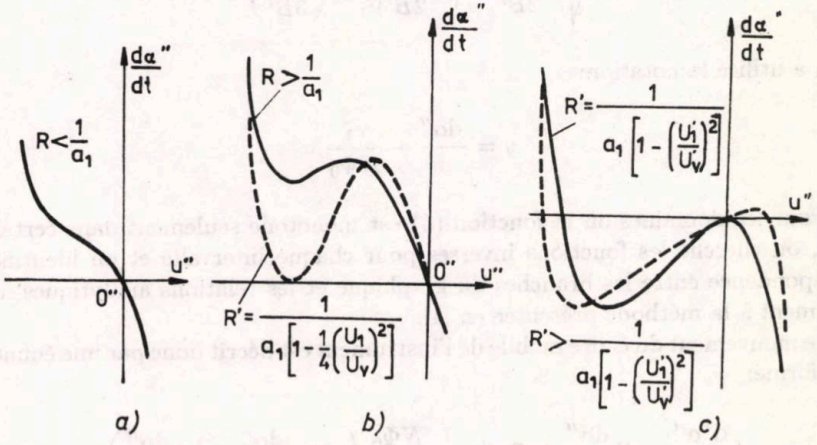

Fig. 3

Pour la détermination des inverses de la fonction (5) dans les intervalles de monotonie on effectue le changement de variable:

$$u'' = x - \frac{N}{3P} = x - U_1'. \tag{6}$$

On obtient la relation:

$$\frac{\mathrm{d}\alpha''}{\mathrm{d}t} - \frac{e_1}{N\Phi_0} = -A'x - B'x^3, \tag{7}$$

où:

$$e_1 = U_1' - R'a_1U_1' + a_3R'U_1'^3; \tag{8}$$

les coefficients A' et B' ont les valeurs données dans les Notes antérieures [1] et [2] à savoir:

$$A' = \frac{1 - R'a_1}{N\Phi_0}, \qquad B' = \frac{R'a_3}{N\Phi_0}, \tag{9}$$

avec a_1 et a_3 – les coefficients du polynôme d'approximation de la caractéristique de la diode tunel.

Pour le domaine de stricte monotonie, l'inverse de la fonction (7) a la forme donnée par les relations de Cardan:

$$u'' = -U_1' + \sqrt[3]{-\frac{y}{2B'} + \sqrt{\frac{y^2}{(2B')^2} + \left(\frac{A'}{3B'}\right)^3}} + \tag{10}$$
$$+ \sqrt[3]{-\frac{y}{2B'} - \sqrt{\frac{y^2}{(2B')^2} + \left(\frac{A'}{3B'}\right)^3}},$$

où on a utilisé la notation:

$$y = \frac{\mathrm{d}\alpha''}{\mathrm{d}t} - \frac{e_1}{N\Phi_0}. \tag{11}$$

Pour les domaines où la fonction (5) est monotone seulement dans certaines zones, on cherche les fonctions inverses pour chaque intervalle et on identifie la correspondence entre les branches du graphique et les relations analytiques, conformément à la méthode présentée en [1].

Le mouvement du cadre mobile de l'instrument est décrit donc par une équation de la forme:

$$J\frac{\mathrm{d}^2\alpha''}{\mathrm{d}t^2} + B\frac{\mathrm{d}\alpha''}{\mathrm{d}t} + C\alpha'' = -\frac{N\Phi_0}{R'}\left(N\Phi_0\frac{\mathrm{d}\alpha''}{\mathrm{d}t} + u''\frac{\mathrm{d}\alpha''}{\mathrm{d}t}\right). \tag{12}$$

On doit faire l'observation que la situation analysée en [1] et [2], quand le point de fonctionnement se trouvait au centre de la zone à pente négative de la caractéristique de la diode tunel, résulte comme un cas particulier de celle présente, à laquelle on arrive pour $U_1' \to 0$.

3. Étude de la stabilité du fonctionnement du circuit dans le domaine de stricte monotonie: $R' \in (0, 1/a_1)$

Si dans l'équation (12) on utilise la substitution:

$$\frac{\mathrm{d}\alpha''}{\mathrm{d}t} = z; \qquad \frac{\mathrm{d}^2\alpha''}{\mathrm{d}t^2} = \frac{\mathrm{d}z}{\mathrm{d}t} = z\frac{\mathrm{d}z}{\mathrm{d}\alpha''}, \tag{13}$$

il résulte:

$$z\frac{\mathrm{d}z}{\mathrm{d}\alpha''} + \frac{B}{J}z + \frac{C}{J}\alpha'' = -\frac{N\Phi_0}{R'J}\left[N\Phi_0 z + u''(z)\right], \tag{14}$$

ou sous la forme équivalente:

$$\frac{\mathrm{d}z}{\mathrm{d}\alpha''} = \frac{-\dfrac{C}{J}\alpha'' - \dfrac{B}{J}z - \dfrac{(N\Phi_0)^2}{R'J} - \dfrac{N\Phi_0}{R'J}u''(z)}{z} = \frac{Q(z,\alpha'')}{P(z,\alpha'')}. \tag{15}$$

Le point singulier de l'équation (15) est situé à $\alpha'' = 0$, $z = 0$. Comme le système est stable du point de vue de la structure, on va négliger la nonlinéarité autour du point singulier, conformément à la première approximation de L y a p o u n o f f, pour obtenir l'expression:

$$\frac{\mathrm{d}z}{\mathrm{d}\alpha''} = \frac{c\alpha'' + dz}{d\alpha'' + bz} \tag{16}$$

pour laquelle on va étudier la stabilité locale. Dans ce but on substitue la fonction $u''(z)$, qui correspond aux termes nonlinéaires, par son approximation linéaire autour du point $z = 0$, c'est-à-dire:

$$u''(z) \cong \left.\frac{\mathrm{d}u''(z)}{\mathrm{d}z}\right|_{z=0} z. \tag{17}$$

Compte tenu que $u''(z)$ est l'inverse (globale ou dans un domaine restreint) de la fonction $z(u'') = \mathrm{d}\alpha''(u'')/\,\mathrm{d}t$, entre les pentes des deux fonctions il y a la relation:

$$\frac{\mathrm{d}u''(z)}{\mathrm{d}z} = \frac{1}{\mathrm{d}z(u'')/\,\mathrm{d}u''}. \tag{18}$$

Comme:

$$\left.\frac{\mathrm{d}z(u'')}{\mathrm{d}u''}\right|_{u''=0} = -A' - 3B'U_1'^2, \tag{19}$$

il résulte, après l'introduction de cette valeur dans les rélations (18) et (17),

$$u''(z) \simeq -\frac{z}{A' + 3B'U_1'^2} \tag{20}$$

et la relation (15) devient:

$$\frac{\mathrm{d}z}{\mathrm{d}\alpha''} = -\frac{\dfrac{B}{J}z + \dfrac{(N\Phi_0)^2}{R'J}z + \dfrac{N\Phi_0}{R'J}\cdot\dfrac{z}{-A' - 3B'U_1'^2} + \dfrac{C}{J}\alpha''}{z}. \tag{21}$$

Les coefficients $a, \ldots, d$ de la relation (16) ont les significations ci-dessous:

$$a = 0,\quad b = 1,\quad c = -\frac{C}{J},\quad d = -\frac{B}{J} - \frac{(N\Phi_0)^2}{R'J} + \frac{N\dot{\Phi}_0}{R'J(A' + 3B'U_1'^2)}. \tag{22}$$

Vu que le signe de d établit le caractère stable ($d < 0$) ou instable ($d > 0$) de la solution du système dans le point respectif, dans ce qui suit on analyse les propriétés de la fonction $d(R')$.

Tous calculs effectués, l'expression de $d(R')$ devient:

$$d(R') = -\frac{BR'a_1\left[1-(U_1'/U_V')^2\right] - B + (N\Phi_0)^2 a_1[1-(U_1'/U_V')^2]}{J[1-R'a_1(1-U_1'^2/U_V'^2)]} \tag{23}$$

et son signe change pour

$$R_1' = \frac{1}{a_1[1-(U_1'/U_V')^2]} - \frac{(N\Phi_0)^2}{B}, \quad R_2' = \frac{1}{a_1[1-(U_1'/U_V')^2]}. \tag{24}$$

Comme $U_1' < U_V'$ et $a_1 > 0$, alors $R_2' > 0$ et $R_1' < R_2'$ et fonction du terme $(N\Phi_0)^2/B$, R_1' peut être positif ou négatif; à savoir il est positif pour:

$$B > (N\Phi_0)^2 a_1[1-(U_1'/U_V')^2] \tag{25}$$

et négatif pour

$$B < (N\Phi_0)^2 a_1[1-(U_1'/U_V')^2]. \tag{26}$$

Le signe du coefficient d est positif, indiquant un fonctionnement instable pour $R' \in (R_1', R_2')$ et négatif pour $R' > R_2'$. Le domaine de fonctionnement instable est maximum, ça veut dire $R' \in (0, R_2')$, dans le cas des mécanismes à faible amortissement, quand la condition (26) est satisfaite. Le même domaine devient plus restreint pour les instruments pour lesquels la relation (25) est valable, donc $R_1' > 0$, qui est d'autant plus proche de R_2' que l'amortissement est plus fort. Ayant en vue que

$$\lim_{R' \nearrow R_2'} d(R') = +\infty \tag{27}$$

on peut affirmer que quelques soient les paramètres de l'instrument utilisé, il y a toujours un domaine pour R' situé à la gauche de R_2' pour lequel le fonctionnement du système est instable.

Pour vérifier la possibilité d'existence d'un cycle limite dans le domaine de fonctionnement instable du système on applique la première proposition de B e n d i x o n [4], qui établit que si la fonction $\partial P/\partial \alpha'' + \partial Q/\partial z$ garde le même signe dans le domaine de variation des variables alors il n'y a pas de cycle limite. Dans le cas étudié:

$$\frac{\partial P}{\partial \alpha''} = 0; \quad \frac{\partial Q}{\partial z} = -\frac{B}{J} - \frac{(N\Phi_0)^2}{R'J} - \frac{N\Phi_0}{R'J} \cdot \frac{\mathrm{d}u''(z)}{\mathrm{d}z}. \tag{28}$$

Utilisant la relation (18) on a:

$$\frac{\partial Q}{\partial z} = -\frac{B}{J} - \frac{(N\Phi_0)^2}{R'J} - \frac{N\Phi_0}{R'J} \cdot \frac{1}{-A' - 3B'(u'' + U_1')^2}, \tag{29}$$

dont le signe doit être étudié dans le domaine D, de variation de u'' en fonction du paramètre R':

$$u'' \in (-2U_V' - U_1'; 2U_V' + U_1') \stackrel{\text{not}}{=} D. \tag{30}$$

Pour la relation (29) on cherche les valeurs de R' pour lesquelles les racines du numérateur et du dénominateur sont réelles, distinctes et situées en D. De l'intersection des intervalles calculés il résulte que pour n'importe quel:

$$R' > \frac{1}{a_1} - \frac{(N\Phi_0)^2}{B} \tag{31}$$

il y a un changement de signe de l'expression $\partial Q(u'')/\partial z$ dans le domaine D.

Si l'on compare l'intervalle (31) à (R_1', R_2'), donné par les relations (24), on constate que pour tout le domaine de fonctionnement instable du système on ne peut pas exclure la possibilité d'existence d'un cycle limite.

4. Résultats expérimentaux

Deux cas ont été étudiés: le premier est celui déjà connu de [1] et [2] quand on a considéré la diode TD716Ge, pour laquelle $a_1 = 0,0202$ et $a_3 = 0,262$ et un instrument magnétoélectrique ayant les paramètres constructifs: $J = 5 \cdot 10^{-7}$ kg m^2, $C = 10^{-5}$ Nm/rad, $N = 80$ sp., $\Phi_0 = 7 \cdot 10^{-5}$ Wb.

Pour le coefficient d'amortissement B on a considéré des valeurs dans le domaine usuel pour les instruments de ce type [5]. La simulation a été réalisée à l'aide d'un ordinateur pour diverses valeurs de R', en dehors et à l'intérieur du domaine d'instabilité (R_1', R_2') déterminé ci-dessus.

Le comportement du système a été celui qu'on attendait, en mettant en évidence la limitation du domaine d'apparition des oscillations mécaniques avec l'augmentation de l'amortissement du circuit. Dans la Fig.4 on présente un exemple de réponse du système pour $B = 10^{-6}$ Nm sec./rad. et $R' = 15\ \Omega$ (Fig.4*a*) respectif $R' = 30\ \Omega$ (Fig.4*b*). Pour les deux situations on donne aussi les diagrammes dans le plan des phases.

Dans le deuxième cas étudié on a utilisé une diode RCA 1N3848 pour laquelle les coefficients du polynôme d'approximation sont $a_1 = 0,048$, $a_3 = 0,79$ et un instrument magnétoélectrique type M4 avec les paramètres modifiés comme il suit: $J = 5 \cdot 10^{-7}$ kg m^2; $C = 1,5 \cdot 10^{-6}$ Nm/rad.; $N = 70$ sp., $\Phi_0 = 1,54 \cdot 10^{-6}$ Wb, $R_{\text{bob}} = 11,5\ \Omega$ et $B = 10^{-9}$ Nm sec./rad.

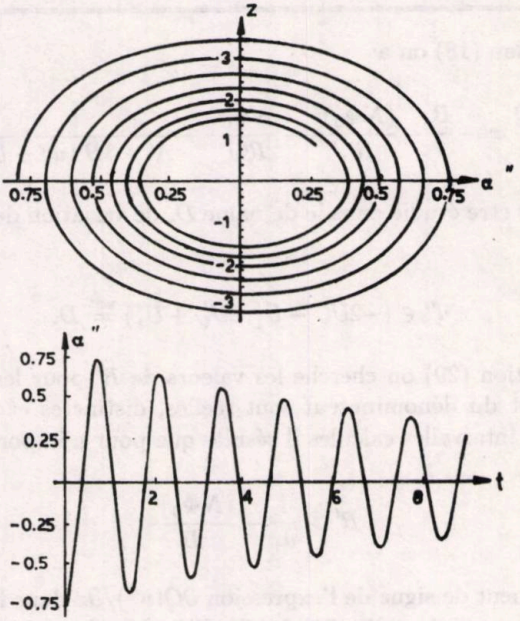
z
3
2
1
-1
-2
-3
0.75
0.5
0.25
0.25
0.5
0.75
α''
α''
0.75
0.5
0.25
-0.25
-0.5
-0.75
2
4
6
8
t

a)

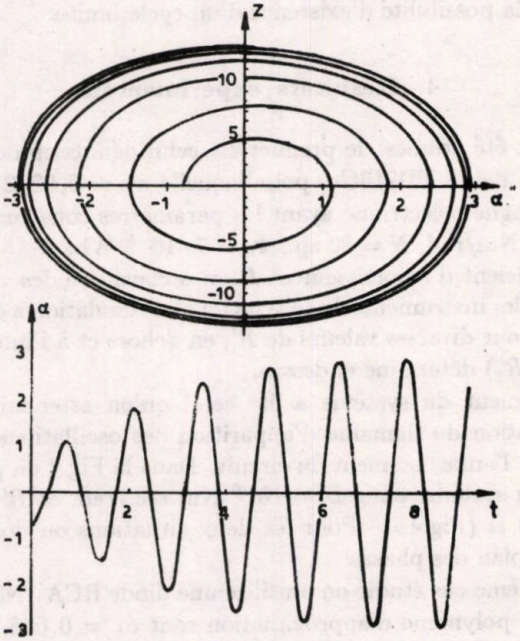
z
10
5
-5
-10
-3
-2
-1
1
2
3
α
α
3
2
1
-1
-2
-3
2
4
6
8
t

b)

Fig. 4

La valeur calculée de la limite de séparation des domaines de fonctionnement stable et instable est $R'_{\text{lim}} = 9,65\ \Omega$, moindre que la résistance minimum du circuit (car $R'_{\text{lim}} < R_{\text{bob}}$).

Pendant les expérimentations on a obtenu des oscillations mécaniques dans tout le domaine de variation de R', ($R' < 1/a_1$) et pour des points de fonctionnement situés n'importe où dans la zone descendante de la caractéristique $i(u)$, donc pour U'_1 variable.

Le même cas simulé à l'aide de l'ordinateur confirme les résultats obtenus par voie expérimentale.

On a observé aussi la possibilité d'apparition des oscillations entretenues pour des valeurs R' supérieures à la limite considérée jusqu'ici, de $1/a_1$, quand la fonction $\mathrm{d}\alpha''/\mathrm{d}t$ n'est plus monotone. L'analyse de ces cas fera le sujet d'une future étude.

5. Conclusions

On présente une extension de l'analyse du fonctionnement du circuit de la Fig.2 pour le cas plus général quand le point de fonctionnement est situé n'importe où dans la zone de pente négative de la caractéristique de la diode tunel.

On a mis en évidence le resserement du domaine d'apparition des oscillations mécaniques par la variation de R', avec l'augmentation du coefficient d'amortissement de l'instrument magnétoélectrique. L'analyse a été effectuée seulement pour le domaine de variation de R' qui assure la monotonie de la fonction $\mathrm{d}\alpha''(u'')/\mathrm{d}t$, caractérisée par la relation (5).

En même temps on a observé, pendant les expérimentations, que les oscillations mécaniques apparaissent aussi pour un domaine plus large de variation de R', cas qui sera analysé ultérieurement.

Reçue le 12 mai 1995

Université Technique „Gh.Asachi", Jassy,
Chaire de Mesures Électriques

BIBLIOGRAPHIE

1. B u z d u g a M., *Conditions pour générer les oscillations mécaniques dans un système électromécanique.* I.*L'établissement des équations du mouvement.* Bul. Inst. polit., Iaşi, **XL (XLIV)**, *1-4*, s.III, 55-58 (1994).

2. B u z d u g a M., *Conditions pour générer les oscillations mécaniques dans un système électromécanique.* II.*Étude de le stabilité des solutions.* Bul. Inst. polit., Iaşi, **XLI (XLV)**, *3-4*, s.III, 55-58 (1995).

3. S a v i n G., G r o v u M., *Elektromechanische Schwingungen, die mit nichtlinearen aktiven Netzwerken selbsterregt werden.* Archiv für Elektrot., **62**, 5-12 (1980).

4. G i b s o n J.E., *Sisteme automate neliniare* (trad. de l'anglais). Ed. Tehn., Bucureşti, 1967.

5. D r y s d a l e C.V., J o l e y A.C., *Electrical Measuring Instruments.* Chapman & Hall, London, 1952.

ASUPRA CONDIŢIILOR DE APARIŢIE A OSCILAŢIILOR MECANICE ÎNTR-UN SISTEM ELECTROMECANIC

III. Extinderea studiului stabilităţii soluţiilor

(Rezumat)

Se determină influenţa parametrilor constructivi ai instrumentului magnetoelectric dintr-un circuit echipat cu o diodă tunel asupra domeniului în care apar oscilaţii mecanice ale sistemului mobil. Analiza se efectuează în cazul când punctul de funcţionare al circuitului se află oriunde pe zona descendentă a caracteristicii diodei tunel şi pentru un domeniu de variaţie al rezistenţei circuitului ce asigură monotonia funcţiei $d\alpha''(u'')/dt$.

BULETINUL INSTITUTULUI POLITEHNIC DIN IAŞI
Tomul XLII (XLVI), Fasc. 1–2, 1996
Secţia III
ELECTROTEHNICĂ. ENERGETICĂ. ELECTRONICĂ

D.C. 621.314.222.3

ABOUT A DIAGRAM FOR THE AUTOMATIC ERROR COMPENSATION IN VOLTAGE TRANSFORMERS

BY

ELENA CREŢU, ADRIAN CREŢU and CARMEN COJOCARU-FILIPIUC

A scheme for the automatic compensation of errors in measuring voltage transformers is proposed and studied.

The scheme we propose comprises a two-stage voltage transformer which is equipped with two additional windings ($N_s = N_c = N_2$), placed on the first magnetic core (the first stage of the transformer), and which is associated with a low power electric amplifier having the input connected in the secondary circuit, N_2, of the transformer, and the output – in the circuit of the additional winding, N_s.

In comparison with other known diagrams, the proposed scheme – which can be applied in the construction of certain standard measuring voltage transformers – requires electronic amplifiers of only low power and shows better operating stability.

1. Introduction

The complex error $\underline{\varepsilon}$ of a voltage transformer which has a single magnetic core (a single stage) has the expression [1]:

$$\underline{\varepsilon} = -\frac{\underline{Z}_1}{\underline{Z}_0} - \frac{\underline{Z}_1 + \underline{Z}'_2}{\underline{Z}'_s}, \tag{1}$$

where: $\underline{Z}_1$ is the impedance of the primary winding, $\underline{Z}_0$ – the impedance of the magnetizing branch, $\underline{Z}'_2$, $\underline{Z}'_s$ – the impedance of the secondary winding, respectively the load impedance, both of them being referred to the primary.

The expression (1) of the complex error renders evident the two components of the complex error, i.e., the no-load operation error:

$$\underline{\varepsilon}_0 = -\frac{\underline{Z}_1}{\underline{Z}_0} \tag{2}$$

and the error due to the load impedance ($\underline{Z}'_s \neq \infty$):

$$\underline{\varepsilon}_s = -\frac{\underline{Z}_1 + \underline{Z}'_2}{\underline{Z}'_s}. \tag{3}$$

With higher-power voltage transformers that are used in the power-network, the error determined by the load impedance (relation (3)) is of highest gravity. As far as low-power voltage transformers are concerned – which are used in electronic equipment and have the secondary connected to an electronic amplifier – the error of no-load operation (relation (2)) is most important [1].

The compensation of the no-load operation error $\underline{\varepsilon}_0$ can be achieved either in an active manner, using various electronic methods [1], [2], or passively, by utilization of a voltage transformer with two stages [3]. Consequently, in case of a two-stage transformer, it is only the error, $\underline{\varepsilon}_s$, determined by the load impedance, which has significant gravity.

In what follows a diagram for the automatic compensation of both components of the voltage transformers error is proposed and studied, which can represents the basis for the construction of certain standard voltage transformers.

2. The Principle Diagram

A few trials to compensate the load impedance error, $\underline{\varepsilon}_s$, are known in the specialized literature. Some special results were obtaind using the compensation diagram proposed by S a n k a r a n, K a n a g a s a b a p a t h y and M u r t i [4]. It has been improved by D e a c o n [5], who applied it to a two-stage voltage transformer so that the elimination of the $\underline{\varepsilon}_0$ component of the complex error was also achieved in this way.

However, even this improved method presents the shortcoming that the electronic device which is to be used must deliver the total current drawn by the load, although it is designed just for the low value of the error voltage. The higher the transformer's rated power is, the more important this shortcoming becomes.

Moreover, experimental tests have shown that for relatively high amplification, $\underline{A}$, of voltage, the stability of the diagram in [4] is low, and the compensation device can oscillate.

In order to eliminate these disadvantages an improvement of the up-mentioned method is proposed. It consists in attaching a compensating winding (Fig.1), which has the number of turns $N_c = N_2$ and it is equipped with a turns-correction, so that, when this winding is connected to a load impedance, $\underline{Z}_s$, equal to the rated impedance, $\underline{Z}_n$, of the voltage transformer, the voltage U_{2c} to be found at its terminals must be rigorously equal to the e.m.f. E_2 induced in the secondary N_2 of the voltage transformer (VT).

In this way the low-power electronic amplifier EA, utilized to compensate errors in a two-stage transformer VT, is associated with two extra windings N_s and N_c which are placed on the first magnetic core (the first stage) – just like the winding N_1 intended to compensation the no-load error ε_0 – and which both have the same number of turns, N_2, as the secondary winding of the voltage transformer.

The input of the electronic amplifier EA is connected in the secondary circuit N_2 of the transformer VT and its output – in the circuit of the supplementary

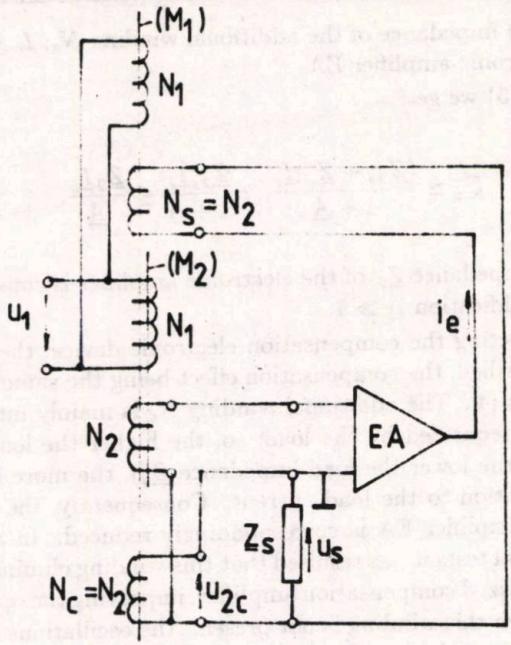

Fig. 1

winding N_s.

As the input impedance, $\underline{Z}_i$, of the electronic amplifier EA is theoretically infinite, the secondary N_2 of the voltage transformer operates in no-load conditions. Therefore, the input voltage of the amplifier EA:

$$\underline{U}_i = \underline{E}_2 - \underline{U}_s = \underline{Z}_2\underline{I}_2, \tag{4}$$

given by the subtraction of the voltage drop $\underline{U}_s$ on the load impedance $\underline{Z}_s$, from the e.m.f. $\underline{E}_2$ induced in the secondary winding N_2, represents the voltage of error determined by the load impedance ($\underline{Z}_s \neq \infty$). When the electronic compensation device is missing, this voltage of error is equal to the voltage drop $\underline{Z}_2\underline{I}_2$ on the secondary winding impedance $\underline{Z}_2$, where $\underline{I}_2$ is the secondary current (before connecting EA).

Applying the Kirchhoff's voltage law to the circuit of the additional winding N_s, we get:

$$\underline{E}_{2s} + \underline{U}_e = (\underline{Z}_{2s} + \underline{Z}_e)\underline{I}_e + \underline{U}_s, \tag{5}$$

where: $E_{2s} = E_2$ represents the e.m.f. induced in the additional winding N_s, which is practically equal to the e.m.f. $\underline{E}_2$ induced in the secondary N_2 of the voltage transformer; $\underline{U}_e = \underline{A}\underline{U}_i$ – the output voltage of the electronic amplifier EA; $\underline{A}$, $\underline{Z}_e$ – the voltage amplification, respectively the output impedance of the amplifier

EA; $\underline{Z}_{2s} \simeq \underline{Z}_2$ – the impedance of the additional winding N_s; $I_e \leq I_2$ – the output current of the electronic amplifier EA.

From (4) and (5) we get:

$$\underline{U}_i \simeq \frac{(\underline{Z}_{2s} + \underline{Z}_e)\underline{I}_e}{1 + \underline{A}} \simeq \frac{\underline{Z}_{2s}\underline{I}_e}{1 + \underline{A}} \leq \frac{\underline{Z}_2 \underline{I}_2}{\underline{A}}, \tag{6}$$

where the output impedance $\underline{Z}_e$ of the electronic amplifier is considered negligible and its voltage amplification $\underline{A} \gg 1$.

Thus, by connecting the compensation electronic device, the voltage of error $\underline{U}_i$ is $\underline{A}$ times diminished, the compensation effect being the same as in case of the method presented in [4]. The additional winding N_c is mainly intended to deliver part of the current requested by the load; so, the higher the load of the voltage transformer VT is (the lower the load impedance $\underline{Z}_s$), the more important is the N_c winding contribution to the load current. Consequently, the power delivered to the load $\underline{Z}_s$ by amplifier EA is correspondingly reduced. In addition to this, from the experimental tests it has resulted that this winding eliminates the possible oscillations of the utilized compensation amplifier, improving the operation stability of the diagram. When this winding is not present, the oscillations of the electronic device could be eliminated, e.g., by connecting capacitors in the feedback of the electronic amplifier (in parallel to the feedback resistance). These capacitors yet decrease the voltage amplification $\underline{A}$ of the electronic device and, consequently, diminish its compensation effect.

3. Conclusions

1. It is presented and studied an electronic diagram for the automatic errors compensation of a two-stage voltage-transformer, which can constitute the basis for the construction of certain standard voltage transformers.

2. Compared to the already known diagrams [4], [5], the proposed diagram requests electronic amplifiers of a lower power, irrespective of the load impedance value and it has definitely superior operation stability.

The higher the rated-power the compensated voltage-transformer is, the more important the up-mentioned advantages become.

3. Experimental results, obtained by modelling, have confirmed the accuracy of the theoretical deductions.

For experimental tests, one and the same electronic device has been used to compensate errors in a voltage-transformer that was connected on a load impedance taking values within the range $Z_n ... Z_n \times 10^{-2}$.

Received, June 27, 1995

Technical University "Gh.Asachi", Jassy,
Department of General Electrotechnics
and Electrical Machines

REFERENCES

1. M i l l e a A., *Măsurări electrice.* Ed. Tehnică, Bucureşti, 1980.
2. C u t k o s k y R.D., *An A.C. Resistance Thermometer Bridge.* J. Res. NBS, **74C**, *1-2*, 15-18 (1970).
3. D e a c o n T.A., H i l l J.J., *Two-stage Inductive Voltage Dividers.* Proc. IEE, **115**, *6*, 888-892 (1968).
4. S a n k a r a n P., K a n a g a s a b a p a t h y P., M u r t i V.G.K., *Electronic Error-Compensation of a Voltage Transformer.* IEEE Trans. Instrum. Meas., **28**, *1*, 86-89 (1979).
5. D e a c o n T.A., *Comments on "Electronic Error-Compensation of a Voltage Transformer".* IEEE Trans. Instrum. Meas., **29**, *1*, 79-80 (1980).
6. C r e ţ u E., C r e ţ u A., *Electronically Compensated Two-Stage Current Transformer.* Modelling, Measurement & Control, AMSE Press, **A**, **67**, *3*, 53-58 (1995).
7. C r e ţ u E., C r e ţ u A., L u c a n u M., *Transformator în două trepte cu compensare automată a erorilor.* Patent România, *87889* (1986).

ASUPRA UNEI SCHEME DE COMPENSARE AUTOMATĂ A ERORILOR TRANSFORMATOARELOR DE TENSIUNE

(Rezumat)

Se propune şi se studiază o schemă de compensare automată a ambelor componente ale erorilor transformatoarelor de tensiune.

Schema propusă cuprinde un transformator de tensiune în două trepte, prevăzut cu două înfăşurări suplimentare ($N_s = N_c = N_2$), plasate pe primul miez (prima treaptă a transformatorului), asociat cu un amplificator electronic de mică putere, având intrarea conectată în circuitul secundar, N_2, al transformatorului, iar ieşirea – în circuitul înfăşurării sale suplimentare, N_s.

Comparativ cu schemele cunoscute, schema analizată aici – posibil de utilizat la construirea unor transformatoare de tensiune etalon – necesită amplificatoare electronice de putere mai mică şi prezintă o stabilitate de funcţionare superioară.

BULETINUL INSTITUTULUI POLITEHNIC DIN IAŞI
Tomul XLII (XLVI), Fasc. 1–2, 1996
Secţia III
ELECTROTEHNICĂ. ENERGETICĂ. ELECTRONICĂ

D.C. 621.317.785

VERIFICATION STAND-ALONE UNIT WITH PC FOR INDUCTION-TYPE INTEGRATING ELECTRICITY METERS

BY

M. CREŢU and C. VOINICIUC

An experimental unit which allows to verify induction meters will be presented. We studied and built an experimental unit and data acquisition interface including soft which verifies induction-type integrating electricity meters.

1. Introduction

Social and economic activities require power demand. In order to eliminate suspicions between partners – producer, dealer and consumer – it is necessary to verify the accuracy of induction meters function.

Traditional verifications of induction meters are effectuated with comparison methods namely: wattmeter and time method and reference meter method. These methods require long durations for experimentation at different loads and analysis of measurement results. This time depends on number of verified induction meters.

2. Experimental Unit

We have studied and built an experimental unit which allows to verify induction meters and displays the curves of errors for different loads. It allows to determine with high accuracy the induction meter operation in optimal time. Experimental unit is shown in Fig.1 and it is constituted by: inputs connecting block for single-phase or three-phase verificatory meters, simulation loads, power supply to the mains single-phase or three-phase, transducers for rotation, reference standard electronic meter, data acquisition interface, computer. The reference standard meter emits number of impulses proportional to energy passed through the load in period Δt, using a generator of rectangular pulses. A transducer with infrared sensor is used to convert the rotational speed of the disc in frequency impulses. The results are acquired by computer through the interface.

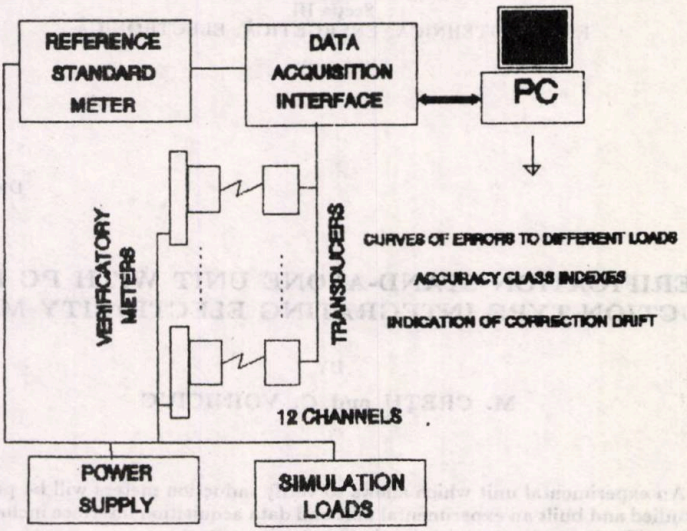

Fig. 1

3. Data Acquisition Interface

The principle of operation for data acquisition interface is shown in Fig. 2. Transducer of revolutions converts rotational speed of disc from verification meter to pulses. Transducer generates output pulses whose number is proportional to revolutions and number of opaque sectors on the width disc. To visualize the moment when the transducer of revolutions "reads" an opaque sector of disc, it is utilized a LED. This is supplied by the "Power Lead" block when at output of the comparator there is "1" logic signal. The output pulses from transducers are selected by "Multiplexer" and processed in amplitude and width in "Processing of Measured Data" block. To minimize the possible errors caused by impulse width, the signal from output of the transducer are derived and triggered in order to obtain a rectangular impulse. The amplitude of output pulses of transducer is of 2...2.5 V. These pulses are applied to input of the comparator circuit to obtain two stable logic states. When the level of applied pulse is bigger than reference (1.2 V) tension, at output of the comparator a signal with 5 V level is obtained, which represents "1" logic. When the previous condition is not satisfied, it is obtained at output of the comparator 0 V, i.e. "0" logic. This impulse is transmitted to PC and to second block "Command Counter". Computer controls the number of revolutions. When computer senses with the help of its soft the second last revolution, it emits the command to stop after the next impulse, which represents the begin of the last revolution of disc and it determines the stop of counting after the last revolution.

The "Command Counter" block allows the opening of the logic "Gate Circuit". The pulses generated by electronic reference standard meter have passed to the "Counter" during opening time of logic gate. The result is transmitted by

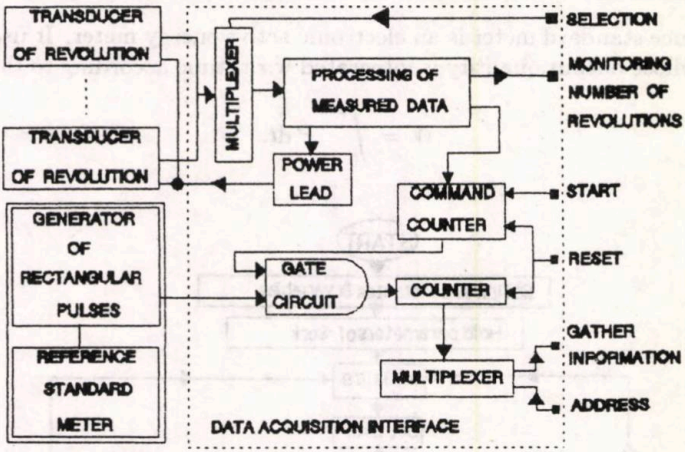

Fig. 2

"Multiplexer" to computer at a certain address. PC computes error and display the error and message. The message refer to accuracy class indexes and indication of correction drift. Computer begins automatically a new cycle if doesn't another option. Computer gives commands "Reset" and "Start" to data acquisition interface. Human operator has the possibility to change option condition of practice or "End" for running program. Option condition of practice refers as follows: selection of a certain induction type meter in order to be verified by multiplexer, number of revolutions, constants of electronic reference standard meters, constants of verificatory meters.

4. Numerical Approach

The number of revolutions N_V effectuated by the disc time during interval Δt is totalized by the integral w.r.t. time of the rotation speed:

$$N_V = k_1 \int_0^{\Delta t} \left(\frac{\mathrm{d}\alpha}{\mathrm{d}t} \right) \mathrm{d}t = k_2 \int_0^{\Delta t} UI \cos\phi \, \mathrm{d}t = \frac{W_V}{C_V}. \tag{1}$$

The fraction-of-indication error of the verification meter is determined with:

$$\epsilon = \frac{W_V - W}{W} \cdot 100 = \left(\frac{N_V}{N} \cdot \frac{C}{C_V} - 1 \right) \cdot 100, \quad [\%], \tag{2}$$

where: W_V represents the registered energy by the verification meter; W – the true value of energy passed; C_V – constant of the verification meter; C – constant of reference standard meter; N_V – number of revolution from disc of verification meter; N – number of rectangular pulses generated by reference standard meter.

Reference standard meter is an electronic active energy meter. It uses a power converter whose output quantity is integrated w.r.t. time according to the relation:

$$W = \int_0^{\Delta t} P \, dt. \tag{3}$$

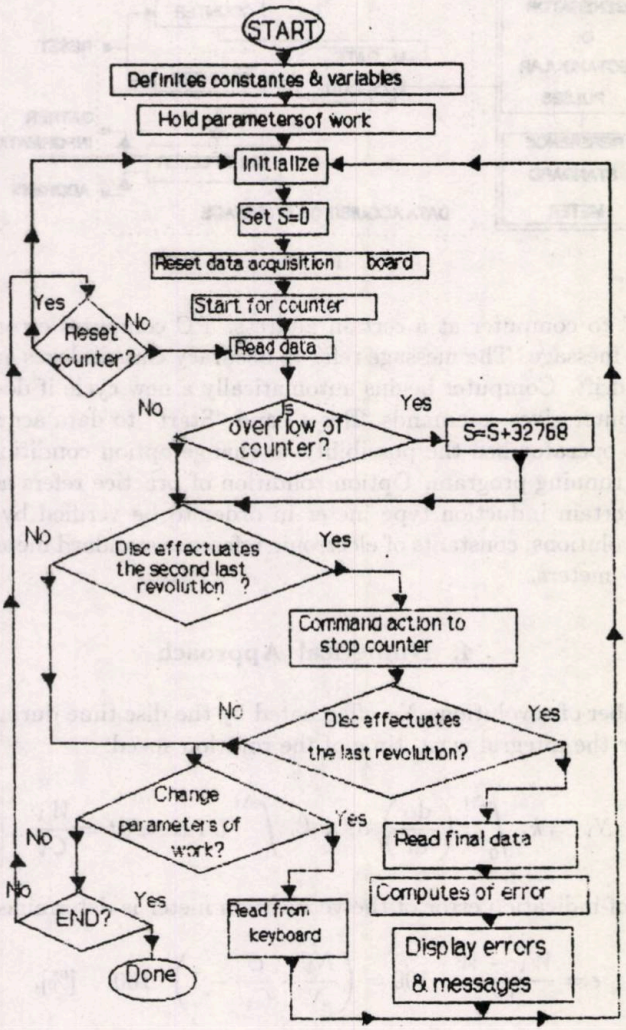

Fig. 3

It consists of a power-to-voltage converter, a voltage-to-frequency converter and a pulse counter. The output voltage, V_{out}, is proportional to active power passed

through load. The voltage-to-frequency converter converts V_{out} to a pulse repetition frequency, f. The reference standard meter has four constants to repetition frequency, f.

The program sequences have consisted of list of instructions and decision boxes which are processed consecutively. The flowchart is shown in Fig.3. Program begins to define variables and constants. The presenting constants are: constant of the verificatory meter, C_V=480 rot./kWh; constant of reference standard meter, C=24 Hz; number of revolutions of the disc, N_V=1.

The next step is to change from keyboard presetting constants and variables. After that the computer initializes variables. The variable S is used for the maximum incremental capacity of counter. Than the computer resets interface and it commands the start of counter. Computer reads data from input port. It will change variable S with S+32,768 if counter is overflow. The program continues with computing of errors and the display of the message. Than it begins automatically a new cycle. When doesn't want to run a new cycle, operator commands the stop from keyboard.

5. Conclusions

We studied and built an experimental unit and data acquisition interface including soft which verifies induction-type integrating electricity meters.

The proposed method is fast and in concordance with the metrological norms and conventions for exploitation of induction meter.

The experimental unit allows simultaneous of many identical type induction meters in optimal time and high accuracy.

The computer emits the metrological certificates of quality for every tested induction meter with the curves of errors to different loads and accuracy class indexes.

Received, April 14, 1995

Technical University "Gh.Asachi", Jassy,
Department of Electrical Measures

REFERENCES

1. Apruzzese G., Frauly C., *IBM PC du laboratoire à l'industrie: interfaces, liaisons, adaptations.* Dunod, Paris, 1986.
2. Cerr M., *Instrumentation industrielle.* Technique & Documentation – Lavoisier, Paris, 1993.
3. Gotte K., Hart H., Jeschke G., *Taschenbuch Betriebsmeßtechnik.* VEB Verlag Technik, Berlin, 1974.
4. Schrufer E., *Elektrische Meßtechnik.* Carl Hanser Verlag, München–Wien, 1990.
5. Lang T.T., *Électronique des systèmes de mesures.* Masson, Paris, 1993.

STAND DE VERIFICARE CU PC PENTRU CONTOARELE ELECTRICE

(Rezumat)

Se prezintă un stand realizat pentru verificarea contoarelor electrice cu ajutorul calculatorului. Calculatorul afişează pe monitor curba erorilor funcţie de curentul de sarcină, clasa de precizie şi observaţii privind corecţiile.

BULETINUL INSTITUTULUI POLITEHNIC DIN IAŞI
Tomul XLII (XLVI), Fasc. 1–2, 1996
Secţia III
ELECTROTEHNICĂ. ENERGETICĂ. ELECTRONICĂ

C.D. 621.318.3

SUR LE FONCTIONNEMENT D'UN RELAIS TYPE FERRORÉSONANT

PAR

ADRIAN BARABOI

On analyse le fonctionnement d'un relais de type ferrorésonant, dont le schéma fait l'objet d'un brévet de l'auteur. On met en évidence la possibilité d'agrandir les valeurs du rapport de maintien du relais par l'emploi avantageux, comme élément de circuit, d'une bobine nonlinéaire ayant le noyau magnétisé orthogonalement.

1. Le relais de type ferrorésonant est un appareil électromagnétique statique, sans contacts, dont la partie active est un circuit ferrorésonant. Le fonctionnement d'un tel type de relais est basé sur les phénomènes de saut du signal de sortie, dues à la variation de l'un des paramètres du signal d'entrée.

On connaît des variantes constructives nombreuses de relais sans contacts, réalisés à l'aide des circuits ferrorésonants et ayant comme élément nonlinéaire une bobine, noncommandée ou commandée longitudinalement.

Vu qu'on est intéressé à diminuer les valeurs du rapport de maintien qui caractérise le fonctionnement d'un relais ferrorésonant, on a proposé une variante constructive originale, [1], se basant sur l'utilisation d'une bobine nonlinéaire à noyau magnétisé orthogonalement (BNNMO) comme élément nonlinéaire du circuit ferrorésonant de base.

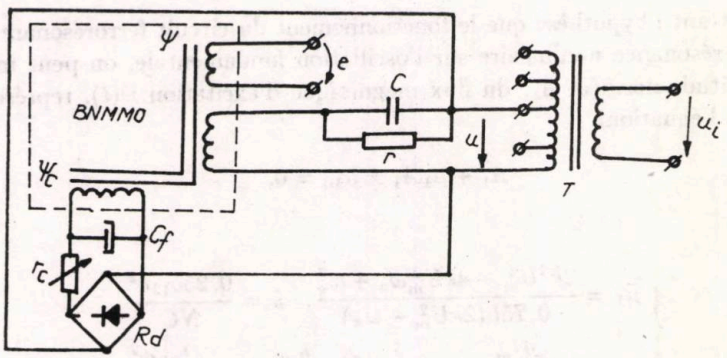

Fig. 1

Cette variante-ci, dont le schéma électrique est représenté dans la Fig.1, fonctionne avec des signaux d'entrée alternatifs, qui peuvent être des tensions ou des courants. Dans ce but le relais contient le transformateur d'adaptation T, dont l'enroulement de sortie est muni par des prises qui permettent le réglage par bonds de la tension de commande.

Le signal d'entrée, ainsi adapté, est appliqué au circuit ferrorésonant série, contenant l'enroulement d'excitation de la BNNMO. Comme signal de commande pour la BNNMO on utilise un courant continu, proportionnel par rapport au signal d'entrée.

Le signal de sortie du relais est obtenu sous la forme de la t.e.m. $e(t)$, induite dans un enroulement supplémentaire, fonctionnant en couplage magnétique avec celui d'excitation de la BNNMO.

Étant donnée une variation continue de l'amplitude du signal d'entrée, $u(t)$, on obtient une variation par saut de l'amplitude du signal de sortie, $e(t)$, ainsi qu'au schéma électrique représenté dans la Fig.1 on peut attacher la caractéristique statique de la Fig.2, où par U_m, Y on a noté les amplitudes des signaux d'entrée, respectivement de sortie.

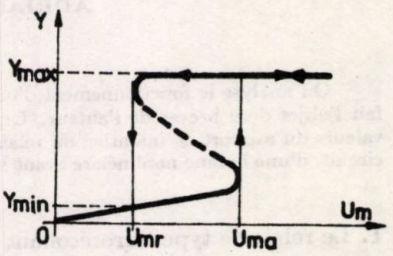

Fig. 2

2. Pour analyser le fonctionnement d'un tel type de relais on fait appel à quelques résultats obtenus antérieurement, [2], dans l'étude du régime forcé des circuits ferrorésonants qui contiennent une BNNMO.

Soit le signal adapté d'entrée (v. la Fig.1) de la forme:

$$u(t) = U_m \cos \omega t \tag{1}$$

et le flux magnétique de commande, ψ_{cm}, proportionnel à la tension U_m:

$$\psi_{cm} = cU_M. \tag{2}$$

Admettant l'hypothèse que le fonctionnement du circuit ferrorésonant a lieu près de la résonance nonlinéaire sur l'oscillation fondamentale, on peut montrer que l'amplitude normée, A_1, du flux magnétique d'excitation $\psi(t)$, représente la solution de l'équation:

$$A_1^3 + \mu_1 A_1 \pm \mu_{10} = 0, \tag{3}$$

où:

$$\begin{cases} \mu_1 = \dfrac{2k^2U_m^4 - 4kU_m^2\omega_\pi + \omega_\pi^2}{0,75h(2kU_m^2 - \omega_\pi)}, \quad k = \dfrac{0,25b_{12}c^2}{NC}, \\ \mu_{10} = \dfrac{\omega U_m}{0,75h\psi_0}, \quad \omega_\pi = \omega^2 - \dfrac{b_{10}}{NC}, \quad h = \dfrac{b_{30}\psi_0^2}{NC}. \end{cases} \tag{4}$$

Dans les relations (3), (4) on a utilisé les suivantes notations: ψ_0 – la valeur de repère du flux magnétique d'excitation; b_{10}, b_{12}, b_{30} – les coefficients du polynôme d'approximation de la caractéristique de la BNNMO, N – le nombre de spires de l'enroulement d'excitation, C – la capacité du circuit ferrorésonant (Fig.1).

Vu qu'on est intéressé à trouver, par voie graphique, les solutions de l'équation (3) sous la forme d'une fonction $|A_1| = f(U_m)$ qui représente, exceptant un facteur de proportionnalité, la caractéristique $Y(U_m)$ du relais (v. la Fig.2), on détermine les expressions des asymptotes (C_s), respectivement du lieu géométrique (L_V) des points où les courbes de résonance admettent des tangentes verticales; celles-ci résultent de la forme:

$$(5) \qquad \begin{cases} |A_1| = \sqrt{\dfrac{\omega_\pi}{0,75h}}, & (C_s), \\ 3A_1^2 + \mu_1 = 0, \quad U_m = \pm\sqrt{\dfrac{\omega_\pi}{2k}}, & (L_V). \end{cases}$$

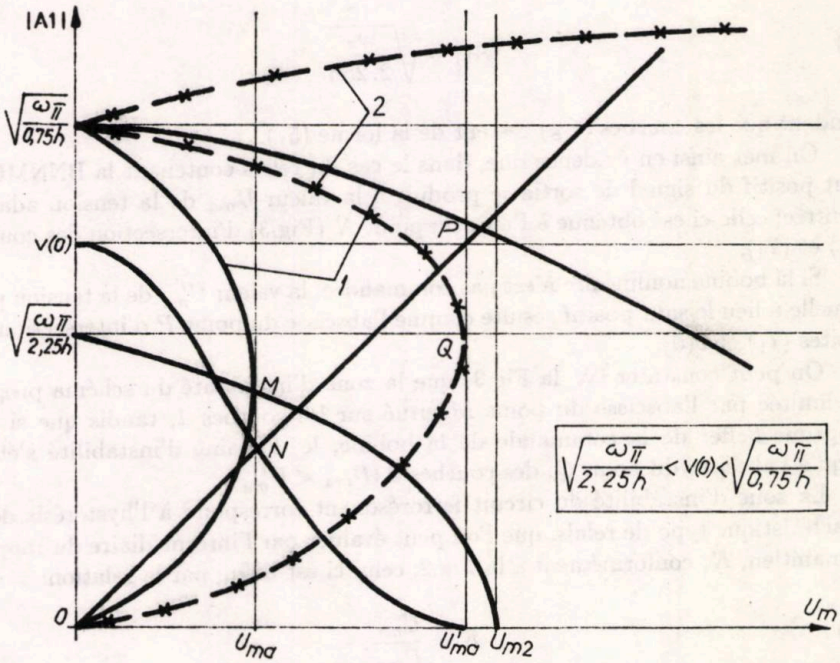

Fig. 3

Dans la Fig.3 on a représenté les courbes résultées, $|A_1| = f(U_m)$. La tension U_{ma}, pour laquelle se produit le saut positif du signal de sortie, est obtenue par l'intersection des courbes (3), (5), donc comme solution de l'équation:

$$(6) \qquad U_{ma} = \frac{h\psi_0}{2\sqrt{3}\omega}[-\mu_1(U_{ma})]^{3/2},$$

où $\mu_1(U_m)$ a l'expression (4).

On a déterminé la solution de l'équation (6) par voie grapho-analytique, en obtenant sa solution, U_{ma}, à l'intersection des courbes:

$$y(U_m) = U_m, \quad v(U_m) = \frac{h\psi_0}{2\sqrt{3\omega}}[-\mu_1(U_m)]^{3/2}. \tag{7}$$

Afin de comparer le fonctionnement du relais proposé avec celui d'un relais ferrorésonant dont la bobine nonlinéaire n'est pas commandée, on considère interrompu le courant de commande de la BNNMO (Fig.1). De (4), avec $k = 0$, on obtient:

$$\mu_1 = \mu_1(0) = -\frac{\omega_\pi}{0,75h}. \tag{8}$$

Dans ce cas, les courbes (L_V) résultent de la forme:

$$|A_1| = \sqrt{\frac{\omega_\pi}{2,25h}}, \tag{9}$$

pendant que les courbes (C_S) restent de la forme (5_1).

On met ainsi en évidence que, dans le cas du relais contenant la BNNMO, le saut positif du signal de sortie se produit à la valeur U_{ma} de la tension adaptée d'entrée; celle-ci est obtenue à l'aide du point N (Fig.3) d'intersection des courbes (7_1) et (7_2).

Si la bobine nonlinéaire n'est pas commandée, la valeur U'_{ma} de la tension pour laquelle a lieu le saut positif résulte comme l'abscisse du point P d'intersection des droites (7_1) et $v(0)$.

On peut constater (v. la Fig.3) que la zone d'instabilité du schéma proposé est limitée par l'abscisse du point M situé sur les courbes *1*, tandis que si l'on supprime l'effet de la commande de la bobine, le domaine d'instabilité s'étend jusqu'à l'abscisse du point Q, des courbes *2* ($U_{ma} < U'_{ma}$).

La zone d'instabilité du circuit ferrorésonant correspond à l'hystérésis de la caractéristique type de relais, que l'on peut évaluer par l'intermédiaire du rapport de maintien, K, conformément à la Fig.2; celui-ci est défini par la relation:

$$K = \frac{U_{mr}}{U_{ma}}. \tag{10}$$

L'analyse effectuée par voie théorique démontre que le schéma du relais préconisé, représenté dans la Fig.1, permet l'amélioration du rapport de maintien; expérimentalement on a constaté que celui-ci atteint des valeurs $K > 0,9$, tandis que, dans le cas des relais ferrorésonants usuels, ce rapport-ci ne dépasse pas la valeur $K = 0,7$.

Conclusions

1. On étudie le fonctionnement d'un relais sans contacts de type ferrorésonant, dont le schéma original est constitué par un circuit oscillant contenant une BNNMO, convenablement commandée.

2. Par voie grapho-analytique on met en évidence que le schéma préconisé permet l'augmentation appréciable des valeurs du rapport de maintien, caractérisant le relais; des essais expérimentaux confirment les résultats théoriques obtenus.

Reçue le 22 juin 1994

Université Technique „Gh. Asachi", Jassy,
Chaire d'Énergétique

BIBLIOGRAPHIE

1. B a r a b o i A., *Releu static ferorezonant de tensiune sau curent.* Brevet Roum., *69826* (1978).
2. B a r a b o i A., *Contribuţii la studiul şi aplicaţiile magnetizării în câmpuri ortogonale.* Thèse de doctorat, Inst. Polyt., Jassy, 1980.

ASUPRA FUNCŢIONĂRII UNUI RELEU DE TIP FEROREZONANT

(Rezumat)

Se analizează funcţionarea unui releu ferorezonant de concepţie originală, evidenţiindu-se influenţa avantajoasă a utilizării, drept element neliniar în schema electrică, a unei bobine comandate ortogonal; valorile obţinute pentru factorul de revenire depăşesc pragul de 0,9.

BULETINUL INSTITUTULUI POLITEHNIC DIN IAŞI
Tomul XLII (XLVI), Fasc. 1–2, 1996
Secţia III
ELECTROTEHNICĂ. ENERGETICĂ. ELECTRONICĂ

D.C. 621.313.333.021.2

ON THE EQUIVALENT CIRCUITS DIAGRAMS OF THE TWO-PHASE UNSYMMETRICAL INDUCTION MOTORS

BY

I. ANDRONE and ADRIANA PRISĂCARU

The expressions of the two magnetizing reactances of the two different phase windings of a two-phase unsymmetrical induction motor were derived. The equivalent numbers of phases from magnetically point of view of the two-phase unsymmetrical stator windings were defined. These numbers may be fractional, not only integers.

1. Introduction

The operation of a two-phase induction motor (TPIM) can be described starting from the examination of the single-phase machine. Its operation may be explained by the revolving magnetic field theory namely, the single-phase alternating magnetic field is considered as one produced by the superposition of two magnetic fields rotating in opposite directions at constant angular velocity.

The voltage equations of a single-phase machine, in complex quantities, are [1]:

$$\underline{U}_1 = (R_1 + \mathrm{j}X_{1d})\underline{I}_1 + \mathrm{j}X_m(\underline{I}_1 + \underline{I}'_{2f}) + \mathrm{j}X_m(\underline{I}_1 + \underline{I}'_{2r}),$$

$$0 = \left(\frac{R'_2}{s} + \mathrm{j}X'_{2d}\right)\underline{I}'_{2f} + \mathrm{j}X_m(\underline{I}_1 + \underline{I}'_{2f}), \tag{1}$$

$$0 = \left(\frac{R'_2}{2-s} + \mathrm{j}X'_{2d}\right)\underline{I}'_{2r} + \mathrm{j}X_m(\underline{I}_1 + \underline{I}'_{2r}),$$

where all the quantities associated with the stator (primary) are indexed with "1" and those with the rotor (secondary), with "2", the symbols underlined denote complex quantities, the sign ($'$) denotes rotor quantities referred (or transferred) to the stator side, subscript d is utilised for leakage reactances, m – for magnetizing reactances, f – for "forward" and r – for "reverse" sequence, s is the rotor slip w.r.t. forward revolving magnetic field and $2-s$, the same but w.r.t. reverse one.

The equivalent circuit diagram of single-phase motor corresponding to the equation (1) is drawn in Fig. 1, neglecting the iron (core) losses.

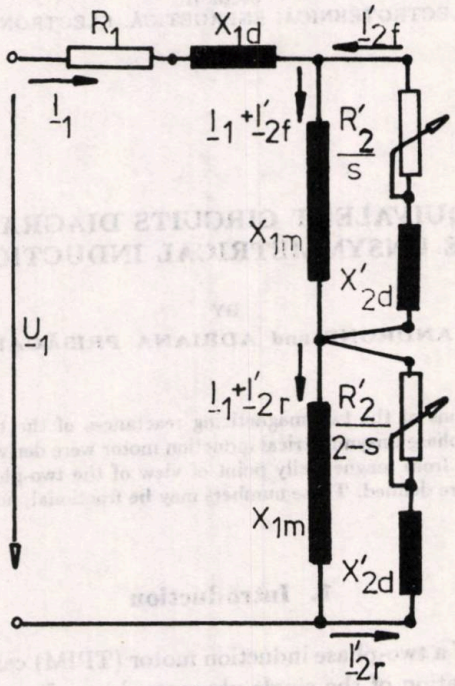

Fig. 1

For the TPIM the effects of the two phases are superimposed. The two phase windings are spaced arround the stator periphery and its currents are phase-shifted. The two phase windings are generaly different (as number of turns, winding factors, etc.) and their currents have different magnitudes. The aim of this papers is to estimate the effects of these differences on the equivalent circuits diagrams of the TPIM without use the method of symmetrical components.

2. The Two-phase Motor Equations

Let us consider an unsymmetrical TPIM with the stator phases labelled with the letters a and b and a squirrel-cage rotor (Fig. 2). The two phase windings are spaced apart by 90 degrees.

The voltage equations for phase windings are:

$$
\begin{aligned}
\underline{U}_{1k} &= (R_{1k} + \mathrm{j}X_{1dk})\underline{I}_{1k} + \mathrm{j}X_{mfk}(\underline{I}_{1k} + \underline{I}'_{2kf}) + \mathrm{j}X_{mrk}(\underline{I}_{1k} + \underline{I}'_{2kr}),\\
0 &= \left(\frac{R'_{2fk}}{s} + \mathrm{j}X'_{2fdk}\right)\underline{I}'_{2kf} + \mathrm{j}X_{mfk}(\underline{I}_{1k} + \underline{I}'_{2kf}),\\
0 &= \left(\frac{R'_{2rk}}{2-s} + \mathrm{j}X'_{2rdk}\right)\underline{I}'_{2kr} + \mathrm{j}X_{mrk}(\underline{I}_{1k} + \underline{I}'_{2kr}),
\end{aligned}
\tag{2}
$$

where $k = a, b$.

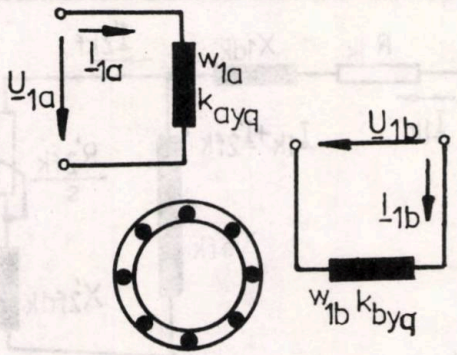

Fig. 2

The equivalent circuits diagrams corresponding to Eqs.(2) are drawn in Fig. 3. In this figure the higher loop corresponds to the forward revolving magnetic fields and the lower loop to the reverse ones. The rotor quantities reffered to the stator side in Eqs.(2) and in Fig. 3 are marked by ($'$), X_{mfa} and X_{mfb} are the phase magnetizing reactances corresponding to the forward revolving magnetic field and X_{mra} and X_{mrb} – the phase magnetizing reactances corresponding to the reverse magnetic field. The expressions of these magnetizing reactances are different in comparison with those in literature, and for this reason the interest is focused on them.

3. The Magnetizing Reactances

The magnetizing reactance of each phase winding in two-phase motor is greater than the one of a phase winding in single-phase motor by a number of times that equals a half of the ratio between the magnitudes of two-phase revolving and single-phase alternating magnetic fields [2]. Consequently the magnetic fields set up by stator windings will be examinated.

The two currents of phase windings a and b set up by tensions u_{1a} and u_{1b} are:

$$i_{1a} = \sqrt{2} I_{1a} \cos(\omega_1 t + \gamma_a), \quad i_{1b} = \sqrt{2} I_{1b} \cos(\omega_1 t + \gamma_b), \tag{3}$$

where $\omega_1 = 2\pi f_1$ is the common angular frequency of feeding voltage and γ_a and γ_b – initial phases. The phase-shift between the two phases currents is:

$$\gamma_{ab} = \gamma_a - \gamma_b. \tag{4}$$

The radial component of magnetic induction (magnetic flux density) set up in air gap (assumed to be uniform) by current i_{1a} is:

$$b_{1a}(\alpha_1, t) = B_{1a} \cos p\alpha_1 \cos(\omega_1 t + \gamma_a) \equiv b_{1af} + b_{1ar}, \tag{5}$$

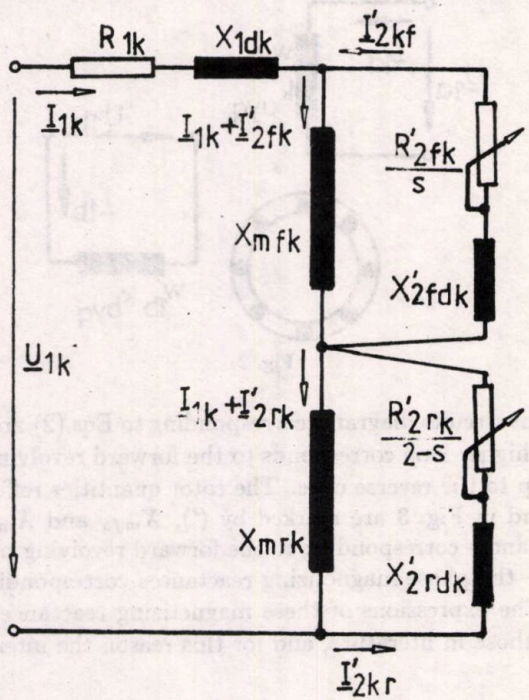

Fig. 3

where α_1 is stator angular coordinate, p – the number of pole pairs, b_{1af} and b_{1ar} – the two revolving magnetic fields, forward (f) and reverse (r):

$$
\begin{aligned}
b_{1af}(\alpha_1,t) &= \frac{1}{2}B_{1a}\cos(p\alpha_1-\omega_1 t-\gamma_a)=\frac{1}{2}B_{1a}\cos(p\alpha_1-p\Omega_1 t-\gamma_a),\\
b_{1ar}(\alpha_1,t) &= \frac{1}{2}B_{1a}\cos(p\alpha_1+\omega_1 t+\gamma_a)=\frac{1}{2}B_{1a}\cos(p\alpha_1+p\Omega_1 t+\gamma_a).
\end{aligned}
\tag{6}
$$

Here $\Omega_1=\omega_1/p$ is the angular velocity of revolving magnetic fields w.r.t. stator winding,

$$
B_{1a}=\mu_0\frac{2\sqrt{2}w_{1a}k_{ayq}I_{1a}}{\pi p\delta}
\tag{7}
$$

– the amplitude of alternating single-phase a magnetic field, δ – equivalent air-gap and $\mu_0=4\pi\times10^{-7}$ H/m – the magnetic permeability of air-gap.

Similary, for phase b:

$$
b_{1b}(\alpha_1,t)=B_{1b}\cos\left(p\alpha_1-\frac{\pi}{2}\right)\cos(\omega_1 t+\gamma_b)\equiv b_{1bf}+b_{1br}.
\tag{8}
$$

The two revolving magnetic fields (b_{1bf} and b_{1br}) have the expressions:

$$
\begin{aligned}
b_{1bf}(\alpha_1,t) &= \frac{1}{2}B_{1b}\cos\left[p\alpha_1-\omega_1 t-\left(\frac{\pi}{2}+\gamma_b\right)\right]= \\
&= \frac{1}{2}B_{1b}\cos\left[p\alpha_1-p\Omega_1 t-\left(\frac{\pi}{2}+\gamma_a\right)\right], \\
b_{1br}(\alpha_1,t) &= \frac{1}{2}B_{1b}\cos\left[p\alpha_1+\omega_1 t-\left(\frac{\pi}{2}-\gamma_b\right)\right]= \\
&= \frac{1}{2}B_{1b}\cos\left[p\alpha_1+p\Omega_1 t-\left(\frac{\pi}{2}-\gamma_b\right)\right],
\end{aligned}
\tag{9}
$$

where:

$$
B_{1b}=\mu_0\frac{2\sqrt{2}w_{1b}k_{byq}I_{1b}}{\pi p\delta}. \tag{10}
$$

The magnetic fields revolving in the same directions are added and set up a resultant magnetic field, forward or reverse revolving:

$$
\begin{aligned}
b_{1f}(\alpha_1,t) &= b_{1af}+b_{1bf}=B_{1f}\cos(p\alpha_1-p\Omega_1 t+\beta_{1f}), \\
b_{1r}(\alpha_1,t) &= b_{1ar}+b_{1br}=B_{1r}\cos(p\alpha_1+p\Omega_1 t+\beta_{1r}).
\end{aligned}
\tag{11}
$$

Through identification, having in view (6), (9) and (11), it follows that:

$$
B_{1f}=\frac{1}{2}\sqrt{B_{1a}^2+2B_{1a}B_{1b}\sin\gamma_{ab}+B_{1b}^2}, \tag{12}
$$

$$
\tan\beta_{1f}=-\frac{B_{1a}\sin\gamma_a+B_{1b}\sin\left(\frac{\pi}{2}+\gamma_b\right)}{B_{1a}\cos\gamma_a+B_{1b}\cos\left(\frac{\pi}{2}+\gamma_b\right)} \tag{13}
$$

for the forward revolving magnetic field, and:

$$
B_{1r}=\frac{1}{2}\sqrt{B_{1a}^2-2B_{1a}B_{1b}\sin\gamma_{ab}+B_{1b}^2}, \tag{14}
$$

$$
\tan\beta_{1r}=\frac{B_{1a}\sin\gamma_a-B_{1b}\sin\left(\frac{\pi}{2}-\gamma_b\right)}{B_{1a}\cos\gamma_a+B_{1b}\cos\left(\frac{\pi}{2}-\gamma_b\right)} \tag{15}
$$

for the reverse one.

If the notation

$$
\frac{B_{1a}}{B_{1b}}=k_{ab}=\frac{1}{k_{ba}} \tag{16}
$$

is made, it follows from (12),...,(15):

$$B_{1f} = \frac{1}{2} B_{1a} \sqrt{1 + 2k_{ba} \sin \gamma_{ab} + k_{ba}^2} = \frac{1}{2} B_{1b} \sqrt{1 + 2k_{ab} \sin \gamma_{ab} + k_{ba}^2}, \tag{17}$$

$$\tan \beta_{1f} = -\frac{\sin \gamma_a + k_{ba} \sin \left(\frac{\pi}{2} + \gamma_b\right)}{\cos \gamma_a + k_{ba} \cos \left(\frac{\pi}{2} + \gamma_b\right)} = -\frac{k_{ab} \sin \gamma_a + \sin \left(\frac{\pi}{2} + \gamma_b\right)}{k_{ab} \cos \gamma_a + \cos \left(\frac{\pi}{2} + \gamma_b\right)} \tag{18}$$

and:

$$B_{1r} = \frac{1}{2} B_{1a} \sqrt{1 - 2k_{ba} \sin \gamma_{ab} + k_{ba}^2} = \frac{1}{2} B_{1b} \sqrt{1 - 2k_{ab} \sin \gamma_{ab} + k_{ba}^2}, \tag{19}$$

$$\tan \beta_{1r} = \frac{\sin \gamma_a - k_{ba} \sin \left(\frac{\pi}{2} - \gamma_b\right)}{\cos \gamma_a + k_{ba} \cos \left(\frac{\pi}{2} - \gamma_b\right)} = \frac{k_{ab} \sin \gamma_a - \sin \left(\frac{\pi}{2} - \gamma_b\right)}{k_{ab} \cos \gamma_a + \cos \left(\frac{\pi}{2} - \gamma_b\right)}. \tag{20}$$

The ratios between the magnitudes of revolving and alternating single-phase magnetic fields are:

$$\frac{B_{1f}}{B_{1a}} = \frac{1}{2} k_{fa}, \tag{21}$$

$$\frac{B_{1f}}{B_{1b}} = \frac{1}{2} k_{fb}, \tag{22}$$

for the forward revolving magnetic field and:

$$\frac{B_{1r}}{B_{1a}} = \frac{1}{2} k_{ra}, \tag{23}$$

$$\frac{B_{1r}}{B_{1b}} = \frac{1}{2} k_{rb}, \tag{24}$$

for the reverse one, where the following notations are utilised:

$$k_{fa} = \sqrt{1 + \frac{2 \sin \gamma_{ab}}{k_{ab}} + \frac{1}{k_{ab}^2}} = \sqrt{1 + 2k_{ba} \sin \gamma_{ab} + k_{ba}^2}, \tag{25}$$

$$k_{fb} = \sqrt{1 + 2k_{ab} \sin \gamma_{ab} + k_{ab}^2} = \sqrt{1 + \frac{2 \sin \gamma_{ab}}{k_{ba}} + \frac{1}{k_{ba}^2}}, \tag{26}$$

$$k_{ra} = \sqrt{1 - \frac{2 \sin \gamma_{ab}}{k_{ab}} + \frac{1}{k_{ab}^2}} = \sqrt{1 - 2k_{ba} \sin \gamma_{ab} + k_{ba}^2}, \tag{27}$$

$$k_{rb} = \sqrt{1 - 2k_{ab} \sin \gamma_{ab} + k_{ab}^2} = \sqrt{1 - \frac{2 \sin \gamma_{ab}}{k_{ba}} + \frac{1}{k_{ba}^2}}. \tag{28}$$

The expressions (25),...,(28) represent more as simply notations having a physical signification. They are the equivalent numbers of phases of the two-phase stator unsymmetrical winding from magnetical point of view. Thus, k_{fa} is the equivalent number of phases reffered to the forward revolving magnetic field and to the phase a, k_{fb} – to the phase b, k_{ra} reffered to the reverse revolving magnetic field and to the phase a and k_{rb} – to the phase b. The equivalent numbers of phases (25),...,(28) may be fractional numbers not only integers.

If the magnetizing reactances in single-phase motor for windings phases a and b are given by [2]:

$$(29)\qquad X_{ma} = \frac{8}{\pi}\mu_0 f_1 \frac{\tau L}{p\delta} w_{1a}^2 k_{ayq}^2, \qquad (30)\quad X_{mb} = \frac{8}{\pi}\mu_0 f_1 \frac{\tau L}{p\delta} w_{1b}^2 k_{byq}^2,$$

the magnetizing reactances of two-phase motor are:

$$(31)\qquad X_{mfa} = \frac{1}{2}k_{fa}X_{ma}, \qquad (32)\quad X_{mfb} = \frac{1}{2}k_{fb}X_{mb},$$

for the forward revolving magnetic field, and:

$$(33)\qquad X_{mra} = \frac{1}{2}k_{ra}X_{ma}, \qquad (34)\quad X_{mrb} = \frac{1}{2}k_{rb}X_{mb},$$

for the reverse revolving one.

From the above expressions it follows that the variations of the factors (25),..., (28) must be estimate to find the values of magnetizing reactances (31),...,(34). The factors (25),...,(28) are functions of k_{ab} and γ_{ab}.

With the aim to determine the extreme values for expressions (25),...,(28), considered as functions of two variables, k_{ab} and γ_{ab}, the first step is to solve the pair of equations:

$$(35)\qquad \frac{\partial f}{\partial k_{ab}} = 0, \qquad \frac{\partial f}{\partial \gamma_{ab}} = 0,$$

where $f = k_{fa},\ k_{fb},\ k_{ra},\ k_{rb}$. It results:

$$(36)\qquad k_{ab} = \pm 1, \qquad \gamma_{ab} = \pm\frac{\pi}{2}.$$

These values define the so called critical points.

The object of the next step is to sort out from among the critical points those that are relative maximum or minimum points and those that are not. Because the expression

$$(37)\qquad \left[\frac{\partial^2 f}{\partial k_{ab}^2}\cdot\frac{\partial^2 f}{\partial \gamma_{ab}^2} - \left(\frac{\partial^2 f}{\partial k_{ab}\partial \gamma_{ab}}\right)^2\right]_{k_{ab}=\pm 1,\gamma_{ab}=\pm\pi/2},$$

where $f = k_{fa},\ k_{fb},\ k_{ra},\ k_{rb}$, is indetermined, there are not points of extremum.

From technical point of view only one from two quantities k_{ab} and γ_{ab} is variable. Consequently, the study may be carry out for one variable, the other being a parameter.

The extreme values of k_{fa}, k_{fb}, k_{ra} and k_{rb} w.r.t. k_{ab} ratio are found by equalizing with zero the first derivative, γ_{ab} being considered as a parameter:

$$(38)\quad \frac{\mathrm{d}k_{fa}}{\mathrm{d}k_{ab}} = 0, \quad (39)\quad \frac{\mathrm{d}k_{fb}}{\mathrm{d}k_{ab}} = 0, \quad (40)\quad \frac{\mathrm{d}k_{ra}}{\mathrm{d}k_{ab}} = 0, \quad (41)\quad \frac{\mathrm{d}k_{rb}}{\mathrm{d}k_{ab}} = 0.$$

From the above expressions it follows that the values of k_{ab} for which the first derivatives are vanishing and consequently the functions have extremes are, respectively:

$$(42)\quad k_{ab}^{(fa)} = -\frac{1}{\sin\gamma_{ab}}, \qquad (43)\quad k_{ab}^{(fb)} = -\sin\gamma_{ab},$$

$$(44)\quad k_{ab}^{(ra)} = \frac{1}{\sin\gamma_{ab}}, \qquad (45)\quad k_{ab}^{(rb)} = \sin\gamma_{ab}.$$

The extreme (minimum) values of k_{fa}, k_{fb}, k_{ra} and k_{rb} are found having in view relations (25),...,(28). It follows that:

$$(46)\quad (k_{fa})_{\min} = (k_{fb})_{\min} = (k_{ra})_{\min} = (k_{rb})_{\min} = \cos\gamma_{ab}.$$

In Fig. 4 are drawn the variations of k_{fa}, k_{fb}, k_{ra} and k_{rb} versus k_{ab}, with $\gamma_{ab} = \pi/6$ as parameter, for positive values of k_{ab}.

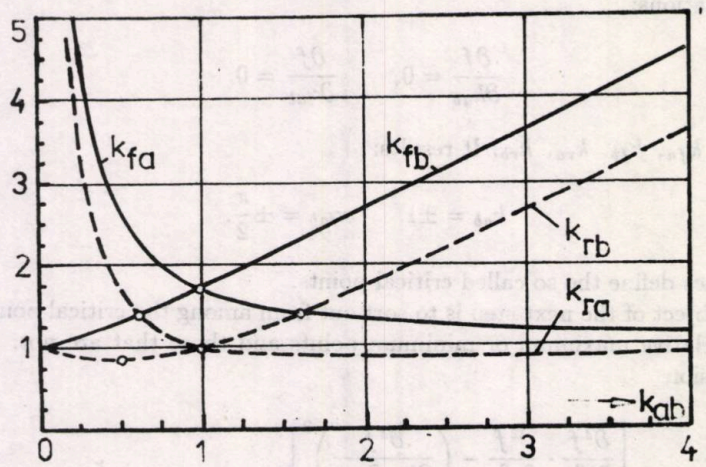

Fig. 4

When the variations of k_{fa}, k_{fb}, k_{ra} and k_{rb} versus γ_{ab}, k_{ab} being considered as a parameter, are studied, first the derivative is found then equalize it with zero:

$$(47)\quad \frac{\mathrm{d}k_{fa}}{\mathrm{d}\gamma_{ab}} = 0, \quad (48)\quad \frac{\mathrm{d}k_{fb}}{\mathrm{d}\gamma_{ab}} = 0, \quad (49)\quad \frac{\mathrm{d}k_{ra}}{\mathrm{d}\gamma_{ab}} = 0, \quad (50)\quad \frac{\mathrm{d}k_{rb}}{\mathrm{d}\gamma_{ab}} = 0.$$

From the above expressions the values $\gamma_{ab} = \pm\pi/2$ are found. The extreme values are given by:

$$(51)\quad (k_{fa})_{\mathrm{extr}} = 1 \pm \frac{1}{k_{ab}}, \qquad (52)\quad (k_{fb})_{\mathrm{extr}} = 1 \pm k_{ab},$$

$$(53)\quad (k_{ra})_{\mathrm{extr}} = 1 \mp \frac{1}{k_{ab}}, \qquad (54)\quad (k_{rb})_{\mathrm{extr}} = 1 \mp k_{ab},$$

where "+" signs are for maximum values and "−", for minimum ones. In Fig. 5 are drawn the variations of k_{fa}, k_{fb}, k_{ra} and k_{rb} versus γ_{ab} with $k_{ab} = 0.5$ as parameter.

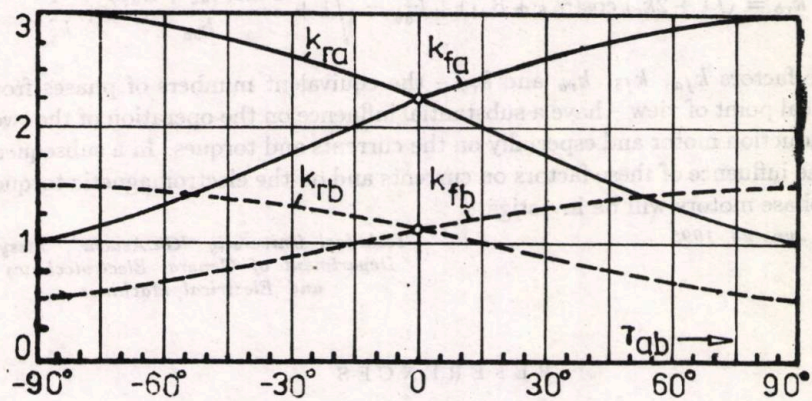

Fig. 5

4. Conclusions

The magnetizing reactance of the phase windings of a two-phase unsymmetrical induction motor is a function of the ratio between the amplitudes set up by the two magnetic inductions of the two phase windings and of the phase-shift between the magnetic inductions.

If the ratio between the magnitudes of magnetic inductions, k_{ab}, is constant and the phase-shift, γ_{ab}, is also constant, then the magnetizing reactances are also constant.

If $k_{ab} = 1$ and $\gamma_{ab} = \pi/2$ the motor is a two-phase symmetrical one ($k_{fa} = k_{fb} = 2$ and $k_{ra} = k_{rb} = 0$), and consequently there is only one revolving magnetic field – forward.

If the two-phase windings are spaced apart by an angle $\alpha_{ab} \neq \pi/2$ electrical radians, then the factors (25),...,(28) become:

$$(55) \quad k_{fa} = \sqrt{1 + \frac{2\cos(\gamma_{ab} - \alpha_{ab})}{k_{ab}} + \frac{1}{k_{ab}^2}} = \sqrt{1 + 2k_{ba}\cos(\gamma_{ab} - \alpha_{ab}) + k_{ba}^2},$$

$$(56) \quad k_{fb} = \sqrt{1 + 2k_{ab}\cos(\gamma_{ab} - \alpha_{ab}) + k_{ab}^2} = \sqrt{1 + \frac{2\cos(\gamma_{ab} - \alpha_{ab})}{k_{ba}} + \frac{1}{k_{ba}^2}},$$

$$(57) \quad k_{ra} = \sqrt{1 + \frac{2\cos(\gamma_{ab} + \alpha_{ab})}{k_{ab}} + \frac{1}{k_{ab}^2}} = \sqrt{1 + 2k_{ba}\cos(\gamma_{ab} + \alpha_{ab}) + k_{ba}^2},$$

$$(58) \quad k_{rb} = \sqrt{1 + 2k_{ab}\cos(\gamma_{ab} + \alpha_{ab}) + k_{ab}^2} = \sqrt{1 + \frac{2\cos(\gamma_{ab} + \alpha_{ab})}{k_{ba}} + \frac{1}{k_{ba}^2}}.$$

The factors k_{fa}, k_{fb}, k_{ra} and k_{rb} – the equivalent numbers of phases from magnetical point of view – have a substantial influence on the operation of the two-phase induction motor and especially on the currents and torques. In a subsequent paper the influence of these factors on currents and on the electromagnetic torques of two-phase motors will be investigate.

Received, June 28, 1995

Technical University "Gh. Asachi", Jassy,
Department of General Electrotechnics
and Electrical Machines

REFERENCES

1. Richter R., *Elektrische Maschinen.* Vierter Band, Verlag Birkhäuser, Basel – Stuttgart, 1954.
2. Richter R., *Elektrische Maschinen.* Zweiter Band, Verlag Birkhäuser, Basel – Stuttgart, 1953.

ASUPRA SCHEMELOR ECHIVALENTE ALE MOTORULUI ASINCRON BIFAZAT NESIMETRIC

(Rezumat)

Se determină dependenţa reactanţelor utile ale celor două faze (diferite) ale unui motor asincron bifazat nesimetric ca funcţie de raportul şi defazajul dintre inducţiile produse de cele două faze, fără a folosi metoda componentelor simetrice. Se introduce noţiunea de număr echivalent de faze din punct de vedere magnetic, număr ce poate fi şi fracţionar.

BULETINUL INSTITUTULUI POLITEHNIC DIN IAŞI
Tomul XLII (XLVI), Fasc. 1–2, 1996
Secţia III
ELECTROTEHNICĂ. ENERGETICĂ. ELECTRONICĂ

D.C. 621.43.044

AN ELECTRONIC INJECTION AND IGNITION MICROPROCESSOR CONTROL UNIT FOR SPARK IGNITION ENGINES

BY

ANGEL-RADU-PETRICĂ TODEREAN,
IULIAN RĂDUCANU and LAURENŢIU DIMITRIU

A sequential management system for injection and ignition control in s.i. engines is presented. The main functions of the system are described and some technical solutions exposed. The control structure assures optimization of engines features.

1. Introduction

The engine control has been evolved from simple electronic ignition to modern closed-loop systems that operate in extreme conditions and compensate the engine wear, maladjustment and variation in fuel quality. Concern the environment it has led government limits on permitted emissions from new vehicles, conditions which must be met through the life of the vehicle. The catalytic converters have been used to control the emissions, but they reduce engine efficiency and can only be used with unleaded fuel. The real solution lies in better ignition and fuel injection control [1]. A modern engine control systems requires components which perform accurate analog to digital conversion, precise timing of ignition and provide exact control of start and timing of injection.

Best performances have been obtained using control units based on microprocessor or microcontroller technique [2].

2. Functions of Management System

The experiments effectuated on computer-controlled test-bed have put into evidence some advantage for the timed sequential fuel injection such as: improved torque, better fuel efficiency and fewer emissions. The fuel injection and ignition should be controlled jointly and matched to one another. Every operating condition must be sensed and taken into consideration during fuel metering and ignition point

determination.

Based on these functions a microprocessor control system has been designed, and main functions of an electronic engine control system are specified, namely: a) individual cylinder injection timing control, b) individual cylinder start injection control, c) ignition control, d) controlled number of injection/cycle (1 or 2 – used for starting), e) starting enrichment, f) cold-starting control, g) warm-up enrichment control, h) overrun injection suppressing, i) constant time ignition pulse, j) cylinder in admission phase identifying, k) digital engine speed measurement, l) digital load measurement, m) development hardware resources provided.

So, it results that the management system must assure a complex ensemble of functions, be enough developed concerning hardware resources to allow fine tuning (in real traffic).

3. Block Diagram

The block diagram of a management system which materializes described functions is shown in Fig. 1. In accordance with this block diagram, the next functional grouping of the blocks results: a) microprocessor unit, b) sensors (load, engine speed, complex, auxiliary), c) input signal block, d) A/D converter, e) ROM memory (software, ignition characteristic-map, injection characteristic-map, correction constants, labels), f) RAM memory (temporary storage of necessary data), g) injection control circuits, h) ignition control circuits, i) idle speed control circuit, j) Lambda control circuit, k) signalizing circuits, l) auxiliary circuits (clock, reset, power supply).

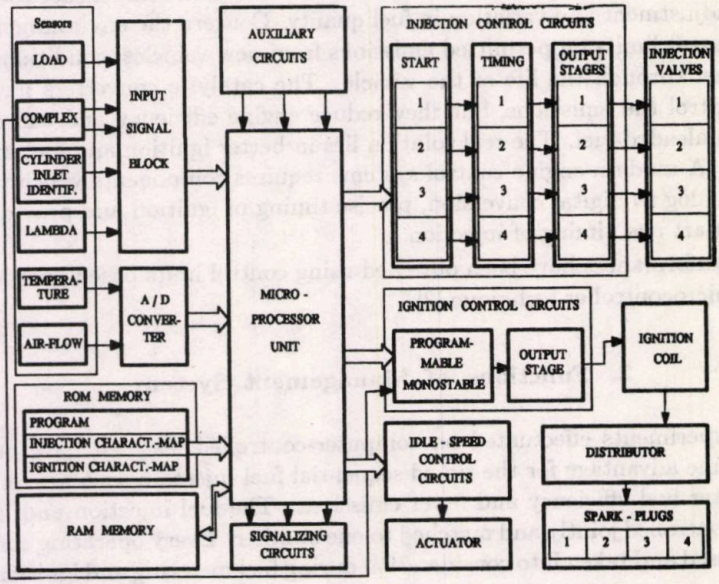

Fig. 1

In what follows the main functions of these blocks and principle of operation are presented.

a) *Microprocessor Unit* uses a Z80 one. Its internal registers assure current necessary of memory. The address-bus and data-bus are accordingly buffered. The unit assures data management, reading the input parameters and forming the adequate addresses to read from the memory the time injection and the ignition advance (expressed in crank-angle degrees before the top dead center – TDC), converted to time in accordance to a reference time. These values are written into adequate control timers to assure the control pulses for the injection and ignition. An adequate software assures the optimum adaptation to various operating conditions: start, post-start, warm-up, overrun, full load.

b) *Sensors* are used in the management system to assure primary information. They are: 1° load sensor [3], digital type, measures throttle angular position (6 bits, Gray code), 2° complex sensor [4], pulse working, provides the engine speed measurement (by timing every half engine rotation), reference mark (maximum advance angle) and TDC pulse identifying, 3° inlet cylinder identifying (using a 2 bits Gray code), 4° temperature sensors (resistive type) for: intake manifold air, engine (coolant liquid), fuel, 5° Lambda sensor, 6° air-flow (hot-wire air-mass meter).

c) *Input Signal Block* is designed to assume system input signals: 1° load, by throttle angle (digital, 6 bits), 2° engine speed, by rotation period, 3° reference mark, corresponding to the maximum advance angle (pulse, 1 bit), 4° inlet cylinder identification (digital, 2 bits, Gray code), 5° Lambda control signal (1 bit) for the engines using catalytic converters.

d) *A/D Converter* is used to convert useful input analog signals to digital ones. A sufficient resolution (8 bits) is provided. The input signal is selected by an analog multiplexer (8 to 1).

e) *ROM Memory* (EPROM type) contains the working program, the test program, and the constant labels (2 ko); the injection characteristic-map (2 ko); the ignition characteristic-map (4 ko).

f) *RAM Memory* (static type, 1 ko) is provided to assure a high system flexibility (for the development phase).

g) *Injection Control Circuit* use programmable timers (8253 type), one for each cylinder to assure individually control the injection pulse time. Other programmable timers (one for each cylinder also) assure the fuel injection start, timed in accordance with inlet valve opening. In this way a sequential multi-point injection system is obtained. Adequate output stages assure the injection valves control. The basic injection time is calculated using measured input quantities and is subjected to matching corrections. The injection valves are located in the intake manifolds, near inlet valves, and they spray the fuel onto the heads of the inlet valves.

h) *Ignition Control Circuit.* The microsystem calculates the ignition angle for all operating condition using the input quantities. The ignition angle can be set to the optimum position for every operating point by reading the characteristic-

map stored in ROM memory. The ignition moment is obtained using a timer (programmable monostable), gate-controlled by the reference-mark pulse. The ignition output stage essentially provides the current amplification and controls the primary current of the ignition coil.

i) *Idle-speed Control Circuits.* An idle-speed actuator is installed in a bypass tubing of the throttle. The opening cross-section of the actuator determines the engine idle-speed. Also, the injected fuel quantity changes accordingly. The required data regarding the actual speed is fed to the control unit from the complex sensor. The actual speed is compared to the set one. From the difference the control unit generates the actuator control signal which is fed to the idle-speed actuator as a pulse train. An oscillator and a pulse-width modulator are used to generate this pulse train.

j) *Lambda Control Circuit* provides closed-loop control of the injected quantities of fuel, so that the air/fuel mixture enables a virtually complete combustion to take place. The Lambda sensor is used to measure the oxygen content in the exhausted gas. If the oxygen components are still present in the exhausted gas, even with a rich mixture, then the sensor signal is a measure of the mixture composition. The principle of the sensor operation is based on the fact that, starting temperatures of roughly 350°C the ceramic material used conducts ions. If the percentage of oxygen present on both sides of the sensor is different, a step-like voltage curve in the area of $\lambda = 1$ is generated on the basis of the special properties of the material used. The voltage is amplified and used to correct basic injection duration. So, the closed-loop control consists in the engine (the controlled system), the Lambda sensor (the measuring element), the microprocessor unit (the controller) and the injection valves (the final controlling element).

k) *Signalizing Circuits* provide information about system and blocks state. There are useful during the system development phase.

l) *Auxiliary Circuits* provide useful signals like: clock (2 MHz, crystal), reset (automatically and manual).

4. Conclusions

The designed engine management system provides the following improvements: a) reduction of the fuel consumption; b) increase in the specific engine power; c) providing closed-loop control of the mixture, it becomes possible to use catalytic converters for the exhaust and thus to achieve the maximum improvement in exhausted gas possible at the present time; d) constant, low emissions and economical idling ensured under the most various conditions.

Received, April 5, 1995

Technical University "Gh.Asachi", Jassy,
Department of Applied Electronics

REFERENCES

1. A r a m ă C., G r ü n w a l d B., *Motoare cu ardere internă. Procese şi caracteristici.* Ed. Tehn., Bucureşti, 1966.
2. M e t z e r m a e k e r s D., V e l d h u i z e n E., *Engine Management with PCB 83C552 Single-Chip 8-bit Microcontroller.* PHILIPS, Electronic Components and Applications, **9**, *1*, 2-13 (1989).
3. D i m i t r i u L. et. al., *Traductor de sarcină pentru motoare cu ardere internă cu aprindere prin scânteie.* Patent, Romania, No.*98669* (1990).
4. D i m i t r i u L. et. al., *Traductor complex pentru motoare cu aprindere prin scânteie.* Patent, Romania, No.*98960* (1991).

SISTEM ELECTRONIC CU MICROPROCESOR PENTRU CONTROLUL INJECŢIEI ŞI AL APRINDERII LA MOTOARE CU APRINDERE PRIN SCÂNTEIE

(Rezumat)

Este prezentată schema bloc a unui sistem cu microprocesor realizat pentru controlul electronic, secvenţial, al injecţiei şi al aprinderii la motoare cu aprindere prin scânteie. Sistemul foloseşte microprocesorul Z80, pe 8 biţi, ca unitate centrală ce controlează un bloc de timere programabile, de tip 8253, programate să genereze impulsurile corespunzătoare întârzierii şi timpului de injecţie pentru fiecare injector electromagnetic în parte, precum şi impulsurile de aprindere corespunzătoare diferitelor regimuri de lucru ale motorului. Temperatura blocului motor, a lichidului de răcire, compoziţia gazelor eşapate (controlul Lambda) sunt prevăzute ca bucle de control ale sistemului, informaţia analogică fiind convertită digital cu ajutorul unui CAD de tipul ADC0808, pe 8 biţi. Pentru o uşoară urmărire a sistemului de control sunt prevăzute şi circuitele de semnalizare corespunzătoare.

BULETINUL INSTITUTULUI POLITEHNIC DIN IAŞI
Tomul XLII (XLVI), Fasc. 1–2, 1996
Secţia III
ELECTROTEHNICĂ. ENERGETICĂ. ELECTRONICĂ

D.C. 621.316.719; 621.313.333.021.2

THE SELFBRAKING METHOD OF A TWO-PHASE ASYNCHRONOUS MOTOR SUPPLIED BY A PWM INVERTER

BY

C. POŞA, D. ALEXA and RADU MUNTEANU

The paper presents an original PWM transistor inverter control method, which improve the transient behaviour of a two-phase electric motor. The transistors are controlled only 3/4 of the period. Each one is off during a quarter of a period. Considering the transient state equations for the asynchronous motor, its equivalent circuit is presented according to the suggested method. A simulation in PSPICE of the dynamic state of the motor is give too.

1. Introduction

Generally, the methods that have the quick damping of the transient components of the currents by the windings of the machine, of high complexity, try to keep constant the flux into the machine airgap.

The method described below is based upon a certain behaviour in the transient condition of the inverter. The method is applied to the inverters based on the PWM principle in comparison with the PAM one. An inverter achieved with bipolar transistors or with IGBT following the PWM principle, for the supplying of a two-phase asynchronous motor is represented in Fig. 1. This inverter meant for the supplying of the voltage and variable frequency of the biphased motor may be, in its turn, supplied from the monophased network by means of a rectifyer.

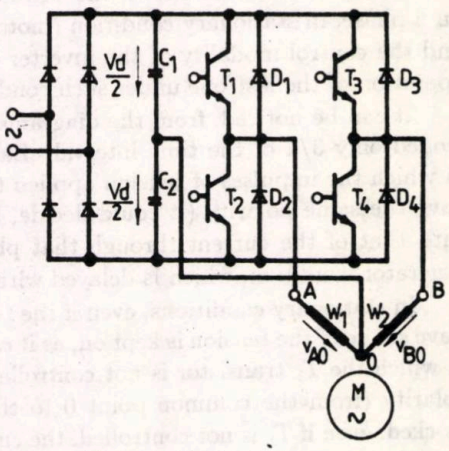

Fig. 1.– Basic diagram of the two-phase PWM inverter.

2. Description of the Self-braking Method

If the biphased machine passes from the motor condition to the generator one (changing the revolution way or the supplying tensions frequency) the compared resistance of the motor becomes negative and the current through the motor changes the direction of its rotation.

In Fig. 2 there are shown the tensions and currents diagrams in the two situations. It is noticed that in generator conditions the phase difference within the tension fundamentals and the current on each phase is bigger than $\pi/2$.

If the interval ε/ω_1, in which can appears this phase difference supplementarily to $\pi/2$, the transistor control which connects the respective phase to the tension with the polarity in the direction of the current remained behind, is blocked, on this phase, during all this interval (ε/ω_1) the tension remains constant (it is no longer pulse width modulated).

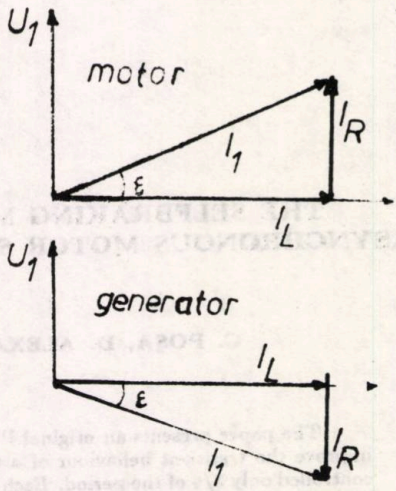

Fig. 2.– The phase diagram for the motor and generator state.

This tension impulse, widened on the whole interval of supplementary delay, which may reach at least a quarter of the period, increases the tension applied on phase and the motor which is in generator conditions is strongly braked. It appears that a self-adjusting phenomenon of the acceleration field, depending on the angle, decides a reduction of the speed oscillation.

In Fig. 3 there are shown the wave shapes of the tension and of the current on a phase, in stationary condition (motor) and in dynamic condition (generator) and the control modality of the inverter transistors from Fig. 1, necessary to the operation of the last one under such conditions.

It can be noticed, from the diagrams of Fig. 3*c*, that the transistors are controlled only 3/4 of the time interval. Each is blocked in the quarter of a period in which the impulses of tension applied to the windings by this transistor should have the same polarity (it could decide, by winding, a current of the same way) with that of the current through that phase in the situation of its operation in generator condition, which is delayed with $\pi/2 + \varepsilon/\omega_1$.

In stationary conditions, even if the respective transistor is not controlled, the wave shape of the tension is kept on, as it can be observed in Fig. 3*a*. In the interval in which the T_1 transistor is not controlled $(3\pi/2, 2\pi)$, the current has a negative polarity (from the common point 0 to the end of the A phase) and when T_2 is blocked, even if T_1 is not controlled, the current goes on through D_1 to $+U/2$. The same happens, too, in the interval of time when T_2 is not controlled, the current

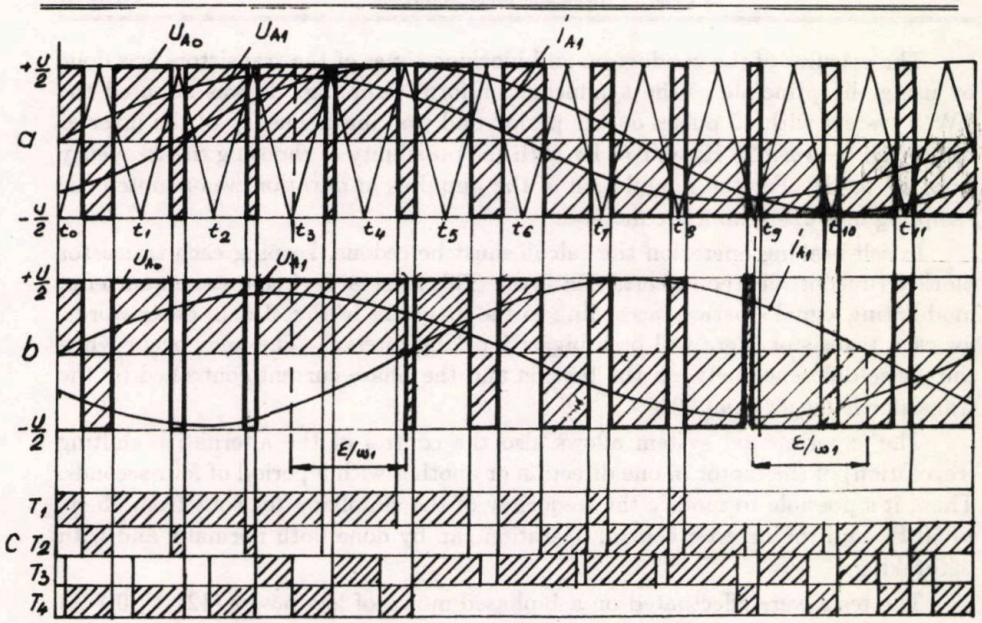

Fig. 3.– Voltage and current waveform in the motor and generator state and the transistors control program.

going on through D_2, being positive, this time.

In generator conditions, the current is left behind with $\pi/2 + \varepsilon/\omega_1$ and as it can be observed from Fig. 3*b*, while when T_1 is not controlled, the current has a positive polarity (from A to the common 0) during ε/ω_1. If it does not enter T_1 in conduction, it keeps on the winding a negative tension due to the maintaining of the current through D_2 after the blocking of T_2. For the voltage applied on the phase (pulse widths modulated) it appears as a negative impulse with a duration a little larger than the ε/ω_1 interval. It may be added at the most a period of the rectangular signal modulated in duration.

The phenomenon takes place identically for the T_3 and T_4 transistors, which forms the PWM voltage of B phase. It appears, therefore, on each phase, a supplementary braking phase in generator conditions, which decides a quicker damping of the rotor oscillation.

3. Experimentally Results

The inverter operation in both analysed situations was experimentally tried. The inverter was achieved following the scheme of Fig.1, using as switching elements, the bipoled transistors, types BUR 608D, which have a diode antiparalelly incorporated. The control of the transistors was done by means of a system based upon the Z80 microprocessor completed by an interface.

The calculus of the conduction and blocking times of the transistors was done by using the principle of the symmetric uniform sampling. It was adopted the PWM system with 12 pulses on the period and working frequency of the inverter comprised between 25 Hz and 75 Hz with the possibility of choosing the frequency from Hz to Hz. For the modulation of the impulses in duration was adopted the sampling uniform symmetric method.

In self-braking operation the calculi must be redone, keeping each transistor blocked (uncontrolled) on a certain interval. This interval is choosen as a quarter of modulating signal's period, according to the diagrams of Fig. 3*c*. In other words, for each transistor there will be a bigger blocking interval. This may occur when the phase difference between the tension and the phase current controlled by the transistor is bigger than 90°.

The experimental system allows also the control of the alternative shifting (revolution) of the motor in one direction or another with a period of four seconds. Then, it's possible to modify the frequency of the supplying tensions from 25 Hz to 50 Hz and the inverter control operation can by done both normally and with selfbraking.

The tests were effectuated on a biphased motor of low power (127 V; 0.1 A) and on a linear motor with three pairs of reduced tension poles (24 V), but of high inertia. It was noticed a decreasing of the motor returning time in the case of the inverter control in selfbraking conditions, compared to the normal case. The effect is stronger at higher powers.

4. The Simulation of the Dynamic State in PSPICE

To emphasize exactly the phenomenon we made apply to the simulation a computer of inverter operation. We use PSPICE electronic circuit's simulation.

It can be noticed from Fig. 1 that each of the two branchs ($T_1 - T_2$ and $T_3 - T_4$) works independent, as two dephased monophased PWM inverters, so we considered enough the analysis of one branch operation.

The power transistors' control is simulated with E_1 and E_2 tension sources, which are controlled by the tension from the out comparator voltage, which achieves the modulation in duration by comparing an angular signal (carrier) with that of a sinusoidal one (modulator). In this way the control is modulated by means of the eight-couplings.

For the switching transistors there were used the catalogue data of the BUR 608D transistors. These transistors have antiparallel incorporated diode, but for the analysis in PSPICE we defined separately the parameters for the transistor and for diode. For the transistors there were considered the following catalogue data: $I_e = 10^{-10}$ A; $\beta = 20$; $C_{je} = 409$ pF; $C_{jc} = 242$ pF; $T_R = 0.8$ μs; $T_E = 0.1$ μs; $R_e = 1$ Ω; $R_c = 0.2$ Ω and for the diode: $I_e = 10^{-10}$ A; $R_e = 5.4$ m; BV= 300 V; $I_{ev} = 100$ μA; $C_{j0} = 10$ pF; $M = 0.33$; TT= 1.2 μs; $N = 2$; $V_j = 0.7$ V.

In Fig. 4 there are presented the waveforms of the phase voltage and of the phase current for a period. The analysis was made for a 50 Hz frequency of the sinusoidal signal and for 24 phases per period. This result does not bring anything new. It was just used for the checking of the correctness of operation of the scheme used in the modelling of the inverter – biphased motors ensemble. The phase voltage has the PWM form and the phase current has an almost sinuous shape, easy-toothed, having the frequency of the pulses' width modulated.

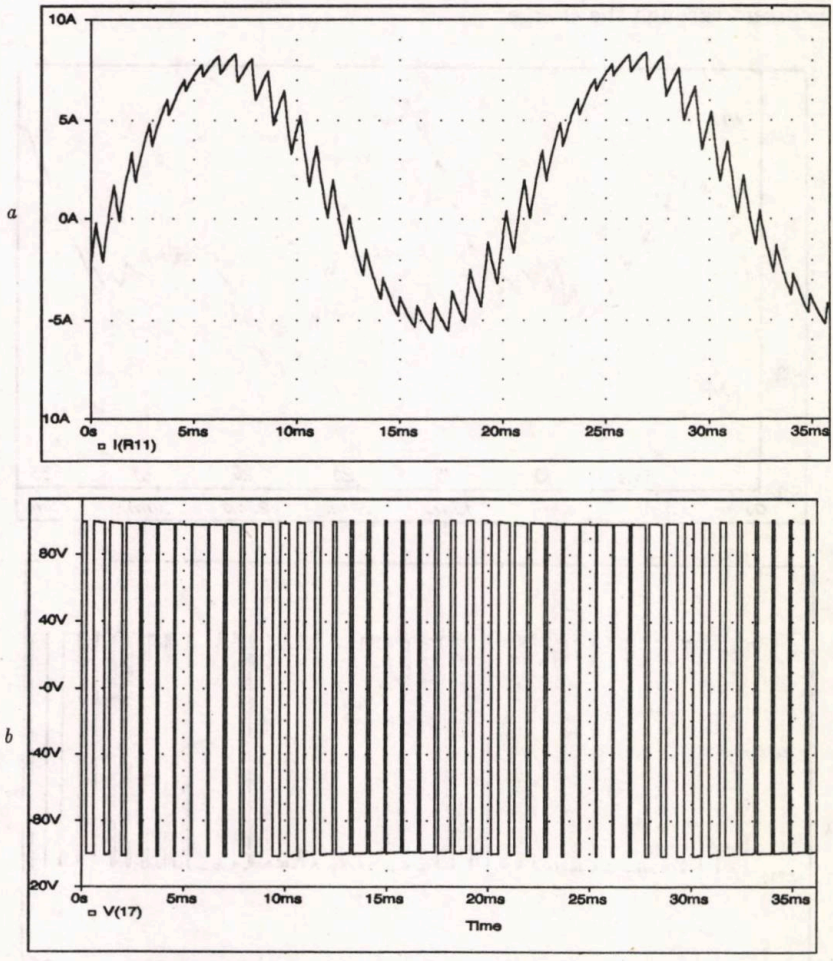

Fig. 4.– Results diagram of the: a – phase current and b – voltage in the motor state.

For the blocking of the transistors for one quarter of period (for example: T_1 in the last quarter and T_2 in the second quarter) in view of getting the way

of operation of the inverter with the possibility of motor selfbraking there was introduced in the main circuits of the switching transistors two supplementary sources. These sources supply a negative impulse on the blocking interval, which summed with the modulated tension E_1 or E_2, lowers the impulses of the latest under the opening limit of the transistors.

In normal motor state, this supplementary blocking of the transistors on the mentioned intervals does not affect, as was previously explained and as there were got as a sequence of the analysis (s. Fig. 4), the shapes of wave of the tension and of the current through the charge.

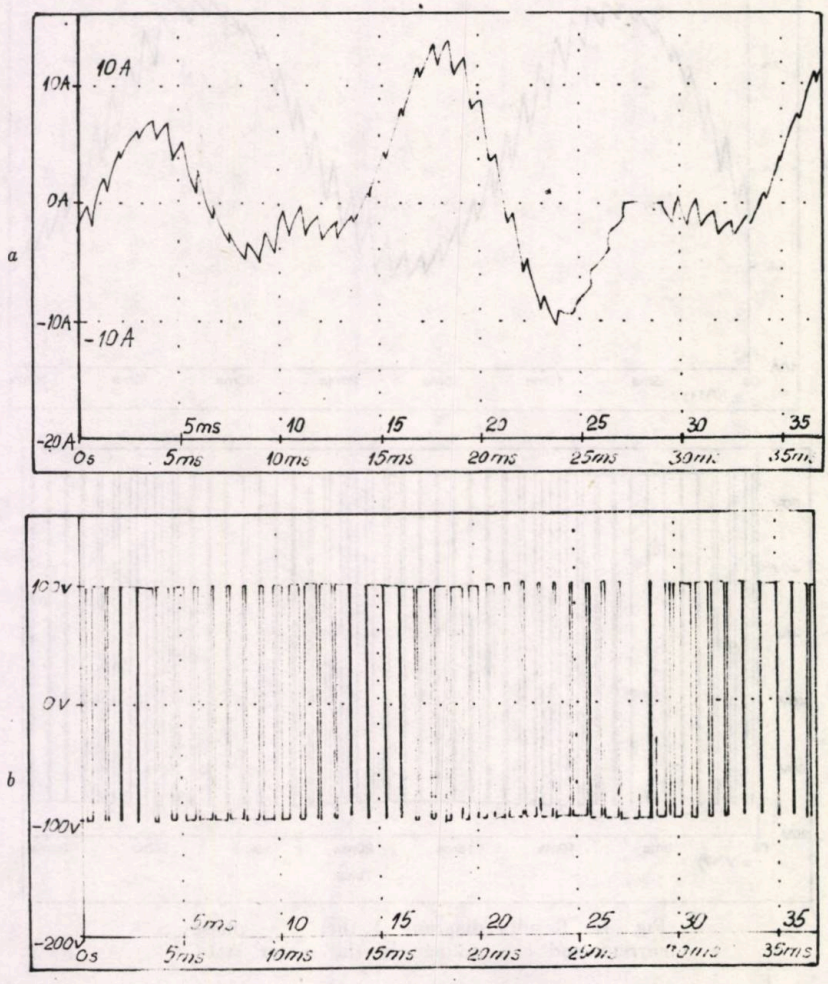

Fig. 5.– Results diagram of the: *a* – phase current and *b* – phase voltage in case of changing of the motor speed.

For simulation of the generator conditions and particularly of the selfbraking operation, it must be introduced in the engine equivalent circuit a sinuous voltage (counterelectromotive tension). This, for simulate the generator conditions which appear when the rotor has a higher speed than the pulsing of the tension supplied by the inverter, it must have a frequency bigger than the supplying one and an effective value big enough to decide a change of direction of the current through the motor.

In Fig. 5 there are represented the waveforms for the situation when the engine (one phase) is supplied with a 24-pulses tension per period, in case of changing of the motor speed. The sinusoidal modulated voltages change the frequency after 10 ms, from 100 Hz to 50 Hz. The counterelectromotive tension has the frequency of 100 Hz and the amplitude of 100 V. The operation condition with selfbraking (the appearance of a supplementary tension because of the coming toghether of several pulses) was obtained just in the last quarter of the period (for details, s. Fig. 6), when T_1 is off and the current through the charge (a phase of the motor) are positive. In the second quarter (when T_2 was off) the phenomenon did not appear because, as it can be observed in the figure, the current through the charge is positive on the whole interval and the diode placed in parallel with T_2 cannot lead (it is inversely polarized).

The getting of this widened impulse (the gathering of several impulses) decides, in fact, an overincreasing of the tension applied on the motor and thus its quicker braking. There are reduced, as we mentioned, the oscillations of the rotor when changing the working conditions.

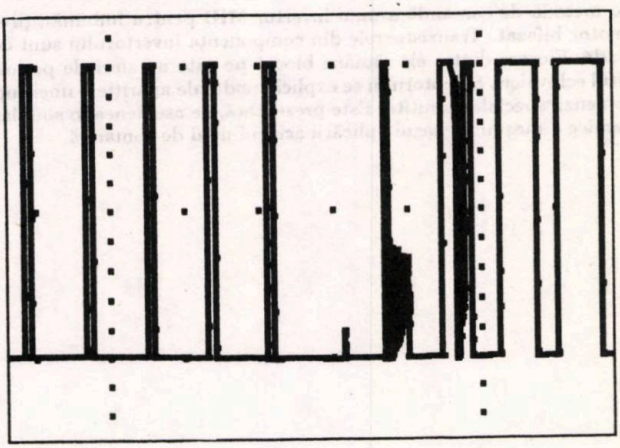

Fig. 6.– The detail of Fig. 5*b* for the last period quarter.

5. Conclusions

By choosing a certain control program of the semiconductor power devices

included in the PWM inverter, high dynamic performances can be obtained in the transient operation of the asynchronous two-phase motor supplied by this inverter, by the appearing a supplementary voltage at the inverter outputs. This voltage results in a faster damping of the transient currents in the motor, also in accelerating the process of establishing the excitation current i_0 at the value corresponding to the new steady state.

Received, March 1, 1995

Technical University "Gh.Asachi", Jassy,
Department of Applied Electronics

REFERENCES

1. Leonhard W., *Control of Electrical Drives.* Springer Verlag, Berlin, 1985.
2. Alexa D., *Static Frequency Converter for Supplying an Asynchronous Two-phase Motor.* IEE Proc., **134**, Pt. **B**, *1*, 57-60 (1987).
3. Alexa D., Neacşu D., *PAM GTO Inverter with Quasi Resonant d.c. Link.* Archiv für Elektrotechnik, **77**, *5*, 351-359 (1994).
4. Poşa C., Munteanu R., Ilieş B., *Une possibilité de simulation avec SPICE d'un ondouleur biphasé réalisé par la méthode MID.* Int. Conf. "Development and Application System", Suceava, 1994, **5**, 251-256.

METODĂ DE AUTOFRÂNARE A UNUI MOTOR ASINCRON BIFAZAT ALIMENTAT DE UN INVERTOR MID

(Rezumat)

Se propune o metodă de comandă a unui invertor MID pentru îmbunătăţirea comportării dinamice a unui motor bifazat. Tranzistoarele din componenţa invertorului sunt comandate numai 3/4 din perioadă. Fiecare dintre ele rămâne blocat pe câte un sfert de perioadă. Luând în consideraţie circuitul echivalent al motorului se explică modul de apariţie a unei supratensiuni de frânare în cazul comenzii speciale amintite. Este prezentată, de asemenea, o simulare în PSPICE a comportării dinamice a maşinii în cazul aplicării acestui mod de comandă.

BULETINUL INSTITUTULUI POLITEHNIC DIN IAŞI
Tomul XLII (XLVI), Fasc. 1–2, 1996
Secţia III
ELECTROTEHNICĂ. ENERGETICĂ. ELECTRONICĂ

D.K. 621.313.333.021.3

BESTIMMUNG DER INNEREN PARAMETER UND DEREN EINFLUß AUF DIE GARANTIERTEN BEMESSUNGS-BETRIEBSPARAMETER VON DREHSTROM-ASINCHRONMOTOREN

VON

KARL SAAL

A calculus method for the analytical determination of the internal parameters of the three phase induction motors is presented, which comes to meet the necessities of the drive engineers. The input data are the rated parameters, guaranteed by the machine factory. The influence of the internal parameters on the catalogue data of the motor is studied, assuming that only one of the catalogue data takes value in comparison to its rated value.

1. Einleitung

In den mit Drehstrom-Asynchronmotoren versehenen elektrischen Antrieben ist die Kenntnis der inneren Parameter dieser Motoren für verschiedene Zwecke notwendig (künstliche Kennlinien, transiente Vorgänge, Einfluß auf die Bemessungs-Betriebsparameter, usw.). In der Praxis verfügt leider der Antriebsingenieur nur selten über diese Parameter, auch die experimentelle Bestimmung weist Schwierigkeiten auf.

Die dimensionlosen Bemessungs-Betriebsparameter (BB) der Drehstrom-Asynchronmotoren sind folgende: η – Wirkungsgrad; $\cos\varphi$ – Leistungsfaktor; $M_{A^*} = M_K/M_R$ – relatives Kipp– oder maximales Drehmoment; $I_{A^*} = I_A/I_R$ – relativer Anlaufstrom. Im Katalog oder den Normen sind üblicherweise diese BB für Nennbetrieb angegeben, wobei unter M_K und M_R das Nenn-Drehmoment bzw. der Nenn-Anlaufstrom zu verstehen sind. Allgemein kennt man auch die Nenngrößen: U_{1N} – Strangspannung im Ständer, P_N – aktive mechanische Leistung und f_N – Netzfrequenz.

Aufgrund der obigen BB kann man eine Rechenvorschrift zur analytischen Bestimmung der inneren Parameter des Drehstrom-Asynchronmotors entwickeln. Ein einfaches Rechenprogramm führt bequem und rasch zum Erhalt der gewünschten inneren Parameter. Indem man annimmt, daß sich nur einer der vom Hersteller garantierten BB, M_{A^*}, M_K und I_A – im Rahmen der von DIN-Normen akzeptierten Toleranzen – verändert, stellt man die relativen inneren Parameter, die verant-

wortlich für solche Abweichungen sind, fest. Die vorgeschlagene Methode wird an einem konkreten Drehstrom-Asynchronmotor ($P_N = 200$ kW, $n_N = 2978$ min^{-1}) veranschaulicht.

2. Berechnungshypothesen

Man setzt symmetrische stationäre und quasistationäre Betriebszustände voraus, die die klassischen Ersatzschaltbilder des Drehstrom-Asynchronmotors (Abb. 1) und das Zeigerbild im Motorbetrieb (Abb. 2) rechtfertigen [1]. Einige Vereinfachungen werden im weiterem Text getroffen. Die Ummagnetisierungsverluste im Läufer werden vernachlässigt.

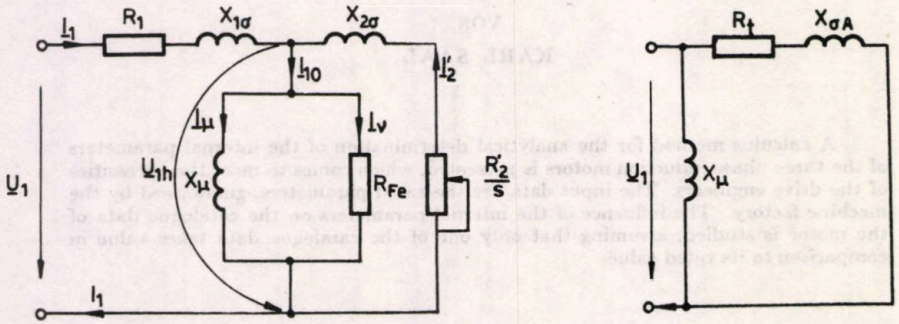

Abb. 1.– Ersatzbildschaltungen des Drehstrom-Asynchronmotors: *a* – in normalem Betrieb; *b* – im Anlauf ($s = 1$).

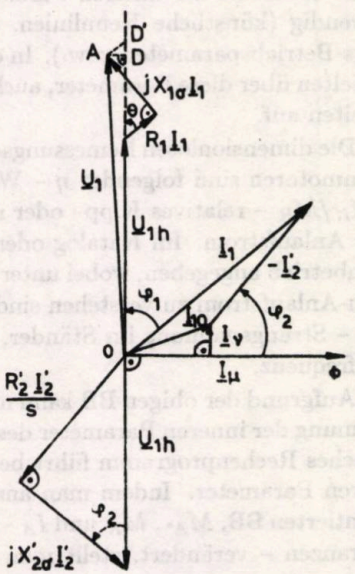

Abb. 2.– Zeigerbild im Nennmotorbetrieb der Asynchronmaschine mit Käfigläufer.

3. Rechenvorschrift zur Berechnung der inneren Parameter des Drehstrom-Asynchronmotors

Die Nennimpedanz der Strangwicklung im Ständer sei

$$Z_N = \frac{U_{1N}}{I_N}. \tag{1}$$

Die relativen inneren Strangparameter sind:

$$R_{1\bullet} = \frac{R_1}{Z_N};\quad R'_{2\bullet} = \frac{R'_2}{Z_N};\quad X_{1\sigma\bullet} = \frac{X_{1\sigma}}{Z_N};\quad X'_{2\sigma\bullet} = \frac{X_{2\sigma}}{Z_N}. \tag{2}$$

Die Berechnungsmethode der inneren Parameter, die hier geschildert wird, benutzt die Katalog- oder Normendaten des Motors und stützt sich hauptsächlich auf die Arbeit [2], mit einigen vom Verfasser unternommenen Verfeinerungen. Zuerst führt man die Koeffizienten

$$k_e = \frac{U_{1h}}{U_{1N}} < 1,\quad k_s = \frac{R'_{2\bullet}}{s_N} = \frac{k_e \cos\varphi_2 \cos(\varphi_2 + \varphi_\mu)}{\cos\varphi_N} < 1, \tag{3}$$

ein. Man schreibt die Gleichung der Ständer-Spannungen und führt im Abb.2 die Annäherungen:

$$\theta \approx \varphi_N,\quad \text{Punkt}\, D \approx \text{Punkt}\, D',\quad OA = OA', \tag{4}$$

ein (OD' entspricht U_{1N}). Somit erhält man:

$$k_e \approx 1 - (R_{1\bullet}\cos\varphi_N + X_{1\sigma\bullet}\sin\varphi_N). \tag{5}$$

In Gl.(3) hat man die Winkel:

$$\begin{gathered}\varphi_\mu \approx \arctan(X_{1\sigma\bullet}\cos\varphi_N),\\ \varphi_2 = \arctan\left(\frac{X'_{2\sigma}}{k_s}\right) = \arctan\left[\frac{X'_{2\sigma\bullet}}{k_e\cos\varphi_2\cos(\varphi_2+\varphi_N)}\right]\end{gathered} \tag{6}$$

aufzeichnet.

Die relative Kurzschluß-Streureaktanz sei:

$$X_{\sigma\bullet} = X_{1\sigma\bullet} + X_{2\sigma\bullet}. \tag{7}$$

Jetzt müssen die Koeffizienten k_e und k_s ermitellt werden. Aus dem Ausdruck des Motorkippschlupfes:

$$s_k = \frac{R'_{2\bullet}}{\sqrt{R_{1\bullet}^2 + X_{\sigma\bullet}^2}} = \frac{k_s s_N}{\sqrt{R_{1\bullet}^2 + X_{\sigma\bullet}^2}}, \tag{8}$$

kann das Verhältnis s_N/s_k berechnet werden. Andererseits ergibt sich von der K l o s s'schen Gleichung, in einer dem Nennbetrieb entsprechenden Form geschrieben:

$$\frac{2M_{K\bullet}}{s_K/s_N + s_N/s_K} = 1. \tag{9}$$

Weiterhin ergibt sich:

$$\frac{s_N}{s_K} = b = M_{K\bullet} - \sqrt{M_{K\bullet}^2 - 1} = \frac{\sqrt{R_{1\bullet}^2 + X_{\sigma\bullet}^2}}{k_s}. \tag{10}$$

Die Kurzschluß-Streureaktanz wird zu:

$$X_{\sigma\bullet} = \sqrt{b^2 k_s - R_{1\bullet}^2}.. \tag{11}$$

Wie man weiß, kann man ungefähr

$$X_{1\sigma\bullet} \approx X'_{2\sigma\bullet} = 0,5\sqrt{b^2 k_s - R_{1\bullet}^2} = \frac{X_{\sigma\bullet}}{2} \tag{12}$$

annehmen. Nur aus diesen wenigen Bemessungs-Nennparametern kann eine bessere Genauigkeit nicht erreicht werden. Um den Widerstand $R_{1\bullet}$ zu schätzen, wird der Ausdruck des Nennkippmomentes im Motorbetrieb:

$$M_{KN} = \frac{3U_{1N}^2}{2\Omega_0\left(R_1 + \sqrt{R_1^2 + X_\sigma^2}\right)} \tag{13}$$

benutzt. Die obige Gleichung wird *per unit* zu:

$$\frac{M_{KN}}{M_N} = M_{K\bullet} = \frac{1 - s_N}{2\cos\varphi_N \eta_N (R_{1\bullet} + bk_s)}. \tag{14}$$

Indem das elektromagnetische Nennmoment M_N durch das Nutzmoment M_{NN} approximiert, erhält man:

$$M_N \approx M_{NN} = \frac{P_N}{\Omega_N} = \frac{3U_{1N} I_{1N} \eta_N \cos\varphi_N}{\Omega_0(1 - s_N)}. \tag{15}$$

Mit Hilfe von Gl.(14) kann man den Strangwiderstand im Ständer wie folgt

$$R_{1\bullet} = a - bk_s \tag{16}$$

schreiben, wobei

$$a = \frac{1 - s_N}{2M_{K\bullet}\eta_N \cos\varphi_N}. \tag{17}$$

Durch Einsetzen von $R_{1\bullet}$ aus Gl.(10) in Gl.(14) kann man jetzt die Kurzschluß-, Streureaktanz ausrechnen:

$$X_{\sigma\bullet} = \sqrt{a(2bk_s - a)}. \tag{18}$$

Um den Koeffizient k_s zu bestimmen, muß man die Winkel φ_2 und φ_μ als Funktionen von k_s schreiben:

$$\begin{cases} \varphi_2 = \arctan\left(\frac{X_{\sigma\bullet}}{2k_s}\right) = \arctan\left[0,5\sqrt{\frac{a}{k_s}\left(2b - \frac{a}{k_s}\right)}\right], \\ \varphi_\mu = \arctan(0,5X_{\sigma\bullet}\cos\varphi_N) = \arctan\left[0,5\cos\varphi_N\sqrt{a(2bk_s - a)}\right]. \end{cases} \tag{19}$$

Setzt man k_e aus Gl.(5) in die zweite Gl.(3) ein, ergibt sich eine transzendentale Gleichung in k_s und zwar:

(20)

$$k_s = \left\{1 - \left[(a - bk_s)\cos\varphi_N + 0,5\sin\varphi_N\sqrt{a(2bk_s - a)}\right]\right\}\frac{\cos\varphi_2\cos(\varphi_2 + \varphi_\mu)}{\cos\varphi_N}.$$

Man bemerkt gleich die Anwesenheit von k_s in den Ausdrücken beider Winkel φ_2, φ_μ, gemäß Gl.(19). Obwohl anscheinend kompliziert, kann Gl.(20) ohne Schwierigkeiten numerisch gelöst werden, wenn man eine iterative metode (z.B. das Verfahren der sukzessiven Approximationen) benutzt wird. Der anfänglich gegebene Wert von k_s soll kleiner als 1 und positiv sein, entsprechend den Ungleichungen:

$$1 \geq k_s > \frac{a}{2b}. \tag{21}$$

Nach einigen Iterationen, gewöhnlich unter 10, erreicht man schon eine bessere Genauigkeit als 10^{-5} in der Bestimmung von k_s. Nachdem k_s ermittelt worden ist, wird der Koeffizient k_e durch die geschweifte Klammer von Gl.(20) oder mit Hilfe folgenden Ausdrucks:

$$k_e = \frac{k_s\cos\varphi_N}{\cos\varphi_2 + \cos(\varphi_2 + \varphi_\mu)} \tag{22}$$

ausgerechnet.

Aus der zweiten Gl.(3) ergibt sich:

$$R'_{2\bullet} = k_s s_N. \tag{23}$$

Die Magnetisierungsreaktanz wird zu:

$$X_\mu \approx \frac{k_e}{\sin\varphi_N - \cos\varphi_N\tan(\varphi_2 + \varphi_\mu)}. \tag{24}$$

Der relative fiktive Widerstand der Eisenverluste ist:

$$R_{\mathrm{Fe}\bullet} = \frac{R_{\mathrm{Fe}}}{Z_N} = \frac{k_e^2}{P_{0N\bullet}\eta_N \cos\varphi_N}, \tag{25}$$

wobei

$$P_{0N\bullet} = \frac{1}{\eta_N - (1 + P_{JN\bullet})}, \tag{26}$$

die relative Gesamtverlustleistung im Leerlaufbetrieb ist. Die relative Joule'sche Gesamtverlustleistung des Motors im Nennbetrieb wird durch die Beziehung

$$P_{JN\bullet} = \frac{R'_{1\bullet}}{\eta_N \cos\varphi_N} + \frac{k_e R'_{2\bullet}}{k_s \eta_N} \tag{27}$$

bestimmt. Der relative Leerlaufstrom, I_{0N}, und der entsprechende Leistungsfaktor im Leerlauf, $\cos\varphi_{0N}$, werden wie folgt

$$I_{0N\bullet} = k_e \frac{\sqrt{R^2_{\mathrm{Fe}\bullet} + X^2_{\mu\bullet}}}{R_{\mathrm{Fe}\bullet} X_{\mu\bullet}}; \quad \cos\varphi_{0N} = \frac{P_{0N}\eta_N \cos\varphi_N}{I_{0N\bullet}} \tag{28}$$

berechnet.

Die Parameter des einphasingen Ersatzschaltbildes beim Anlauf des Motors sollen die Stromverdrängung in den Ankerstäben – wenn die Maschine ein Kurzschlußmotor ist – sowie die magnetische Sättigung im Augenblick des Anlaufes, berücksichtigen der Läuferwiderstand wird zu:

$$R'_{2A\bullet} = kR'_{2\bullet}, \qquad (k > 1) \tag{29}$$

und die Reaktanz $X_{\sigma\bullet}$ vermindert sich k_x-mal:

$$X_{\sigma A\bullet} = k_x X_{\sigma\bullet}, \qquad (k_x < 1). \tag{30}$$

Mit

$$R_{t\bullet} = R_1 R'_{2A\bullet}, \tag{31}$$

kann das Anlaufdrehmoment $M_{A\bullet}$ und der Anlaufstrom $I_{A\bullet}$ wie folgt:

$$M_{A\bullet} = \frac{R'_{2A\bullet}}{R^2_{t\bullet} + X^2_{\sigma A\bullet}}, \qquad I^2_{A\bullet} = \frac{M_{A\bullet}}{R'_{2A\bullet}} \tag{32}$$

erhalten werden. Mit Hilfe dieser Gleichungen ergibt sich jetzt der Läuferwiderstand im Anlauf:

$$R'_{2A\bullet} = \frac{M_{A\bullet}}{I^2_{A\bullet}}. \tag{33}$$

Da $R'_{2A\bullet} = k_r R'_{2A}$ und $R'_{2\bullet} = k_s s_N$ sind, kann man demnach den Fakto.

$$k_r = \frac{M_{A\bullet}}{I^2_{A\bullet} k_s s_N} \tag{34}$$

ermitteln.

Die Kurzschlußstreureaktanz beim Anlauf, die in der ersten Beziehung (32) vorkommt, nimmt die Form:

$$X_{\sigma A\bullet} = \frac{1 - R^2_{t\bullet} I^2_{A\bullet}}{I_{A\bullet}} \tag{35}$$

an. Der Verminderungsfaktor der Anlaufkurzschlußreaktanz wird durch den folgenden Ausdruck berechnet:

$$k_A = \frac{X_{\sigma A\bullet}}{X_{\sigma\bullet}}. \tag{36}$$

Schließlich wird der Anlaufleistungsfaktor wie folgt:

$$\cos\varphi_A = \frac{R_{t\bullet}}{R^2_{t\bullet} + X^2_{\sigma A\bullet}} = R_{t\bullet} I_{A\bullet} \tag{37}$$

ermittelt. Mit dieser letzten Beziehung ist die vorgestellte Rechenvorschrift der inneren Parameter der Drehstrom-Asynchronmotoren, aufgrund ihrer Katalog- oder Normendaten, vollständig dargestellt.

4. Einfluß der Veränderung innerer Parameter auf die Bemessungs-Betriebsparameter

Das Problem der Beeinflußung garantierter BB eines Drehstrom-Asynchronmotors durch seine inneren Parameter ist gleichzeitig wichtig und schwierig. Die Normen sind sehr streng, was die Beibehaltung von zwei BB, Wirkungsgrad und Leistungsfaktor, anbelangt. Deshalb studiert man hier den Einfluß der inneren Parameter, ihre ungünstigten tolerierten Abweichungen und deren numerische Werte, im Falle eines konkreten Drehstrom-Asynchronmotors mit Kurzschlußläufer und dem Einsatzgebiet in einer Umgebung mit Explosionsgefahr, Typ MIB2 Ex d II BT4, 315 M 70-2 [3]. Seine Bemessungsdaten sind: P_N=200 kW, U_{1N}=500 V (verkettete Spannung), f_{1N}=50 Hz, n_N=2978 min.$^{-1}$, η_N=0,94, $\cos\varphi_N$=0,93, $M_{K\bullet}$=2,2, $M_{A\bullet}$=1,25, $I_{A\bullet}$=6.

Der im § **3** vorgelegten Berechnungsvorschrift nach haben die Koeffizienten k_s und k_e die Werte 0,9724, bzw. 0,9347. Was die relativen inneren Parameter anbelangt, so wurden diese wie folgt, nach einem eigenen Rechenprogramm, festgestellt: $R_{1\bullet}$=0,025; $R'_{2\bullet}$=0,0071; $X_{1\sigma\bullet} \approx X_{2\sigma\bullet}$=0,118; $X_{\mu\bullet}$=6,09; $R_{\mathrm{Fe}\bullet}$=35,82. Im Leerlauf hat man: $P_{0N\bullet}$=0,0279; $I_{0N\bullet}$=0,156; $\cos\varphi_{0N}$=0,156 gefunden. Im

Tabelle 1

Einige garantierte Bemessungs-Betriebsparameter, ihre ungünstigste tolerierte Abweichungen und von diesen betroffenen Werten

Garantierte Parameter	Werte	Ungunstigste Abweichungen[1)]	Garantierte, am ungünstigsten betroffenen Parameter
Anlaufdrehmoment, M_A	1,25	$-0{,}15\ M_A$	1,063
Kippdrehmoment, M_K	2,2	$-0{,}1\ M_K$	1,988
Anlaufstrom, I_A	6,0	$+0{,}2\ I_A$	7,200

[1)] VDE 0530, Teil 1/1.66

Tabelle 2

Bezogene innere Parameter eines Drehstrom-Asynchronkurzschlußmotors, welche zu verschiedenen Anlaufdrehmomenten $M_{A\bullet}$ führen

$M_{A\bullet}$	1,0864	1,1098	1,1331	1,1565	1,1799	1,2032	1,2266	1,2500
$R'_{2A\bullet}$	0,030	0,031	0,032	0,032	0,033	0,033	0,034	0,035
$X_{\sigma A\bullet}$	0,158	0,157	0,157	0,157	0,157	0,157	0,156	0,156
$\cos\varphi_A$	0,327	0,331	0,335	0,339	0,343	0,346	0,350	0,354
k_r	4,232	4,323	4,414	4,505	4,496	4,687	4,778	4,869
k_x	0,677	0,677	0,676	0,675	0,674	0,673	0,671	0,670

N o t e. Für alle Fälle hat man k_e=0,935 und k_s=0,972 ermittelt.

Anlaufbetrieb des Motors wurden der aktive Strangwiderstand im Läufer, auf die Ständerwindungszahl bezogen, $R'_{2A\bullet}$=0,037, sowie der Anlaufleistungsfaktor $\cos\varphi_A$=0,37 ermittelt. Der Zunahmefaktor des Läuferwiderstandes beim Anlauf, k_r, und der Verminderungsfaktor, k_x, der Anlaufstreureaktanz wiesen die Werte 4,89, bzw. 0,664 auf.

Um das studium nicht zu verkomplizieren, nimmt man an, daß nur einer der drei Parameter $M_{A\bullet}$, $M_{K\bullet}$ und $I_{A\bullet}$ eine Abweichung im Rahmen ihrer tolerierten Abweichungen (Tabelle 1) zu seinem Bemessungswert aufweist und die anderen Parameter ihren Nennwerten entsprechen. Unter diesen Bedingungen wird die Veränderung des Anlaufsdrehmomentes $M_{A\bullet}$ und Anlaufstromes $I_{A\bullet}$ nur von Änderung der Anlaufparameter hervorgebracht (Tabellen 2, bzw. 4). Die Veränderung des Kippdrehmomentes $M_{K\bullet}$ wird aber von der Änderung fast der gesamten inneren Parameter des Motors verursacht (Tabelle 3). Der Leser kann selber verfolgen welche inneren Parameter des Motors am stärksten die besprochenene garantierten BB beeinflußen.

5. Schlußfolgerungen

Mit Hilfe des in Arbeit [2] beschriebenen analytischen Verfahrens und einiger vom Verfasser unternommenen Verfeinerungen, kann man die inneren Parameter eines Drehstrom-Asynchronmotors mit Käfigläufer bestimmen. Die dargelegte

Tabelle 3

Relative inneren Parameter eines Drehstrom-Kurzschlußmotors, welche zu verschiedenen Kippdrehmomenten $M_{K\bullet}$ führen

$M_{K\bullet}$	2,1725	2,1450	2,1175	2,0900	2,0625	2,0350	2,0075	1,9800
$R_{1\bullet}$	0,025		0,026			0,027		0,028
$R'_{2\bullet}$	0,007							
$X_{\sigma\bullet}$	0,235	0,0238	0,241	0,245	0,248	0,251	0,254	0,258
$X_{\mu\bullet}$	6,220	6,342	6,473	6,614	6,767	6,932	7,112	7,309
$R_{\mathrm{Fe}\bullet}$	35,218	35,687	36,181	36,701	37,249	37,827	38,437	39,081
I_{0N}	0,520	0,149	0,146	0,143	0,140	0,136	0,133	0,129
$\cos\varphi_N$	0,162	0,163	0,164	0,165	0,166	0,168	0,169	0,170
P_{J1N}	0,028	0,029	0,030		0,031			
P_{J2N}	0,007							
P_{JN}	0,036			0,037		0,038		0,039
$R'_{2A\bullet}$	0,035							
$\cos\varphi_A$	0,356	0,359	0,361	0,363	0,366	0,368	0,371	0,373
$X_{\sigma A\bullet}$	0,56				0,155			
k_r	4,878	4,888	4,897	4,907	4,917	4,928	4,939	4,951
k_x	0,662	0,653	0,644	0,635	0,626	0,618	0,609	0,600
k_e	0,934	0,933	0,932	0,931	0,930	0,929	0,928	0,927
k_s	0,971	0,969	0,967	0,965	0,963	0,961	0,959	0,956

Tabelle 4

Relative inneren Parameter eines Drehstrom-Asynchronkurzschlußmotors, welche zu verschiedenen Anlaufströmen $I_{A\bullet}$ führen

$I_{A\bullet}$	6,00	6,15	6,30	6,45	6,60	6,75	6,90	7,05	7,20
$R'_{2A\bullet}$	0,035	0,033	0,032	0,030	0,029	0,027	0,026	0,025	0,024
$X_{\sigma A\bullet}$	0,156	0,152	0,149	0,145	0,142	0,139	0,136	0,133	0,130
$\cos\varphi_A$	0,354	0,353	0,352	0,351	0,35	0,349	0,349	0,349	0,349
k_r	4,869	4,635	4,417	4,214	4,024	3,847	3,682	3,527	3,382
k_x	0,670	0,654	0,639	0,635	0,611	0,597	0,584	0,572	0,560

N o t e. Für alle Fälle hat man k_e=0,935 und k_s=0,972 ermittelt.

Rechenvorschrift benutzt die BB, die im Katalog oder Normen angegeben sind. Der Rechenansatz gilt für die Antriebsingenieure, die keinen weiteren Parameter zur Verfügung haben.

Nach der analytischen Bestimmung der inneren Parameter konnte des weiteren der Einfluß der Veränderung innerer Parameter eines Motors auf die wichtigsten BB ($M_{A\bullet}$, $M_{K\bullet}$ und $I_{A\bullet}$, bzw. relative Anlaufdrehmoment, Kippdrehmoment und Anlaufstrom) untersucht werden. Bei jedem dieser drei BB hat man Abweichungen im Rahmen ihrer größten Abweichungen zu ihren Nennwerten vorausgesetzt.

Die in der Arbeit vorgestellten Berechnungen können als ausreichend genau für die Bedürfnisse des Konstrukteurs der elektrischen – mit Drehstrom-Asynchronmo-

toren ausgestatteten – Antriebe angesehen werden.

Formelzeichen

I_A – Anlaufstrom,
M_A – Anlaufdrehmoment,
M_K – Kippdrehmoment,
M_N – Nenndrehmoment,
P_N – nützliche mechanische Nennleistung,
R_1 – Strangwiderstand im Ständer,
R_2 – Strangwiderstand im Läufer,
R_{Fe} – fiktiver Widerstand der Eisenverluste,
s_K – Kippschlupf,
$X_{1\sigma}$ – Streureaktanz im Ständer,
$X_{2\sigma}$ – Streureaktanz im Läufer,
X_μ – Magnetisierungsreaktanz,
η – Wirkungsgrad.

Indizes

A – Anlauf-
Fe – Eisen-
1 – Ständer,
2 – Läufer,
* – relative (bezogene) Werte,
$'$ – auf die Ständerwindungszahl bezogene Maschinengröße.

Eingegangen am 22. Juli 1995

FH Regensburg, Deutschland

LITERATURVERZEICHNIS

1. V o g e l J., *Grundlagen der elektrischen Antriebstechnik mit Berechnungsbeispielen.* Dr. Alfred Hüthig Verlag, Heidelberg, 1985.
2. M i h a l a c h e M., *Bestimmung der inneren Parameter des Asynchronmotors nach den Katalogdaten* (Rum.). Electrotehnica, **34**, *6*, 261-264 (1986).
3. * * * *Erzeugnissennomenklatur, Niederspannungsmotoren* (Rum.). MIMUEE-CIMAE: Electroputere, Craiova, 1984.
4. S a a l K., S z a b o W., *Elektrische Antriebssysteme. Bestimmung der Betriebsparameter* (Rum.). Editura Tehnică, Bucureşti, 1981.

DETERMINAREA PARAMETRILOR INTERNI ŞI INFLUENŢA LOR ASUPRA PARAMETRILOR DE FUNCŢIONARE IMPUŞI, GARANTAŢI, AI MOTOARELOR ASINCRONE TRIFAZATE

(Rezumat)

Se propune un procedeu de calcul în vederea determinării analitice a parametrilor interni ai unui motor asincron trifazat, venind în întâmpinarea necesităţilor inginerilor specialişti în domeniul Acţionărilor electrice. Datele de intrare sunt parametrii impuşi, garantaţi de uzina producătoare. Se studiază influenţa parametrilor interni asupra datelor de catalog ale motorului, considerând că numai una dintre acestea are o altă valoare decât cea prescrisă.

BULETINUL INSTITUTULUI POLITEHNIC DIN IAŞI
Tomul XLII (XLVI), Fasc. 1–2, 1996
Secţia III
ELECTROTEHNICĂ. ENERGETICĂ. ELECTRONICĂ

D.C. 621-83; 669

NUMERICAL SIMULATION OF THE STABILIZED FUNCTIONING REGIME OF SOME ELECTRICAL DRIVE SYSTEMS USED IN METALLURGICAL INDUSTRIES

BY

IULIAN GRAUR, GR. TAŞCĂ, M. ALBU,
ADRIAN MAREŞ, V. HORGA and DORIN LUCACHE

Utilizing a numerical simulation, the stabilized working regime of electrical drives system of rolling mills are studied.

1. Introduction

In order to determine the main working parameters ($M_m(t) = f_1(t)$; $\Omega_m(t) = f_2(t)$), in the numerical simulation of the stabilized functioning regime of electrical drive systems (EDS) of great importance is the value of the factors these parameters depend on [1],...,[3].

The electromechanical time constant determines the correct design of the electrical drive systems.

2. Numerical Application

In order to underline the advantages of the proposed computation method in [4], established under the specific form (5) [5] (s. also Figs. 1 and 2, and Tables 1,...,4 [5]), there are presented the obtained results for the specific case of a load diagram for a rolling mill, stated in [1], with (s. Fig. 1) and without pause torque (s. Fig. 2). Simulation of the stabilized load state for a cycle has been effectuated for two values of the electromechanical time constant of EDS: T_m=3 s and T_m=6 s. The parameters of loading diagrams are indicated in Tables 1,...,4.

For computerized simulation of the system we used the program established in [5] transcribed in TURBO PASCAL language.

The program gives the value of the torque and of the speed for the whole period of time taken into account.

The input data are: n – number of time intervals considered; T_m – time

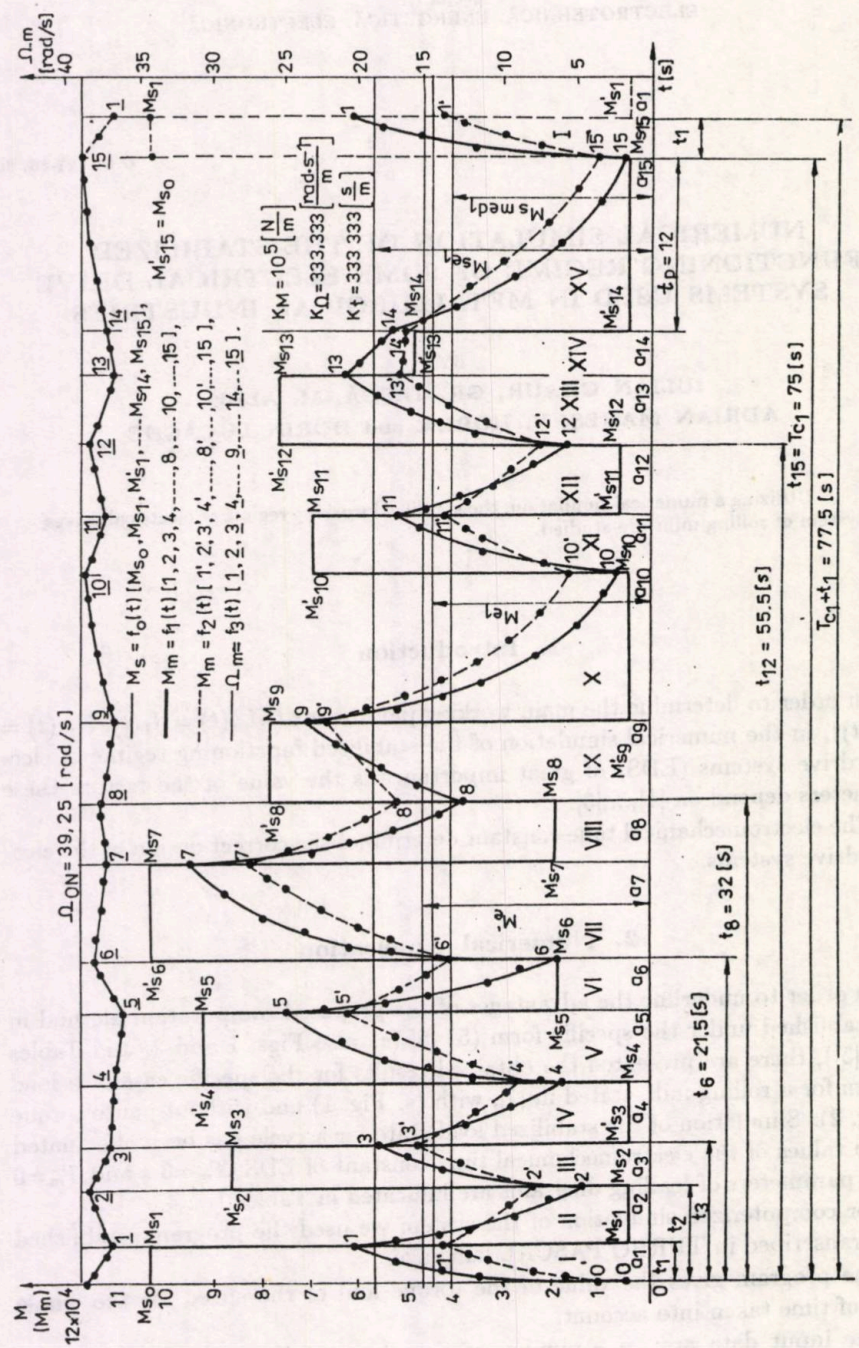
Ω.m [rad/s]
M (Mm) 12x10⁴
Ω0N = 39,25 [rad/s]
Ms = f0(t) [Mso, Ms1, Ms1', ..., Ms14, Ms15],
Mm = f1(t) [1, 2, 3, 4, ..., 8, ..., 10, ..., 15],
Mm = f2(t) [1', 2', 3', 4', ..., 8', ..., 10', ..., 15],
Ωm = f3(t) [1, 2, 3, 4, ..., 9, ..., 14, ..., 15].
Ms15 = Mso
KM = 10⁵ [N/m]
KΩ = 333,333 [rad·s⁻¹/m]
Kt = 333 333 [s/m]
t [s]
tp = 12
t1
t2
t3
t6 = 21,5 [s]
t8 = 32 [s]
t12 = 55,5 [s]
t15 = Tc1 = 75 [s]
Tc1+t1 = 77,5 [s]

Fig. 1

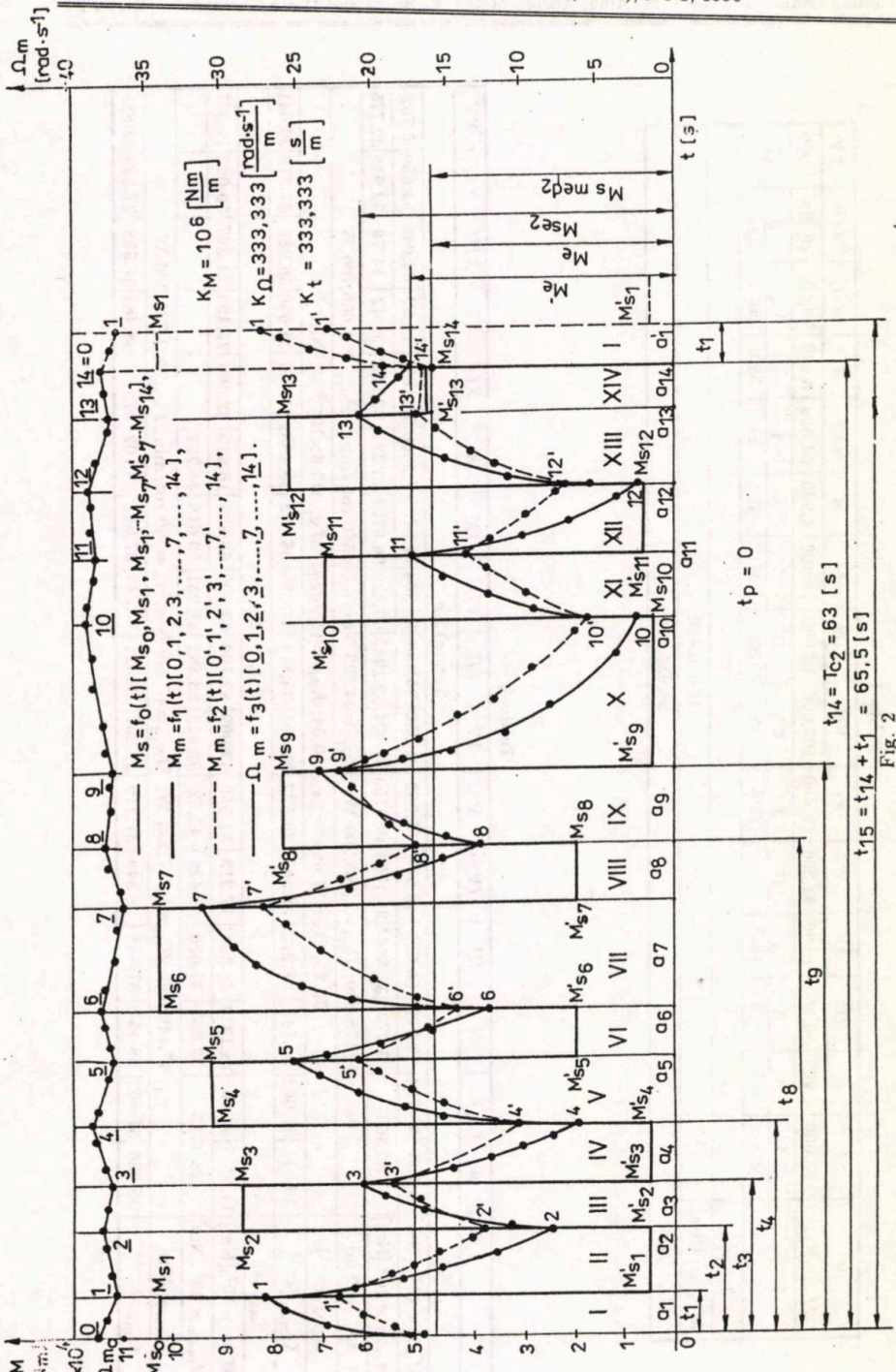
Ωm [rad·s⁻¹]
M [Nm]
t [s]
Ms = f0(t) [Ms0, Ms1, Ms1', ..., Ms7, Ms7', ..., Ms14],
Mm = f1(t) [0, 1, 2, 3, ..., 7, ..., 14],
Mm = f2(t) [0', 1', 2', 3', ..., 7', ..., 14],
Ωm = f3(t) [0, 1, 2, 3, ..., 7, ..., 14].
KM = 10^6 [Nm/m]
KΩ = 333,333 [rad·s⁻¹/m]
Kt = 333,333 [s/m]
Ms med2
Me
Ms e2
tp = 0
t14 = Tc2 = 63 [s]
t15 = t14 + t1 = 65,5 [s]

Fig. 2

Table 1

0	*I*	*II*	*III*	*IV*	*V*	*VI*	*VII*	*VIII*	*IX*	*X*	*XI*	*XII*	*XIII*	*XIV*	*XV*
M_{sk}, [Nm]	103,000	4,900	86,200	4,900	92,200	19,600	103,000	19,000	78,400	4,900	69,600	6,000	76,400	48,200	4,900
t_k, [s]	2.5	4	3	4	45	3.5	6.5	4	5	10	1	43	4	3	12
	2.5	6.5	9.5	13.5	18	21.5	28	32	37	47	51	55.5	60.0	63	75
T_c, [s]	75														
$M_{s\,\mathrm{med}}$, [Nm]	41,070.666														
M_{se}, [Nm]	56,936.816														

Table 2

	0	*I*	*II*	*III*	*IV*	*V*	*VI*	*VII*	*VIII*	*IX*	*X*	*XI*	*XII*	*XIII*	*XIV*	*XV*
T_{m1}, [s]	3; t_p=12 s															
$M_{mk} \times 10^3$, [Nm]	5.793	50.754	13.972	56.625	18.577	75.763	21.350	95.450	39.594	71.0705	7.2606	53.1675	16.52	63.040	53.650	5.792
$M_{mek} \times 10^3$,[Nm]	36.863		3,973	37.3844	39.1724	49.9753	51.034	62.1943	69.420	56.0734	43.281	32.993	36.42	11.79	32.946	32.775
M_{me1},[Nm]	44,175.900; $P_{e_{11}}$= ,665.300 W; $M_{N_{11}}$=44,200 Nm; n_N=360 rot./min., $P_{N_{11}} \cong$ 1,666,180 W															
Ω_{ON}, [s^{-1}]	39.25; Ω_N=37.68 s^{-1}; s_N=0.04; $K_M = \Omega_{ON} S_N / M_{N_{11}}$=3.6×$10^{-5}$ s^{-1}Nm^{-1}															
Ω_{mk}, [s^{-1}]	39.041	37.063	38.747	37.212	38.582	36.522	38.481	35.814	37.825	36.692	38.988	37.336	38.656	36.980	37.319	39.041
T_{m2}, [s]	6; t_p=12 s															
$M_{mk} \times 10^3$,[Nm]	11.0117	42.360	24.1314	48.554	27.313	61.550	43.009	82.700	62.000	66.924	16.615	42.400	23.194	51.267	50.060	11.067
$M_{mek} \times 10^3$,[Nm]	28.1785		33.660	37.020	38.426	45.52	52.553	63.891	57.931	59.618	44.222					
M_{me2},[Nm]	47,146.500; $P_{e_{12}}$=1.777,250 W; $M_{N_{12}}$=47,200 Nm; n_N=360 rot/min, $P_{N_{12}} \cong$ 1,780,000 W															
Ω_{mk}, [s^{-1}]	38.886	37.852	38.454	37.648	38.349	37.219	37.307	36.521	37.340	37.041	38.702	37.[illegible]0	38.484	37.558	37.598	38.885

Table 3

0	*I*	*II*	*III*	*IV*	*V*	*VI*	*VII*	*VIII*	*IX*	*X*	*XI*	*XII*	*XIII*	*XIV*
M_{sk}, [Nm]	103,000	4,900	86,200	4,900	92,200	19,600	103,000	19,600	78,400	4,900	69,600	6,000	76,400	48,200
t_k, [s]	2.5	4	3	4	4.5	3.5	6.5	4	5	10	1	4.3	4.5	3
	2.5	6.5	9.5	13.5	18	21.5	28	32	3	47	51	55.5	60.0	6.3
T_c, [s]	63													
$M_{s\,\mathrm{med}}$,[Nm]	47,960.317													
M_{se}, [Nm]	62,086.340													

Table 4

	0	*I*	*II*	*III*	*IV*	*V*	*VI*	*VII*	*VIII*	*IX*	*X*	*XI*	*XII*	*XIII*	*XIV*
T_{m1}, [s]	3; t_p=0 s														
$M_{mk} \times 10^3$,[Nm]	35.060	31.560	25.065	62.400	20.056	76.103	37.200	95.462	39.600	71.071	7.2085	53.171	7.2753	62.850	53.914
$M_{ek} \times 10^3$,[Nm]	08.088		55.770	45.0583	43.002	50.073	57.754	58.430	59.430	56.076	43.2642	32.977	32.9996	38.560	58.2444
M_{e2}, [Nm]	52,061.343; $P_{e_{21}}$=1,962,522 W; $M_{N_{21}}$=52,100 Nm; $P_{N_{21}}$=1,962,000 W														
Ω_{mk}, [s^{-1}]	37.640	36.803	38.497	37.378	38.648	36.967	38.134	36.386	38.062	37.118	39.034	37.655	39.032	37.365	37.545
T_{m2}, [s]	6; t_p=0														
$M_{mk} \times 10^3$,[Nm]	50.061	58.1062	37.343	55.762	31.4244	63.500	44.091	83.067	52.18	67.01	16.63	42.41	23.200	51.27	50.620
$M_{mek} \times 10^3$,[Nm]	59.313		53.470	46.855	44.156	48.357	54.0865	64.567	68.2088	59.749	44.277	30.444	33.270	38.106	50.946
M_e, [Nm]	50,638.610; $P_{e_{22}}$=1,908,890 W; $M_{N_{22}} \cong$ 51,000 Nm; $P_{N_{22}}$= 1,922,514 W														
Ω_{mk}, [s^{-1}]	37.700	37.140	38.093	37.522	38.276	37.282	37.884	36.675	37.633	37.173	38.377	37.935	38.531	37.661	37.681

electromechanical constant; MS – a vector with $n+1$ elements containing the input data values; CON=O_{ON} – angular speed of synchronizing; M_N – nominal torque; s_N – nominal sliding; t – a vector with $n+2$ elements containing the values of the ends of the time intervals considered; the first two values of the vector are 0; h – time sample step.

First the programme calculates the values of C'_k and E'_k stocking them in vectors C and E with $n+1$ elements, and them the values of the torque and of the speed for the whole time interval considered with time sample step h.

Specifying relations (5), (6), (1 b) for the case of the mentioned load diagram and for the values of the electromechanical time constant there are obtained the variations lows of $M_m(t) = f_1(t)$ and $O_e(t) = f_2(t)$, (s.(2), (3), (5), (6), Tables 1,...,4 and Figs. 1, 2).

a) $T_{m_1} = 3$ s, $t_p = 12$ s, $T_{c_1} = 75$ s

$$(1) \qquad \underset{t_p\neq 0}{M_s(t)} = \begin{cases} M_{s_1} = M_{s_0} = 103,000 \text{ Nm}, & t \in [0, t_1], \\ M_{s_2} = M_{s_1} = 4,900 \text{ Nm}, & t \in [t_1, t_2], \\ M_{s_3} = M_{s_2} = 86,200 \text{ Nm}, & t \in [t_2, t_3], \\ \dots\dots\dots\dots & \dots\dots\dots \\ M_{s_6} = M_{s_5} = 19,600 \text{ Nm}, & t \in [t_5, t_6], \\ \dots\dots\dots\dots & \dots\dots\dots \\ M_{s_{15}} = M_{s_{14}} = 103,000 \text{ Nm}, & t \in [t_{14}, t_{15} = t_{c_1}]; \end{cases}$$

(2)

$$M_m(t) = \begin{cases} M_{m_I}(0) = 5,793.03 \text{ Nm}, t = 0 \\ M_{m_I}(t) = -97,206.911\,\mathrm{e}^{-t/3} + 103,000 \text{ Nm}, t \in [0, t_1], \\ \dots\dots\dots\dots\dots\dots\dots\dots \\ M_{m_{VIII}}(t) = 857,774,641\,\mathrm{e}^{-t/3} + 19,600 \text{ Nm}, t \in [t_7, t_8], \\ \dots\dots\dots\dots\dots\dots\dots\dots \\ M_{m_{XV}}(t) = 64,304,519.4 \times 10^6 \mathrm{e}^{-t/3} + 4,900 \text{ Nm}, t \in [t_{14}, t_{15} = t_{c_1}]; \end{cases}$$

$$(3) \quad \Omega_m(t) = \begin{cases} \Omega_{m_I}(0) = 39.041 \text{ rad/s}, t = 0, \\ \Omega_{m_I}(t) = 39.25 + 3.5\,\mathrm{e}^{-t/3} - 3.708 \text{ rad/s}, t \in [0, t_1], \\ \dots\dots\dots\dots\dots\dots\dots\dots \\ \Omega_{m_{VIII}}(t) = 39.25 - 30,879.89\,\mathrm{e}^{-t/3} - 0.7056 \text{ rad/s}, t \in [t_7, t_8], \\ \dots\dots\dots\dots\dots\dots\dots\dots \\ \Omega_{m_{XV}}(t) = 39.25 - 23.15\,\mathrm{e}^{-t/3} - 0.1764 \text{ rad/s}, t \in [t_{14}, t_{15} = t_{c_1}]. \end{cases}$$

b) $T_{m_2} = 6$ s, $t_p = 12$ s

$$(4) \qquad M_m(t) = \begin{cases} M_{m_I}(0) = 11,011.7 \text{ Nm}, \ t = 0 \\ M_{m_I}(t) = -91,988.303\,\mathrm{e}^{-t/6} + 103,000 \text{ Nm}, \ t \in [0, t_1], \\ \dots\dots\dots\dots\dots\dots\dots\dots \\ M_{m_{VIII}}(t) = 6,709,709.8\,\mathrm{e}^{-t/6} + 19,600 \text{ Nm}, \ t \in [t_7, t_8], \\ \dots\dots\dots\dots\dots\dots\dots\dots \\ M_{m_{XV}}(t) = 1,654,923.92 \times 10^3 \mathrm{e}^{-t/6} + 4,900 \text{ Nm}, \ t \in [t_{14}, t_{15} = t_{c_1}]. \end{cases}$$

$$(5)\quad \Omega_m(t) = \begin{cases} \Omega_{m_I}(0) = 38.886 \text{ rad/s},\ t = 0, \\ \Omega_{m_r}(t) = 39.25 + 3.036\,e^{-t/6} - 3.399 \text{ rad/s},\ t \in [0, t_1], \\ \cdots\cdots\cdots\cdots\cdots\cdots\cdots\cdots\cdots\cdots\cdots\cdots \\ \Omega_{m_{VIII}}(t) = 39.25 - 221.42\,e^{-t/6} - 0.6468 \text{ rad/s},\ t \in [t_7, t_8], \\ \cdots\cdots\cdots\cdots\cdots\cdots\cdots\cdots\cdots\cdots\cdots\cdots \\ \Omega_{m_{XV}}(t) = 39.25 - 54.6125\,e^{-t/6} - 0.1617 \text{ rad/s},\ t \in [t_{14}, t_{15} = t_{c_1}]. \end{cases}$$

c) $T_{m_1} = 3$ s, $t_p = 0$ s, $T_{c_2} = 63$ s

$$(6)\quad \underset{t_p=0}{M_s(t)} = \begin{cases} M_{s_1} = M_{s_0} = 103,000 \text{ Nm}, & t \in [0, t_1], \\ M_{s_2} = M_{s_1} = 4,900 \text{ Nm}, & t \in [t_1, t_2], \\ M_{s_3} = M_{s_2} = 86,200 \text{ Nm}, & t \in [t_2, t_3], \\ \cdots\cdots\cdots\cdots\cdots\cdots\cdots\cdots & \\ M_{s_{13}} = M_{s_{12}} = 76,400 \text{ Nm}, & t \in [t_{12}, t_{13}], \\ M_{s_{14}} = M_{s_{13}} = 48,200 \text{ Nm}, & t \in [t_{13}, t_{14} = t_{c_2}]; \end{cases}$$

$$(7)\quad M_m(t) = \begin{cases} M_{m_I}(0) = 53,639.3 \text{ Nm},\ t = 0, \\ M_{m_I}(t) = -49,340.704\,e^{-t/3} + 103,000 \text{ Nm},\ t \in [0, t_1], \\ \cdots\cdots\cdots\cdots\cdots\cdots\cdots\cdots\cdots\cdots\cdots\cdots \\ M_{m_{XIII}}(t) = -6,574,358.85 \times 10^6 e^{-t/3} + 76,400 \text{ Nm},\ t \in [t_{12}, t_{13}], \\ M_{m_{XIV}}(t) = 7,007,293.194 \times 10^6 e^{-t/3} + 48,200 \text{ Nm},\ t \in [t_{13}, t_{14} = t_{c_2}]; \end{cases}$$

(8)

$$\Omega_m(t) = \begin{cases} \Omega_{m_I}(0) = 37.640 \text{ rad/s},\ t = 0, \\ \Omega_{m_I}(t) = 39.25 + 1.48\,e^{-t/3} - 3.09 \text{ rad/s},\ t \in [0, t_1], \\ \cdots\cdots\cdots\cdots\cdots\cdots\cdots\cdots\cdots\cdots\cdots\cdots \\ \Omega_{m_{XIII}}(t) = 39.25 + 197,230,765.5\,e^{-t/3} - 2.292 \text{ rad/s},\ t \in [t_{12}, t_{13}], \\ \Omega_{m_{XIV}}(t) = 39.25 - 210,218,795.82\,e^{-t/3} - 1.446 \text{ rad/s},\ t \in [t_{13}, t_{14} = t_{c_2}]. \end{cases}$$

d) $T_{m_2} = 6$ s, $t_p = 0$ s, $T_{c_2} = 163$ s

$$(9)\quad M_m(t) = \begin{cases} M_{m_I}(0) = 50,061 \text{ Nm},\ t = 0, \\ M_{m_I}(t) = -52,930.322\,e^{-t/6} + 103,000 \text{ Nm},\ t \in [0, t_1], \\ \cdots\cdots\cdots\cdots\cdots\cdots\cdots\cdots\cdots\cdots\cdots\cdots \\ M_{m_{XIV}}(t) = 6,763,432 \times 10^4 e^{-t/6} + 48,200 \text{ Nm},\ t \in [t_{13}, t_{14} = t_{c_2}], \end{cases}$$

$$(10)\quad \Omega_m(t) = \begin{cases} \Omega_{m_I}(0) = 37.7 \text{ rad/s},\ t = 0, \\ \Omega_{m_I}(t) = 39.25 + 1.63\,e^{-t/6} - 3.1724 \text{ rad/s},\ t \in [0, t_1], \\ \cdots\cdots\cdots\cdots\cdots\cdots\cdots\cdots\cdots\cdots\cdots\cdots \\ \Omega_{m_{XIV}}(t) = 39.25 - 2,083.14\,e^{-t/6} - 1.485 \text{ rad/s},\ t \in [t_{13}, t_{14} = t_{c_2}]. \end{cases}$$

3. Conclusions

1. For a greater efficiency and precision, the numerical simulation of the stabilized functioning mode of the EDS, especially for the general form graphs, is recommanded to be effectuated using a computer.

2. From the energetical point of view, the load diagram without pause torque and $T_m = 6$ s offers to the electrical drive motor a more convenient and a less energy consumption functioning mode.

Received, March 10, 1994

Technical University "Gh. Asachi", Jassy, Department of Electrical Drives, Utilizations and Automatizations

REFERENCES

1. B r a ş o v a n M. et al., *Acţionări electrice. Aplicaţii industriale.* Ed. Tehnică, Bucureşti, 1978.
2. R u s u N., *Contribuţii la optimizarea funcţionării laminoarelor reversibile de tip bluming.* Ph. D. Diss., Polyt. Inst. "Tr. Vuia", Timişoara, 1981.
3. S a a l C., S z a b o W., *Sisteme de acţionare electrică. Determinarea parametrilor de funcţionare.* Ed. Tehnică, Bucureşti, 1981.
4. T a ş c ă Gr., *Contribuţii la calculul cuplului motor stabilizat al unor motoare rotative funcţionând cu şocuri de sarcină periodice.* Bul. Inst. polit., Iaşi, **XXVI (XXX)**, *1-2*, s.IV, 103-112 (1980).
5. T a ş c ă Gr. et al., *Mathematical Model for Stabilized State of Electrical Drive Systems Used in Metallurgical Industry.* Bul. Inst. polit., Iaşi, **XLI (XLV)**, *3-4*, s.III, 137-142 (1995).

SIMULAREA NUMERICĂ A REGIMULUI DE FUNCŢIONARE STABILIZAT AL UNOR SISTEME DE ACŢIONARE ELECTRICĂ UTILIZATE ÎN INDUSTRIA METALURGICĂ

(Rezumat)

Se prezintă rezultatele obţinute în simularea numerică a regimului de funcţionare stabilizat al sistemelor de acţionare electrică a laminoarelor, în baza programului stabilit în [5].

BULETINUL INSTITUTULUI POLITEHNIC DIN IAŞI
Tomul XLII (XLVI), Fasc. 1–2, 1996
Secţia III
ELECTROTEHNICĂ. ENERGETICĂ. ELECTRONICĂ

C.D. 621.3.064.1

LA DÉTECTION MAGNÉTIQUE DES COURT-CIRCUITS DANS LES RÉSEAUX AÉRIENS DE MOYENNE TENSION

PAR

MIRCEA GUŞĂ, MARCEL ISTRATE, N. GAVRILAŞ et C. ASAFTEI

The replacement of manual operated separators by other switching equipments in resistance earthed medium voltage networks becomes of major importance in order to improve the power delivery in rural areas. The break off function of such a load separator demands the use of either current transformers or magnetic induction type transducers for shortcircuits detection.

The examination of magnetic field intensity around a medium voltage line in different situations (normal symmetric or unsymmetric load, unsymmetric and symmetric faults) offers informations for design and emplacement of the transducers on line supports.

There were taken into account five different line crownings, all types of shortcircuits, different distances between post bus and fault, different fault resistances.

The simultaneous utilisation of both horizontal and vertical components of magnetic field intensity vector in an OR logical function provides the correct information about shortcircuits in all possibles situations.

1. Introduction

La détection des court-circuits dans les réseaux aériens de moyenne tension pose de nouveaux problèmes pour le système énergétique roumain. Une telle détection existe mais, pour la plupart des lignes, elle est installée seulement dans le poste HT/MT ou se trouve le seul disjoncteur automatique pour chaque ligne. Les lignes de moyenne tension dans les zones rurales ont une structure ramifiée, vu que les consommateurs sont dispersés sur grandes espaces et ne sont pas munis qu'avec des séparateurs actionnés localement et par voie manuelle. Par conséquence l'apparition d'un court-circuit, dans n'importe quelle section de la ligne, détermine le déclenchement de toute la ligne. Le réenclenchement, après la séparation du secteur à défaut, peut souvent retarder plusieures heures.

Supposant que le point neutral du réseau est mis à terre à l'aide d'une faible impédance, ces déclenchements sont plus fréquents et, par suite, ils incommodent les consommateurs.

Suivant l'exemple des pays dont la technologie est plus avancée on a commencé, en Roumanie aussi, le remplacement des séparateurs simples par des équipements

de commutation plus simples que les disjoncteurs automatiques, comme les séparateurs de charge enfermés en carcasse métallique, isolés en air où en SF_6, qui peuvent déclencher automatiquement en creux de tension (dans une pause où après le cycle RAR). Par conséquence le réenclenchement prochain du disjoncteur dans le poste va rétablir l'alimentation normale des consommateurs. Ce remplacement devient nécessaire tout d'abord dans les réseaux dont le point neutral est mis à terre par une faible résistance. Si la détection des défauts phase–terre dans les réseaux munis par une bobine d'extinction est bien maîtrisée on peut aussi utiliser les séparateurs à déclenchement automatique.

La détection des court-circuits, en vue de commander le déclenchement des séparateurs de charge, peut être réalisée par plusieurs méthodes.

2. Méthodes pour la détection des court-circuits

Les méthodes de détection se rapportent à l'intensité du courant dans les conducteurs de la ligne parce que l'augmentation de celui-ci jusqu'au niveau de „court-circuit" représente la modification essentielle du régime de fonctionnement. Le moyen classique, utilisé dans toutes les installations électriques, c'est le transformateur de courant dans un montage propre à détecter tous les types de court-circuits. Ce procédé, malgré les avantages d'une solution technique bien connue, est assez couteux compte tenu: a) du grand nombre de transformateurs de courant nécessaires parce que chaque séparateur doit être muni de trois unités et le nombre de séparateurs peut être élevé; b) de la nécessité de développer de nouveaux types de tels transformateurs, soit pour fonctionnement à l'extérieur soit pour SF_6.

Une autre solution, moins coûteuse, mais dont les performances sont limitées, c'est l'utilisations des relais primaires de courant, très simples comme, par exemple, ceux insérés dans les dispositifs de signalisation locale [1]. Leur emplacement au potentiel du conducteur empêche la réalisation d'un isolement suffisant entre le relais el le dispositif déclencheur du séparateur, qui se trouve au potentiel de la terre.

Le changement de l'intensité du courant dans les conducteurs de la ligne détermine une modification similaire de l'intensité du champ magnétique autour de celle-ci. Ce changement peut être saisi à l'aide d'un relais REED réduit à son contact. Ce contact doit être emplacé tout près du conducteur et, par suite, il se trouve au potentiel de celui-ci ce que représente, comme dans le cas précédent, le désavantage essentiel de cette solution.

Les modifications de l'intensité du champ magnétique peuvent être saisies aussi à l'aide d'un traducteur inductif, suffisament éloigné par rapport aux conducteurs pour le situer au potentiel de la terre. La puissance du signal induit étant très réduite, une amplification à l'aide d'une source d'énergie devient nécessaire.

L'utilisation d'un tel traducteur doit s'appuyer sur une analyse de l'intensité du champ magnétique des lignes pour divers régimes de fonctionnement (normal où défaut), pour différents types de couronnements, etc. Cette analyse fournie aussi

des informations concernant la construction et l'emplacement du traducteur.

3. Le champ magnétique d'une ligne polyphasée

Autour d'un conducteur rectiligne mince, assez long, parcouru par un courant d'intensité I, se manifeste un champ magnétique dont l'intensité dans un point situé à la distance r du conducteur est donnée par la formule

$$\mathbf{H} = \frac{I}{2\pi r^2}\mathbf{r} \tag{1}$$

et l'orientation duquel est tangentielle au cercle de rayon r dont le plan est normal au conducteur et le sens donné par la règle du vis droit.

L'hypothèse du conducteur mince est acceptable parce que la distance jusqu'au traducteur est assez grande par rapport au diamètre du conducteur. On peut négliger aussi l'influence du courant de retour dans la terre vu que la profondeur de circulation de celui-ci, à la fréquence industrielle, peut atteindre quelques centaines de mètres.

Les lignes électriques sont polyphasées et, par suite, l'intensité du champ magnétique de la ligne sera la résultante vectorielle des champs engendrés par chaque phase.

Pour un système de n conducteurs parallèles, dont les positions sont connues, parcourus par des courants quelconques (Fig. 1), le module de l'intensité du champ magnétique résultant dans un point de coordonnées (x_M, y_M) est

$$H = \sum_{i=1}^{n} \frac{I_i}{2\pi\sqrt{(x_i - x_M)^2 + (y_i - y_M)^2}}. \tag{2}$$

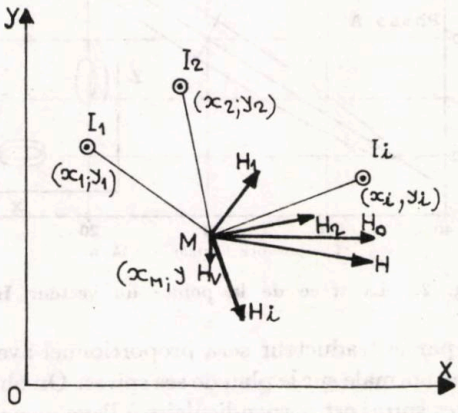

Fig. 1.– Le système de conducteurs parallèles.

Le vecteur champ magnétique résultant a les composantes

$$H_x = \sum_{i=1}^{n} H_i \cos\alpha_i = \sum_{i=1}^{n} \frac{I_i(y_i - y_M)}{2\pi\,[(x_i - x_M)^2 + (y_i - y_M)^2]}, \tag{3}$$

$$H_y = \sum_{i=1}^{n} H_i \sin\alpha_i = \sum_{i=1}^{n} \frac{-I_i(x_i - x_M)}{2\pi\,[(x_i - x_M)^2 + (y_i - y_M)^2]}. \tag{4}$$

Dans le cas particulier d'une ligne triphasée, les courants dans les conducteurs de phase ont les expressions

$$i_1 = \sqrt{2} I_R \sin(\omega t - \phi_R), \quad i_2 = \sqrt{2} I_S \sin(\omega t - \phi_S), \quad i_3 = \sqrt{2} I_T \sin(\omega t - \phi_T),$$

où

$$\phi_R = \varphi_R, \quad \phi_S = \varphi_S + 2\pi/3, \quad \phi_T = \varphi_T + 4\pi/3$$

représentent les déphasages des courants par rapport à la tension de la phase R (origine de phase) et φ sont les déphasages des courants par rapport aux tensions des phases correspondantes.

Il résulte que les composantes H_x et H_y du champ magnétique résultant sont des oscillations périodiques ayant la même fréquence. Vu que les amplitudes de leurs variations, en géneral, ne sont pas les mêmes, la pointe du vector **H** décrit une ellipse dont le centre est le point de calcul considéré et les axes ont des positions qui dépendent de la géometrie de la ligne aussi que du système des courants de phase (Fig. 2). On peut trouver les dimensions de cette ellipse dans [2].

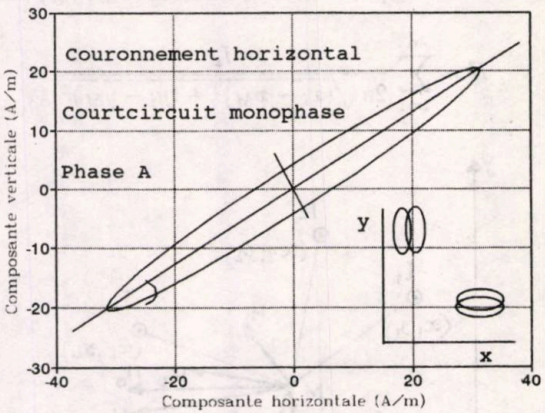

Fig. 2.– La trace de la pointe du vecteur **H**.

Le signal fourni par le traducteur sera proportionnel avec la composante de l'induction magnétique normale sur le plan de ses spires. On obtiendra la sensibilité maximum si le plan des spires est perpendiculaire à l'axe principale de l'ellipse. La position de cet axe peut être déterminée par l'angle β_m:

$$\text{tg}\,\beta_m = \frac{H_{ym}}{H_{xm}}. \tag{5}$$

dont la valeur dépend du type du défaut et les phases qu'il entraîne. Par conséquence, la détection du régime de défaut pourra être réalisée seulement selon les composantes H_x et H_y du champ magnétique résultant. On peut utiliser deux traducteurs inductifs ayant la forme d'une bobine aplatie et emplacés selon les axes d'un système xOy dont le plan est perpendiculaire sur la direction de la ligne (Fig. 2).

4. Étude du champ magnétique des lignes triphasées

L'utilisation d'un traducteur magnétique pour détecter les court-circuits impose que la sensibilité de celui-ci par rapport aux régimes normales de charge (symmétrique ou non symmétrique) soit garantie pour tous les régimes de défaut. Vu que, pour un certain réseau, l'intensité du courant de court-circuit dépend de la distance entre la position du défaut et le jeu de barres (proprement dit de la valeur de l'impédance de court-circuit), il faudra vérifier la sensibilité du traducteur dans le régime minimum de court-circuit par rapport au régime maximum de charge.

Dans ce qui suit on utilise des valeurs numériques communes pour les réseaux aériennes de moyenne tension mais sans être rapportées à un certain réseau.

On a envisagé les situations suivantes concernant la position du défaut: a) un défaut proche, sur un axe dont les conducteurs ont une section de 70 mm^2, à une distance de 10 km du poste; b) un défaut lointain, sur une dérivation dont les conducteurs ont une section de 35 mm^2, à une distance de 5 km du début, la distance sur l'axe jusqu'au poste étant de 30 km.

On a considéré aussi deux valeurs pour la résistance du défaut: a) R_D=0 (défaut métallique); b) R_D=30 Ω (valeur maximum pour la résistance de la prise de terre pour les poteaux de la ligne).

Le régime de charge maximum adopté est caracterisé par:

$$I_m = 100 \text{ A}, \quad \cos\varphi_m = 0,9.$$

En ce qui concerne le type du défaut on a considéré les défauts phase–terre, deux phases–terre, phase–phase et triphasé. On a considéré également que le défaut aurait lieu sur chaque phase (pour les défauts non symmétriques) parce que les positions des conducteurs par rapport au traducteur sont différentes.

Le couronnement de la ligne exerce une certe influence sur le champ résultant. On a considéré les situations plus fréquentes, comme celles de la Fig. 3.

Tenant compte de ces variables, on a déterminé les valeurs: a) des composantes horizontale (H_O) et verticale (H_V) du champ résultant, en fonction de temps; b) de la somme ($H_S = H_O + H_V$) et de la diférence ($H_D = H_O - H_V$) des mêmes composantes, en fonction de temps; c) du maximum du module du vecteur **H** ainsi que sa position dans le système des axes orthogonaux choisi.

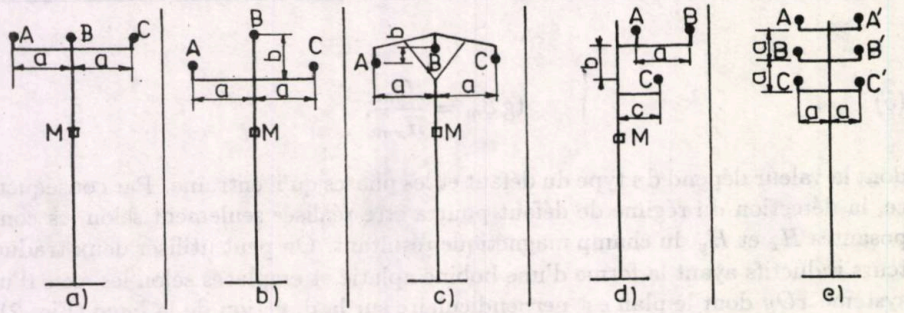

Fig. 3.– Couronnements fréquemment utilisés: *a* – nappe horizontale; *b* – triangle; *c* – nappe voûte; *d* – triangle désaxé; *e* – tonneau double circuit.

Pour l'évaluation de la sensibilité du traducteur de champ magnétique on a rapporté les valeurs maximum des composantes mentionnées dans le régime de défaut aux valeurs des mêmes composantes dans le régime normal. La valeur 2 de ce rapport a été considérée comme minimum acceptable.

Le volume des résultats est très encombrant et ne peut pas être présenté entièrement. La possibilité de détection des défauts est indiqué dans le Tableau 1 par „oui" ou „non". „Oui" signifie que le facteur de sensibilité est supérieur ou égal à 2 pour toutes les situations considérées. „Non", par contraire, signifie qu'il existe au moins une situation pour laquelle la condition mentionnée n'est pas accomplie.

Tableau 1

Les possibilités de détecter les court-circuits

Le couronnement de la ligne	Les composantes du champ magnétique				
	horizontale	verticale	somme	différence	horizontale or verticale
nappe horizontale	Non	Non	Non	Oui	Oui
triangle	Non	Non	Non	Non	Oui
nappe-voûte	Non	Non	Non	Non	Oui
triangle désaxé	Oui	Non	Oui	Oui	Oui
tonneau, double circ.	Oui	Non	Oui	Non	Oui

Par exemple, dans le cas du couronnement en nappe horizontale la détection selon la composante horizontale du champ magnétique n'est pas sûre pour les court-circuits entre deux phases et terre et entre deux phases s'il s'agit des phases extrèmes (A et C). Selon la composante verticale la sensibilité n'est pas assurée pour le cas d'un court-circuit monophasé éloigné sur la phase B, avec R_D=30 Ω.

Pour le couronnement en triangle et en nappe-voûte, la détection n'est pas complètement efficace pour toutes les composantes du champ magnétique.

L'étude des résultats numériques obtenus montre que la sensibilité insuffisante ne se manifeste pas simultanément pour toutes les deux composantes (H_O, H_V) ou leurs combinaisons (H_S, H_D) dans aucune situation de défaut. Par conséquence on

peut utiliser, comme solution générale, une fonction logique „OR" des composantes horizontale et verticale.

En ce qui concerne la valeur maximum du module H, on pourrait assurer la sensibilité imposée dans toutes les situations. Cet avantage ne peut pas être exploité parce que l'orientation du vecteur dans ce moment change de position selon le type de défaut (Fig. 4).

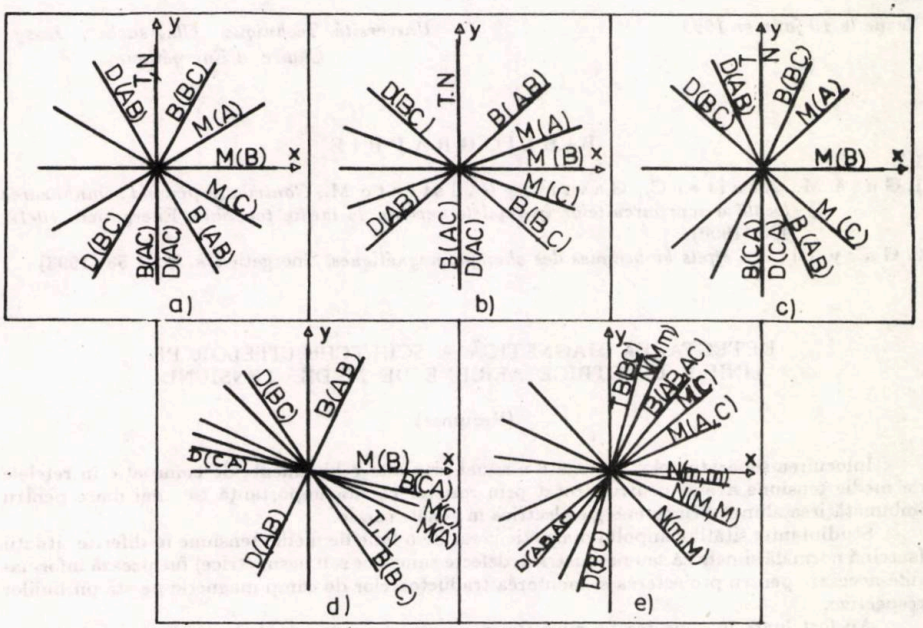

Fig. 4.– L'orientation de l'axe principal de l'ellipse tracée par le vecteur **H**: *a* – couronnement en nappe horizontale; *b* – couronnement en triangle; *c* – couronnement en nappe-voûte; *d* – couronnement en triangle désaxé; *e* – couronnement en tonneau. M – défaut phase–terre, B – défaut phase–phase, D – défaut deux phase–terre, T – défaut triphasé, N – régime normal. En paranthèses: A, B, C – phases de la ligne; M – charge maximum; m – charge minimum.

5. Conclusions

L'utilisation des traducteurs magnétiques pour détecter les court-circuits se présente comme une solution possible et économique pour les lignes aériennes de moyenne tension dans lesquelles on remplace les séparateurs par des équipements de commutation à déclenchement automatique soit sur les dérivations soit sur l'axe et dérivations. Le traducteur magnétique peut être emplacé à une distance sufissament grande par rapport aux conducteurs pour assurer l'isolement conformément à la tension de la ligne.

La détection indubitable des courtcircuits pour tous les régimes de défaut, quel qu'il soit le couronnement de la ligne et la position du défaut, peut être garantie si on utilise une combinaison logique „OR" des composantes horizontale et verticale du vecteur champ magnétique résultant de la ligne.

Le schéma d'un tel détecteur peut englober aussi des blocs de mémoire pour le nombre, le type et les moments des défauts, pour le fonctionnement du séparateur, etc.

Reçue le 10 janvier 1995

Université Technique „Gh. Asachi", Jassy, Chaire d'Énergétique

BIBLIOGRAPHIE

1. Guşă M., Asaftei C., Gavrilaş N., Istrate M., *Contribuţii privind semnalizarea locală a scurtcircuitelor în reţelele aeriene de medie tensiune.* Energetica, *10-12*, 425 (1990).
2. Gary Cl., *Les effets biologiques des champs magnétiques.* Energetica, s. B, *3*, 58 (1993).

DETECTAREA MAGNETICĂ A SCURTCIRCUITELOR PE LINIILE ELECTRICE AERIENE DE MEDIE TENSIUNE

(Rezumat)

Înlocuirea separatoarelor acţionate manual prin alte echipamente de comutaţie în reţelele de medie tensiune având neutrul tratat prin rezistor capătă importanţă tot mai mare pentru îmbunătăţirea alimentării cu energie electrică în zonele rurale.

Studiul intensităţii câmpului magnetic creat de o linie de medie tensiune în diferite situaţii (sarcină normală simetrică sau nesimetrică, defecte simetrice sau nesimetrice) furnizează informaţiile necesare pentru proiectarea şi montarea traductoarelor de câmp magnetic pe stâlpii liniilor respective.

Au fost luate în consideraţie cinci tipuri de coronamente uzuale la medie tensiune, toate tipurile de scurtcircuite, diferite poziţii ale defectelor şi diferite valori ale rezistenţei de defect.

Utilizarea simultană a componentelor orizontală şi verticală ale vectorului câmp magnetic rezultant prin intermediul unei funcţii logice „SAU" poate furniza informaţii corecte asupra producerii scurtcircuitelor în toate situaţiile analizate.

BULETINUL INSTITUTULUI POLITEHNIC DIN IAŞI
Tomul XLII (XLVI), Fasc. 1–2, 1996
Secţia III
ELECTROTEHNICĂ. ENERGETICĂ. ELECTRONICĂ

D.C. 621.317.333.4

THE IMPACT OF THE LAYOUT MODIFICATION IN THE SUPPLY SYSTEMS ON THE ONE-PHASE FAULT LOCATION DEVICES

BY
JAN IGNAT and M. PROFIRE

The layout modification effect of a half-distributor (the distribution of transformer points) in an urban distribution network on the working of signale-phase fault location devices are studied.

1. In [1],...,[3], there was presented a new method that allows the detection and location of the distributor, the section and the phase where the one-phase fault (grounding or short circuit) has been generated.

The method relies on the control of the value determined for the unbalanced currents on the end of each distributor and section by the aid of A_{ij} devices through a homopolar transformer and on the phase differences related to $\underline{U}_a$, $\underline{U}_b$, $\underline{U}_c$ phase voltages directly accessible in the secondary coil of the phase transformers from the transformer points (TP – Fig. 1), with the connection group ΔY-11(5).

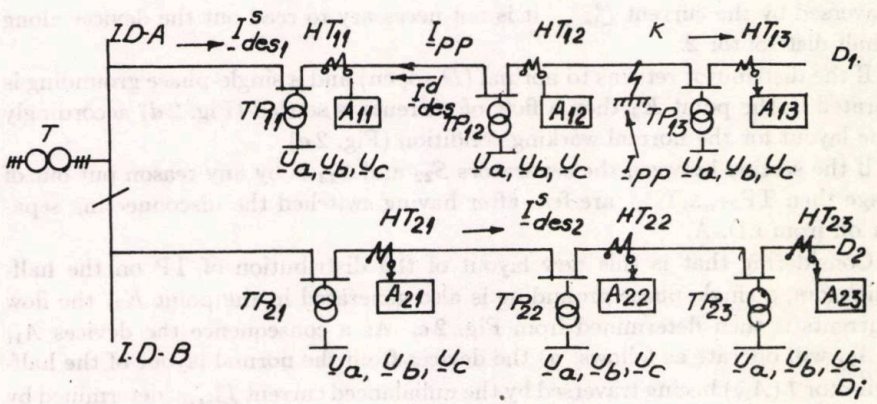

Fig. 1

The method principle also relies on the fact that D_i feeders are supplied just from one end and that is why, under the conditions of a stabilized one-phase fault,

the unbalanced currents have a well-defined flow, determined by the power unit from the end of it (I.D. – Fig. 1).

As a rule, in the local power systems and in order to assure the supply stand-by the feeders may be supplied from both ends (Fig. 2*a*); under normal conditions they operate being sectioned by a selecting separator (D_s), in two half-distributors.

If a single-grounding in K point (Fig. 2*a*) is for instance generated in a power supply system (PSS) with insulated neutral, then $A_{11}, ..., A_{13}$ devices, traversed by the unbalanced current ($\underline{I}^s_{\text{des}}$ – Fig. 2*b*), and accordingly to the method principle proposed in [1], will fall in one of the states I, II, III that indicate the existing fault down R, S, T phase while the other devices (A_{14} and $A_{21}, ..., A_{25}$ respectively) will fall in the state IV, traversed by $\underline{I}^s_{\text{des}_{11}}$, $\underline{I}^s_{\text{des}_{21}}$ current.

While the fault in K_1 is being removed the latter is put out of operation via disconnectors S_{16} and S_{17} and TP_{14} is fed again by from the distributing station-part B and by the half-distributor *2*.

2. If, while the layout of a distributor changes its configuration comparatively to that one specific to the normal working condition (the modification of the TP distribution), an other single-phase grounding is generated in K_2. In this case (Fig. 2*c*) the current changes its flow comparatively to that one presented in Fig. 2*b*, corresponding to the generation of a fault in a PSS whose layout is that of the normal working condition. As a consequence to it and although the device A_{14} is traversed by an unbalanced current $\underline{I}_{\text{des}_{22}}$, it's flow is opposite to $\underline{I}^s_{\text{des}_{11}}$ because it is determined by the voltage from the other end of the distributor (from I.D.-B not I.D.-A). Taking into account the given situation, the device A_{14} will fall in one of the states I, II, III, erroneously indicating the existence of a fault down it is site (as it had been traversed by $\underline{I}^d_{\text{des}_{K_{1,2}}}$).

In this case, the error has no practical effect as this device will not be read out in the field. That is due to the fact that, as the device A_{20} is not operated for it, is traversed by the current $\underline{I}^s_{\text{des}_{22}}$, it is not necessary to read out the devices along the half-distributor *2*.

If the distributor returns to normal (D_s-open) and a single-phase grounding is generated in the point K_3 then a flow of currents is settled (Fig. 2*d*) accordingly to the layout for the normal working condition (Fig. 2*a*).

If the section between the separators S_{22} and S_{23} is by any reason put out of voltage then TP_{22},...,TP_{25} are fed, after having switched the disconnecting separator off from I.D.-A.

Considering that is this new layout of the distribution of TP on the half-distributors, a single-phase grounding is also generated in the point K_3, the flow of currents is then determined from Fig. 2*e*. As a consequence the devices A_{1i} and A_{2j} will operate as follows: a) the devices from the normal layout of the half-distributor *1* (A_{1i}) beeing traversed by the unbalanced current $\underline{I}^d_{\text{des}_{K_3}}$ determined by the normal source (I.D.-A) of this distributor, will fall in the state I, II, III, that is the correct one; b) the devices from the normal layout of the half-distributor *2* that have been still left on this half-distributor (A_{20}) will be traversed by the current

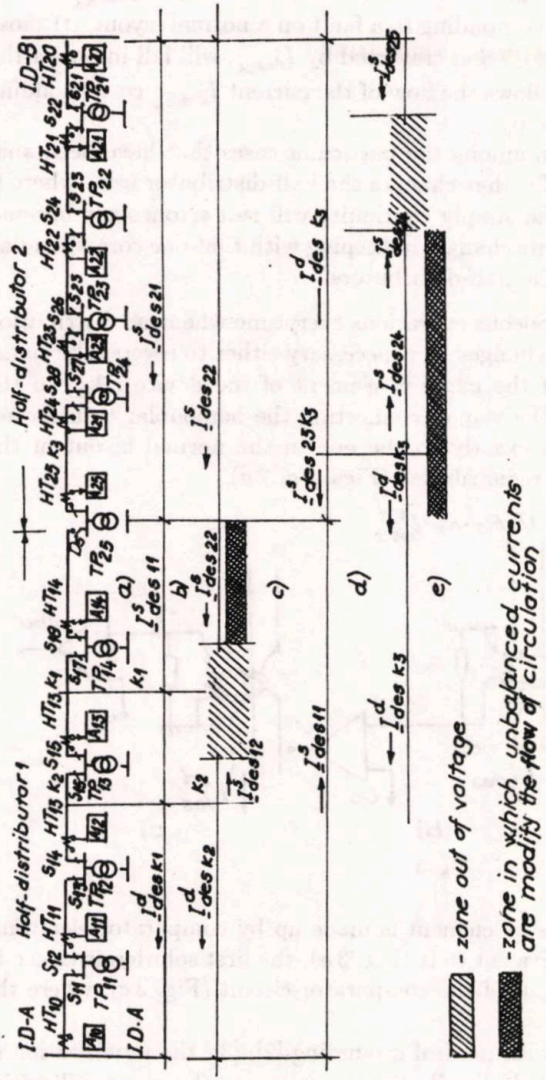
Half-distributor 1
Half-distributor 2
ID-A
ID-B
a)
b)
c)
d)
e)
- zone out of voltage
- zone in which unbalanced currents are modify the flow of circulation

Fig. 2

$\underline{I}^{s}_{\text{des}_{25}}$ and will fall in the correct state IV; c) the devices from the half-distributor *2*, transferred on the half-distributor *1*, will fall in different erroneous states, also in keeping with their position from the fault point as it follows: α) those located up the fault (A_{25}) and traversed by $\underline{I}^{d}_{\text{des}_{K_3}}$ will fall in state IV because $\underline{I}^{d}_{\text{des}_{K_3}}$ follows the flow of the current $\underline{I}_{\text{des}_{23}}$, corresponding to a fault on a normal layout; β) those located down the fault $(A_{24}, ..., A_{22})$ and traversed by $\underline{I}^{s}_{\text{des}_{24}}$, will fall in one of the states I, II, III because $\underline{I}^{d}_{\text{des}_{24}}$ follows the flow of the current $\underline{I}_{\text{des}_{K_3}}$ corresponding to a fault in K_3 on a normal layout.

A single conclusion is drawn among the particular cases that have been analyzed namely all the devices in TP that changes the half-distributor from where it is fed by reasons of assurance the supply continuity will run erroneously because the flow of the unbalanced currents changes in keeping with that one corresponding to the normal layout of TP on the half-distributors.

3. In order to avoid the erroneous operations everytime when the distribution of TP on the half-distributors is changed, it is necessary either to reverse the signal $\underline{U}$ (Fig. 3*c*) from the output of the measure element of the device (A_{ij}) in the redistributed TP, or to change the way of connecting the homopolar transformer (Fig. 3*b*), so that it ressembles exactly to the one in the normal layout of the half-distributor on which it was redistributed (Figs. 3*a*, 2*a*).

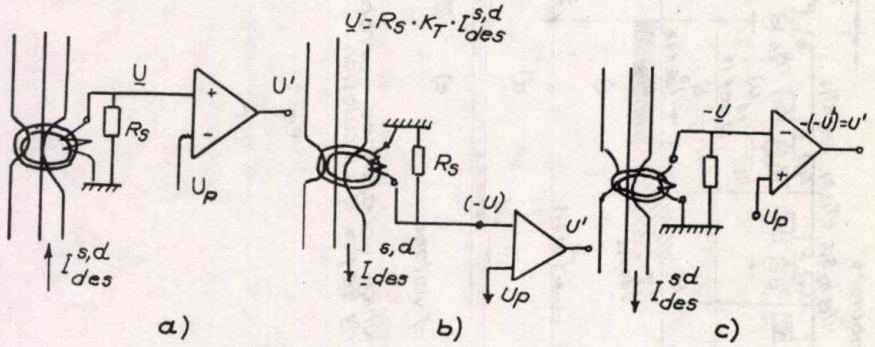

Fig. 3

For the devices whose measure element is made up by comparator electronic circuits of the type A399 or equivalent to it (Fig. 3*a*), the first solution is easier to be achieved by reversing the input of the comparator circuit (Fig. 3*c*), where the signal is applied.

It is obvious that, in PSS with neutral grounding [2], [3], the modification of the distribution of TP on the half-distributions determines the same difficulties in the operation of the devices for which the method of detecting and locating a single-phase fault is used, as the solutions are similar to those for PSS with insulated neutral.

Conclusions

The layout modification of the half-distributors (the distribution of TP) affects the run of the single-phase fault location device. These difficulties can be easily avoided in the case when these devices are made with comparator electronic circuits.

Received, March 20, 1995

Technical University "Gh.Asachi", Jassy,
Department of Installation in
Civil and Industrial Buildings

REFERENCES

1. I g n a t J., *Une nouvelle méthode d'identification et localisation d'une mise a terre dans un réseau de moyenne tension ayant le point neutre isolé.* Bul. Inst. polit., Iaşi, **XXXVII (XLI)**, *1-4*, s.III, 71-76 (1991).
2. I g n a t J., *Sur l'application de la méthode d'identification et localisation d'une mise à terre à l'aide du contrôle des déphasages dans les réseaux électriques de moyenne tension ayant le point neutre mis à terre.* Bul. Inst. polit., Iaşi, **XXXVIII (XLIII)**, *1-4*, s.III, 129-135 (1993).
3. I g n a t J., *Aplicarea metodei bazată pe controlul defazajelor la identificarea şi localizarea scurtcircuitului monofazat.* Bul. Inst. de Energ. al Acad. Republicii Moldova, *7*, 61-67 (1993).

EFECTUL MODIFICĂRII CONFIGURAŢIEI REŢELELOR DE DISTRIBUŢIE ASUPRA DISPOZITIVELOR DE LOCALIZARE A DEFECTULUI MONOFAZAT

(Rezumat)

Se pune în evidenţă efectul modificării configuraţiei unui semi-distribuitor (repartizarea posturilor de transformare) dintr-o reţea de distribuţie urbană asupra funcţionării dispozitivelor de localizare a defectului monofazat şi se indică soluţiile de evitare a efectelor negative ale acestei modificări.

BULETINUL INSTITUTULUI POLITEHNIC DIN IAŞI
Tomul XLII (XLVI), Fasc. 1-2, 1996
Secţia III
ELECTROTEHNICĂ. ENERGETICĂ. ELECTRONICĂ

D.C. 621.316.11

OPTIMAL DESIGN OF THE RURAL ELECTRIC DISTRIBUTION NETWORKS

BY

GH. GEORGESCU and M. GAVRILAŞ

The design of rural electrical distribution networks comprises as an important stage the choice of their optimal route.

An algorithm to solve the problem of the network optimal routing using a step-by-step search method is proposed, that itself creates new branching nodes.

1. Introduction

Medium voltage (MV) rural distribution networks are designed as overhead electric lines in a radial, tree-like configuration. A significant problem that has to be solved in the design stage of these networks is the choice of the route [1]. Also it is necessary to respect both efficiency criteria (total length, cost, etc.) and constraints imposed by the characteristics of the area crossed by the line. At present there is no efficient and accurate method able to determine the optimal route of the line under the conditions above mentioned.

A solution to this problem could be obtained based on a method of successive search on the set of consumer nodes supplied by the network.

2. Mathematical Model

The proposed mathematical model comprises two important steps:

a) S t e p 1: determine a complete graph [3] of minimal length, using the set **S** that contains the source node and all consumer nodes.

b) S t e p 2: optimize the graph built-up in Step 1 by introducing supplementary branching nodes.

2.1. Step 1

To determine the complete, minimal length graph defined on the set of consumer nodes and the source node, a simple and efficient algorithm was used, i.e., the PRIMA algorithm [2]. The principle of this algorithm consists in sequentially

develop a tree-like network using a partition of the set **S** into two subset: **S1** – the subset of those (marked) nodes that at one moment are already included in the PRIMA graph; **S2** – the subset of those (unmarked) nodes, from which the next node to be included in the PRIMA graph will be chosen.

Initially, the subset **S1** contains only the source node SN.

At the very beginning that node, denoted N^{**}, which is the closest to the source node SN, will be selected. Nodes SN and N^{**} determine a new branch in the PRIMA graph. Consequently, the node N^{**} will be marked (it will pass from subset **S2** to subset **S1**). Afterwards the algorithm goes on according to the model described in Box 1, until all nodes are marked.

Box 1
The PRIMA Algorithm

- mark the source node SN : $\mathbf{S1} = \{SN\}$; $\mathbf{S2} = \mathbf{S} - \mathbf{S1}$;
- **repeat**
  - search the node $N^{**} \in \mathbf{S2}$ which is the closest to one of the marked nodes $N^{*} \in \mathbf{S1}$;
  - define branch $N^{*}-N^{**}$ in the PRIMA graph;
  - mark the node N^{**}: $\mathbf{S1} = \mathbf{S1} \cup \{N^{*}\}$; $\mathbf{S2} = \mathbf{S} - \mathbf{S1}$;

until (no more unmarked node exists: $\mathbf{S2} = \{\emptyset\}$)

2.2. Step 2

In the hypothesis that all branching points in the graph are nodes from the set **S**, the graph obtained at the end of Step 1 represents a minimum for the problem.

The length associated to this graph could be reduced on by introducing new, supplementary branching nodes, where no load exists. Each of these nodes is defined in relation with other three nodes, according to the generalized S t e i n e r problem [2] (s. Fig.1).

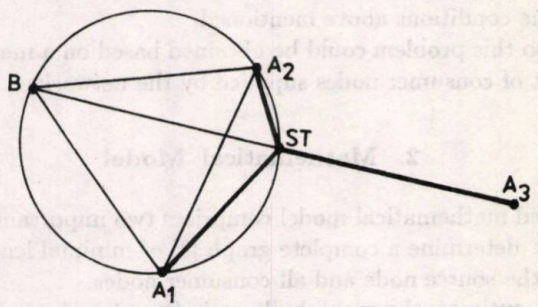

Fig. 1

Let us consider three nodes denoted A_1, A_2, A_3. Using one of the sides between those nodes (for example side A_1A_2), an equilateral triangle is drawn with the apex B in opposition with the third initial node A_3. The intersection of the right line BA_3 with the circle circumscribed to triangle A_1A_2B represents the S t e i n e r node ST, supplementary introduced in the graph. The S t e i n e r node is the

one in the plane of triangle $A_1A_2A_3$ who ensures the minimal length of the radial graph whose branches connect this point whith the three apexes of the triangle.

A S t e i n e r node can be determined if and only if all angles of triangle $A_1A_2A_3$ are less then 120°. Otherwise the S t e i n e r node will coincide with one of the nodes A_1, A_2 or A_3.

3. The Algorithm and the Programme

Using the above mathematical model, a programme was drawn up meant for the optimization of the route of radial, tree-like networks, considering as the optimum criterion the total length of the network.

In comparison with the two steps already described the programme presents few characteristic features:

a) Step 1 is carried out in complete accordance with the principle described, ensuring the global optimum in the hypothesis that only the initial nodes are considered when establishing a branching point.

b) In Step 2 the PRIMA graph is inspected using the order determined by the numbers associated to the nodes in the network, adding – when possible – supplementary S t e i n e r nodes. This step is repeated until no more S t e i n e r nodes could be defined.

c) For Step 2 we observed that, depending on the order of numeration of the nodes in the network, it is possible to obtain different graphs with different lengths, each of such a graph representing a local minimum for the problem. This is the reason why, in order to obtain a minimum as closest as possible to the global one, the programme generates random variants for the numeration of the nodes in the network. In the case of those networks which supply a great number of loads there exists a very large number of such possible variants. In this context the programme comes to end when either a prescribed time or a maximum number of variants are reached.

4. Examples

This programme was used to analyse a series of real cases, in order to establish the optimal route of different rural distribution networks. Fig. 2*a* and *b* show the obtained results for two such examples.

In the case in Fig. 2*a* the network comprises 30 consumer nodes and one source node. The route, drawn with continuous line, corresponds to the PRIMA graph, with a length L_1=48.7 km. After optimizing the PRIMA graph, six S t e i n e r nodes were created and the new route, drawn with dashed line, has a length L_2=43.8 km.

For the second case (a network comprising 18 consumer nodes and one source node – Fig. 2*b*), the same two lengths are L_1=26.0 km and L_2=24.1 km and the number of supplementary S t e i n e r nodes created during the programme running time is three.

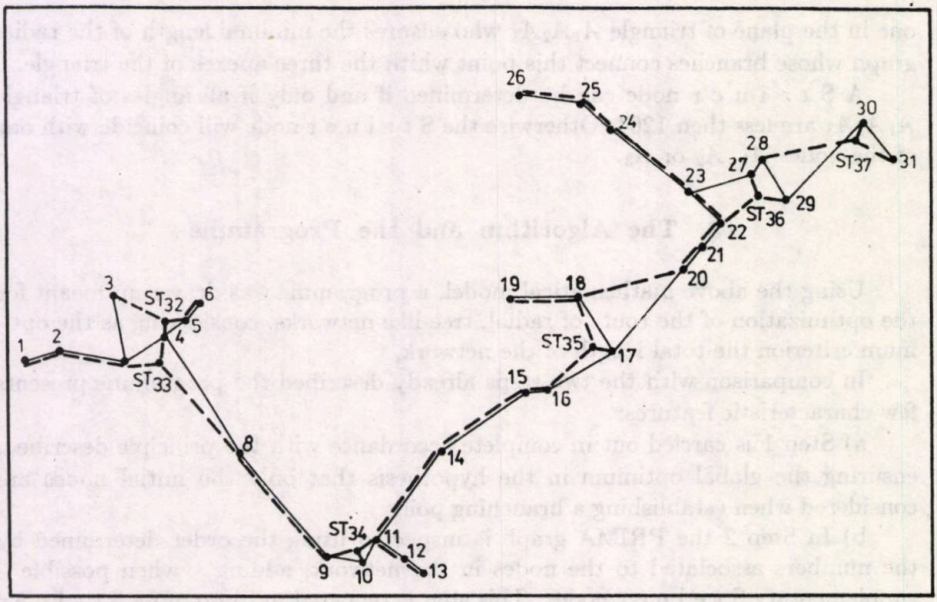
26
25
24
30
28
27
ST37
31
23
29
ST36
22
21
20
19
18
3
ST32
6
5
4
1
2
ST35
17
15
16
ST33
8
14
ST34
11
12
9
10
13

a)

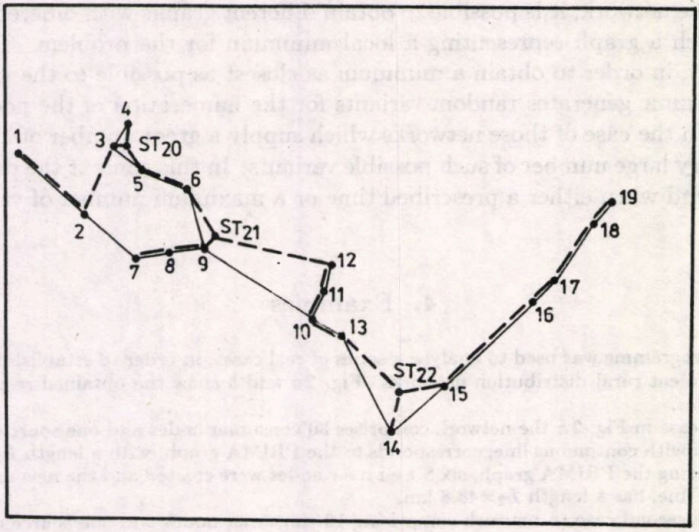
4
1
3
ST20
5
6
19
18
2
ST21
12
7
8
9
11
17
16
10
13
ST22
15
14

b)

Fig. 2

5. Conclusions

The proposed method and programme are efficient tools that could offer useful design information, in order to determine the optimal route of MV rural distribution networks.

Taking into consideration of a sufficiently large number of variants concerning the numeration of the nodes in the network ensures a greater probability to come closer to the global minimum.

Received, February 14, 1995

Technical University "Gh.Asachi", Jassy, Department of Energetics

REFERENCES

1. von Herbert H., Klein L., Wellßow W.H., *Rechnergestützte Planung von städtischen Mittelspannungsnetzen.* Elektrizitätswirtschaft, *22* (1993).
2. Arion V.D., Karatun V.S., *Statičeskie modeli optimizatzii razvitia električeskih setei v SAPR.* Khishin. Polit. Inst. im. "S.Lazo", 1989.
3. Rădescu N., Rădescu E., *Probleme de teoria grafurilor.* Ed. Scrisul Românesc, Craiova, 1982.

PROIECTAREA OPTIMALĂ A REŢELELOR DE DISTRIBUŢIE RURALĂ

(Rezumat)

O etapă importantă în faza de proiectare a reţelelor electrice de distribuţie rurală o reprezintă alegerea traseului optim al acestora. În acest sens se propune un algoritm care, pornind de la mulţimea nodurile definite de sarcini, permite construirea traseului optim pe baza unei metode de căutări succesive şi a introducerii unor puncte suplimentare de ramificaţie.

BULETINUL INSTITUTULUI POLITEHNIC DIN IAŞI
Tomul XLII (XLVI), Fasc. 1–2, 1996
Secţia III
ELECTROTEHNICĂ. ENERGETICĂ. ELECTRONICĂ

RECENZII BOOK REVIEWS

ELDBERM I., *Moderne Berechnungsmethoden in Elektrotechnik und Elektronik.* Expert Verlag, Renningen, 1995, 273 S., ISBN 3-8169-1268-0.

In der klassischen Elektrotechnik und Elektronik waren es hauptsächlich einzelne Bauteile, beispielsweise Spulen, Kondensatoren, Widerstände oder Elektronenröhren, denen als fundamentale Elemente der Gerätetechnik groß Aufmerksamkeit gewidmet wurde. Erst in neuerer Zeit, mit der Entwicklung einer weitverzweigten Halbleitertechnologie, wurde der allen Bauteilen gemeinsame natürliche Kern immer deutlicher. Rechenansätze, mit diesen Gemeinsamkeiten aufgestellt, gelten universell für ganz unterschiedliche technische Konfigurationen.

Heute weiß man: Nicht die Bauteile selbst, sondern nur die formalen Regeln, die ihre Beziehungen untereinander beschreiben und mit denen ihre Wirksamkeiten verknüpft werden können, führen schnell zu neuen Erkenntnissen. Der Mut, die elementbezogene Denkweise zur Abstraktion zu ändern, also in Strukturen zu denken, hat sich als ungeahnt erfolgreich herausgestellt – nicht zuletzt deshalb, weil das Rechnen mit Strukturen sehr viel leichter, bequemer und effektiver ist als der Umgang mit vereinzelten Funktionselementen.

Die an praxisgerechten Ergebnissen interessierten Elektrofachleute mit der so nützlichen und zuverlässig funktionierenden Berechnungsmethode bekannt zu machen, ist Ziel dieses Buchs. Zugleich bringt die ordnende Wirkung eines strukturorientierten Denkansatzes beim Arbeiten mit Computern die Sicherheit, die nötig ist, um den Ergebnissen eines nicht mehr sichtbaren Rechenprozesses zu trauen.

Die Interessenten: Fachleute (oder solche, dies es einmal werden wollen), die eine sicher funktionierende– professionelle und praxistaugliche Berechnungsmethode für lineare und bereichsweise lineare Schaltkreise benötigen.

ALBRECHT F.W. (federführend), *Beschallungstechnik. Theorie und Praxis.* Expert Verlag, Renningen, 1995, 236 S., ISBN 3-8169-0424-6.

Der Leser erhält einen Einblick in die moderne Beschallungstechnik. Angesprochen sind alle, die in ihrer beruflichen Praxis mit der Rundfunk- und Studiotechnik zu tun haben. Ausgehend von den Grundlagen der Schallausbreitung wird über die Besonderheiten bei der Beschallung von geschlossenen Räumen und von Freigeländen berichtet. Die dazu benötigten Schallwandler (Mikrofilme, Lautsprecher) sind ausführlich in gesonderten Kapiteln behandelt. Das gleiche gilt für die Verstärkertechnik und für die Studiotechnik. Es wird gezeigt, wie sich durch eine geeignete Gruppenanordnung von Lautsprechern verschiedene Richtwirkungen erzielen lassen. Ein weiteres Kapitel befaßt sich mit allgemeinen Fragen der Beschallung. Abschließend wird die Technik der drahtlosen Übertragungsanlagen (Hochfrequenz-Technik, Infrarot-Technik) vorgestellt und erläutert.

Die Interessenten: Angesprochen sind alle, die in ihrer beruflichen Praxis mit der Rundfunk- und Studiotechnik zu tun haben, insbesondere: a) Toningenieure und Tonmeister von Theatern, Stadthallen und Konferenzzentren; b) Industriebetriebe, die Schulungen und Konferenzen durchführen; c) Verleiher und Installateure von Beschallungsanlagen; d) Hersteller von ELA-Komponenten.

BONFIG K.W. (federführend), *Temperatursensoren.* Expert Verlag, Renningen, 1995, 187 S., ISBN 3-8169-1261-3.

Der Themenband gibt einen Überblick über die heute in der Industrie und im Labor genutzten Verfahren und die ihnen zugrunde liegenden physikalischen Prinzipien. An eine Darstellung des Prinzips und der Wirkungsweise von Temperatursensoren schließen sich Schwerpunktbeiträge über Metall- und Halbleiterwiderstandsthermometer, Thermoelemente und Schwingquarzthermometer an. Besondere Bedeutung bei schwierigen industriellen Anwendungen haben die Strahlungsthermometer und -pyrometer und die Messung von Temperaturverteilungen und Temperaturprofilen mit infrarotoptischen System. Vor allem die Beiträge über thermische Meßfehler bei Oberflächentemperaturmessungen und über die Meßsignalverarbeitung bei elektrischen Berührungsthermometern werden den Anwender interessieren. Bei allen Kapiteln erfolgt auch eine Darstellung und Erläuterung von typischen Anwendungsbeispielen und Problemlösungen in Forschung, Entwicklung, Prozeßüberwachung und -kontrolle.

Die Interessenten: Das Buch wendet sich an alle, die mit technischer Temperaturmessung befaßt sind, also an Diplom-Ingenieure, Chemiker und Physiker.

SARKOWSKI H., *Meßtechnik bei Elektronikgeräten.* Expert Verlag GmbH, Renningen, 182 S., 1989, ISBN 3-8169-0384-3.

Dieses Buch ist ursprünglich als Begleitmaterial zu den Vorträgen und praktischen Übungen der Lehrgänge der Technischen Akademie Esslingen gedacht. Aber es ist auch als eine sehr gute Informationsquelle zum Selbststudium zu verwenden.

Es ist gut verständlich geschreiben, und unnötige Theorie wurde weggelassen, so daß Ingenieure und Techniker aller Fachrichtungen, die mit elektronischen Hilfsmitteln, Geräten und Anlagen zu tun haben, verwertbare Informationen für die praxisnahe Meßtechnik entnehmen.

Behandelt werden in diesem Buch Meßgrössen und ihre Einheiten, Universal- Meßgeräte, Oszilloskope, Meßbrücken, Funktionsgeneratoren, elektronische Zähler, rechnergesteuerte Meßtechnik, Besonderheiten beim Messen hoher Frequenzen, und schließlich die in den letzten Jahren immer wichtiger gewordenen Meßmethoden in der Digitaltechnik, einschließlich Logikanalyse und Signaturanalyse.

Elektronikingenieure in Labor und Prüffeld sowie Ingenieure und Techniker aller anderen Arbeitsgebiete finden in dem Buch eine systematische Einführung in die praxisnahe Meßtechnik.

ÖRSZÁGOS MŰSZAKI INFORMÁCIÓS KÖZPONT ÉS KÖNYVTÁR 1883

ISSN 0258-9109